JP0550002

JAERI TANDEM ANNUAL REPORT 2003
APRIL 1, 2003—MARCH 31, 2004

December 2004

Department of Materials Science

日 本 原 子 力 研 究 所
Japan Atomic Energy Research Institute

JAERI TANDEM Annual Report 2003
April 1, 2003 – March 31, 2004

Department of Materials Science※

Tokai Research Establishment
Japan Atomic Energy Research Institute
Tokai-mura, Naka-gun, Ibaraki-ken

This annual report describes research activities, which have been performed with the JAERI tandem accelerator and its energy booster from April 1, 2003 to March 31, 2004. Summary reports of 42 papers, and lists of publication, personnel and cooperative research with universities are contained.

原研タンデム加速器
2003 年度年次報告

日本原子力研究所東海研究所
物質科学研究部※

　本年次報告書は、東海研究所の原研タンデム加速器及びブースターを利用し、2003 年 4 月 1 日から 2004 年 3 月 31 日までの間に行われた研究活動をとりまとめたものである。
　(1)加速器の運転状況及び開発　(2)原子核構造　(3)原子核反応　(4)核化学　(5)原子核理論　(6)原子分子物理及び固体物理　(7)材料の照射効果の 7 部門にまたがる 42 編の研究報告、公表された文献、関与した職員及び大学等との協力研究のリストを収録している。

東海研究所：〒319-1195　茨城県那珂郡東海村白方白根 2-4
※（編集者）石井哲朗、竹内末広、大島真澄、永目諭一郎、千葉　敏、左高正雄

Foreword

This report covers research and development activities with the tandem accelerator and its superconducting booster at JAERI, Tokai, for the period of FY 2003 (April 1, 2003 to March 31, 2004). During this period, the accelerator was operated over a total of 188 days and delivered 22 different ions over 111 beam times to experiments in the field of nuclear structure, nuclear reactions, nuclear chemistry, atomic physics, solid state physics and radiation effects in materials. Sixty-three research programs were carried out in collaboration with about 200 researchers from universities and research institutes. The following are some of the highlights in FY 2003.

The JAERI-KEK joint project of developing an ISOL-based radioactive-nuclear beam facility has been running since FY2001. In FY2003, the accelerators (split-coaxial RFQ, IH linac) in KEK were moved to a remodeled room in the tandem accelerator facility. The ion source in the ISOL was developed for the use of a UC_2 target. The ISOL was connected to an ECR charge breeder operating at 18 GHz. An ECR ion source for stable-nuclear beams was also installed. This facility accelerates heavy-ions with $A/q < 7$ up to 1 MeV/nucleon, and named as TRIAC, Tokai Radioactive Ion Accelerator Complex. The first beam is scheduled for the end of 2004.

In the development of the tandem accelerator, all the acceleration tubes were replaced with the compressed-geometry tubes cleaned carefully by high-pressure water rinsing. The terminal voltage recovered 16 MV quickly without heavy high-voltage conditioning. The terminal voltage reached 18 MV by the end of FY2003.

In research of nuclear structure, the first γ-ray experiment of the one-hole-nucleus ^{47}K was carried out by deep-inelastic collisions with a ^{48}Ca beam. The electromagnetic properties of low-lying states in ^{66,68}Zn, ^{78}Se isotopes were determined by projectile Coulomb excitation. High-spin states in ^{169,172,187}Re, ^{145,146}Tb and ^{179}Au, and a high-spin isomer of ^{136}Ba were identified by the γ-ray detector array, GEMINI-II. In one of the heaviest nuclei ^{257}No, the spin-parity of its ground state was determined by α-decay spectroscopy using the ISOL and a He gas-jet system.
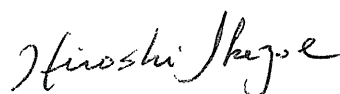
In research of nuclear reactions, fusion cross sections of ^{64}Ni+^{154}Sm and ^{86}Kr+^{134,138}Ba reactions were measured by using the recoil mass separator JAERI-RMS in order to investigate the dependence of sub-barrier fusion on the nuclear deformation and shell structure. The exclusive cross section of ^{8}Li(α,n) reaction was measured with high statistics in the energy region, E_{cm}=0.9-2.8 MeV, of astrophysical interest by using a highly pure

low-energy beam of unstable ^{8}Li nuclei from the JAERI-RMS.

In research of nuclear chemistry, fluoride complexation of element 104, rutherfordium (Rf), produced in the ^{248}Cm(^{18}O,5n)^{261}Rf reaction has been studied by anion-exchange chromatography on an atom-at-a-time scale. The relation between the distribution coefficients K_d of Rf and the concentration of hydrofluoric acid [HF] was determined for the first time for the Rf complex.

In research of nuclear theory, relationship between the Monte-Carlo shell model and mean-field approximation on the structure of unstable nuclei was revealed in terms of the potential energy surface. It was found that the pairing gap of Λ hyperons depends on the background nucleon density through the Dirac effective mass.

In research of solid state physics, long- and short-range disorderings of lithium metatitanate (Li$_2$TiO$_3$) irradiated with energetic Xe or O ions were identified to relate to the electronic stopping power (S$_e$) of the incident ions from the results of X-ray diffraction and Raman spectroscopic analyses. The short-range disordering was caused by the destruction of the cation bonding-structures in the octahedral and tetrahedral coordination sites due to the ion irradiation with the S$_e$ of 20.0 keV/nm. The irradiation with the S$_e$ of 1.2 keV/nm caused only the long-range disordering of lattice planes where the cations lie in the Li$_2$TiO$_3$ structure.

Hiroshi Ikezoe
Deputy Director
Department of Materials Science

Contents

目次

1. Accelerator Operation and Development

This is a blank page.

1. 1 OPERATION AND USAGE OF TANDEM ACCELERATOR AND BOOSTER

S. TAKEUCHI, Y. TSUKIHASHI, T. YOSHIDA, S. KANDA, K. HORIE, I. OUCHI, S. HANASHIMA,
S. ABE, N. ISHIZAKI, H. TAYAMA, M. MATSUDA, T. NAKANOYA, H. KABUMOTO and T. SATO

In the beginning of FY2003, a replacement of the whole acceleration tubes to the new compressed geometry tubes which were cleaned by a high-pressure water jet [1,2] was carried out spending several months and it was successfully finished with a week long conditioning to recover a voltage of 16 MV. The machine time for experiments started June 30 as scheduled. The operations of the tandem accelerator and booster were given to conducting experiments over two machine time periods, June 30 to October 16 and December 8 to March 31. The total operation time of the tandem accelerator was 4,454 hours or 188 days, and 111 different beam deliveries were performed for experiments during the operation time. We had a loss of 8 days in providing beams to experiments scheduled during these periods due to two troubles with a high-voltage power supply for the in-terminal ECR ion source and a charging-chain drive motor.

The experiment proposals and the usage of beam times from June 30, 2002 to March 31, 2003 are summarized in table 1 and table 2, respectively.

Table 1. Experiment Proposals.

Research Proposals Accepted by the Program Committee:

In-house Staff Proposals	11
Collaboration Proposals	33
Number of Experiments Proposed	63
Number of Scientists Participating in Research from out side	201,
in-house	172
Number of Institutions Represented	42

Table 2. Usage of Beam-times in Different Research Fields.

Research fields	Beam Time(days) (percentage)	Number of Experiments Receiving Beam
Nuclear physics	91 (48.4%)	41
Nuclear chemistry	31 (16.5%)	18
Atomic and Solid state physics	55 (29.3%)	45
Material research	9 (4.8%)	5
Accelerator	2 (1.1%)	2
Total	188 (100%)	111

With respect to the accelerator operation, the distribution of the terminal voltages and ion species are listed in table 3 and table 4, respectively.

Table 3. Distribution of Terminal Voltages.

>16	MV	0	days	0.0	%
15-16		61		32.4	
14-15		45		23.9	
13-14		12		6.4	
12-13		10		5.3	
11-12		1		0.5	
10-11		7		3.7	
9-10		8		4.3	
8-9		4		2.1	
7-8		22		11.7	
6-7		3		1.6	
5-6		15		8.0	

All the experiments ended with a terminal voltage below 16 MV because of lack of time for high-voltage conditioning. In the high voltage increasing test done just after the end of the second machine time period, the voltage reached 18 MV in a few days without any heavy discharge activities. It is promising that replacing tubes to new 21 gap compressed geometry tubes, of which inside walls were cleaned by the high pressure jet of clean water, will have an effect on the operation voltage in the near future. The operation voltages spread widely down to 5-6 MV level. At the very low terminal voltages, a beam of ^{7}Li was accelerated to produce ^{8}Li secondary beams for experiments of nuclear astrophysics and Li diffusion in solid materials.

With respect to the ion beams, the accelerator provided a total of 22 different ion species for research.

Table 4. Distribution of Ion Species Accelerated for Experiments.

^{1}H	15	days	^{56}Fe	3	days
^{7}Li	16		^{58,64}Ni	17	
^{11}B	1		^{74}Ge	1	
^{12}C	14		^{80}Kr	11	
^{16,18}O	28		^{82}Se	5	
^{19}F	9		^{90}Zr	1	
^{28}Si	2		^{96}Mo	3	
^{32,33}S	18		^{124}Sn	1	
^{35}Cl	6		^{127}I	3	
^{40}Ar	2		^{136}Xe	22	
^{48}Ca	4		^{197}Au	6	

Among the ions in table 4, inert gas ions Ar, Kr and Xe were accelerated from the in-terminal ECR ion source. The ^{16,18}O beams stood out most in popularity commanding over 15% of all beam time. The ^{136}Xe beams also had a high popularity of 12%.

The super-conducting booster was operated a total of 41 days for boosting 9 different beams from the tandem accelerator to conduct 15 experiments, while the helium refrigeration systems were in operation for 145 days from June 2 in 2003, 115 days from December 8 in 2003. There were no big troubles in FY2003 as before. Forty super-conducting resonators were all in good condition to run and the average acceleration field gradient was 4.2 MV/m at an RF input of 4 watts. The ion species boosted for experiments and their boosted energies and beam times are shown in table 5. All the boosted beams were used for nuclear physics and it meant that 45% of the beam time used for nuclear physics needed an energy boost.

Table 5. Boosted Ion Beams for Experiments:

^{16}O	200	MeV	2 days
^{48}Ca	410		4
^{34}S	180		3
^{64}Ni	360		9
^{82}Se	630		5
^{80}Kr	340		10
^{96}Mo	424		3
^{124}Sn	530		1

With respect to accelerator development activities in FY2003, an radioactive ion beam accelerator(TRIAC) was installed in an extended room in the tandem facility in collaboration with KEK [3,4]. The system is to be reported elsewhere in this annual report. For the up-grade project of the in-terminal ECR ion source from a 10 GHz compact ECR ion source to 14.5 GHz high performance ECR ion source, the gas stripper was removed from the terminal to make a space to install the 14.5 GHz ECR ion source in the next year. A new safety interlock system was in preparation to cope with the addition of TRIAC. We had an up-grade plan of the booster to accept low beta (injection velocity) heavy ions and to improve their beam transmission or increase their beam intensities [4]. A development work of low beta(=0.06) superconducting accelerating cavities started and was in progress.

References

[1] S. Takeuchi, et al, Nucl. Instrum, and Meth., A 513,(2003) 429.

[2] S. Takeuchi, et al, JAERI Tandem Annual Report 2002(2003) pp6-7.

[3] H. Miyatake, et al, Nucl. Instrum. and Meth., B204(2003) 746.

[4] S. Takeuchi, Application of Accelerators in Research and Industry:17th Int'l Conf.; AIP 0-7354-0149-7/03, (2003) pp229-236.

1. 2 ACCELERATION TUBE REPLACEMENT

S. TAKEUCHI, H. KABUMOTO, M. MATSUDA, T. NAKANOYA, Y. TSUKIHASHI,
T. YOSHIDA, S. KANDA, K. HORIE, I. OUCHI, S. HANASHIMA, S. ABE, N. ISHIZAKI,
H. TAYAMA and T. SATO

All of the 120 acceleration tubes were replaced in 2003 to 80 compressed geometry tubes which were cleaned by high-pressure water jets and baked at 200℃, in order to increase the maximum terminal voltages from 16 MV to 18-20MV. Prior to the replacement, we investigated surfaces of the ceramic insulators and the effect of high-pressure water jet sprays. The ceramic surfaces of the new tubes were covered with millions of loosely bound micro-particles and cleaned well by high-pressure water jets [1]. The 3 MV high-voltage test with six new tubes indicated that the high-voltage performance of the tubes was dramatically improved by the cleaning [1,2], i.e. from a noisy state with frequent full sparks at 2.8 MV to a very calm state at 3.2 MV. It was concluded that loosely bound micro-particles were a source of discharge activity in the acceleration tubes.

The replacement took about 4 months and high voltage conditioning was done for a week in the end of June, 2003. The conditioning was carried out in groups of several 1MV modules in the way that the other modules were short-circuited by shorting rods, and took several hours for each. And a high voltage performance of 15.8MV(79%) was obtained for the full column composed of 20 modules. The conditioning was not sufficient, but the machine time resumed because of the schedule.

Every 1MV module was examined in October, 2003. Most of them were stable up to about 1.15 MV(115%) . Every two 1MV modules received a few hours of conditioning in December, 2003, and voltages of about 2.20 MV(110%) were attained by most of them. The three column sections were given several hours of conditioning respectively after the end of the last machine time of FY2003. As a result, the lower column section of 7 modules was free from discharge activities up to 6.80 MV (97%), the middle section of 6 modules 5.57 MV (92%) and the upper section of 7 modules 6.80 MV (98%). And, the full column obtained a high voltage performance of 18 MV(90%).

The pre-treatment with high pressure water jets should have contributed a lot to improving the high voltage performance. There still seemed to be a possibility for the performance to go higher with more conditioning.

References
[1] S. Takeuchi, et al, Nucl. Instrum. and Methods, A 513,(2003) 429.
[2] S. Takeuchi, et al, JAERI Tandem Annual Report 2002(2003) pp6-7.

1. 3 KEK-JAERI JOINT RNB PROJECT

H. MIYATAKE[1] and S. TAKEUCHI
for the TRIAC Collaboration

KEK-IPNS (Institute of Particle and Nuclear Studies) and JAERI-Tokai have been collaborating to construct the radioactive-nuclear-beam (RNB) facility, which consists of the ISOL, a charge-breeding (CB-) ECR, and the heavy-ion linacs (see Fig. 1), since FY2001. From FY2005, the low-energy RNB having its energy up to 1.1 MeV/u will be available at the low-energy experimental hall for scientific subjects of nuclear astrophysics, nuclear physics, material science, and related research fields. Before starting the operation, the acronym of this facility was decided as TRIAC (Tokai Radioactive Ion Accelerator Complex) facility. This is also an abbreviated form of "Tri-ACcelerators" (Split Coaxial RFQ type (SCRFQ-) , Interdigital-H type (IH-), and Super conducting type (SC-) linacs) facility.

In FY2003, all of instruments from KEK have been installed and aligned to the beam line. Fig. 2 shows the CB-ECR placed between the JAERI-ISOL and the SCRFQ-linac at the JAERI RNB experimental room. This ECR takes an important role as an in-flight type charge state breeder of radioactive ions from 1^+ to q^+, for satisfying the mass-to-charge ratios (A/q) for acceleration conditions both of SCRFQ-linac (A/q <30) and IH-linac (A/q <10). An off-line test of the CB-ECR has been performed on a test bench at KEK before its installation. The charge breeding efficiencies defined as number ratios of extracted q^+-ions to injected 1^+-ions for Ar, Kr, and Xe were 13.5% (for q=9), 10.4% (for q=12), and 6.8% (for q=20), respectively. It is noted that the ECR is optimized for the required charge state fulfilling the condition A/q < 7.
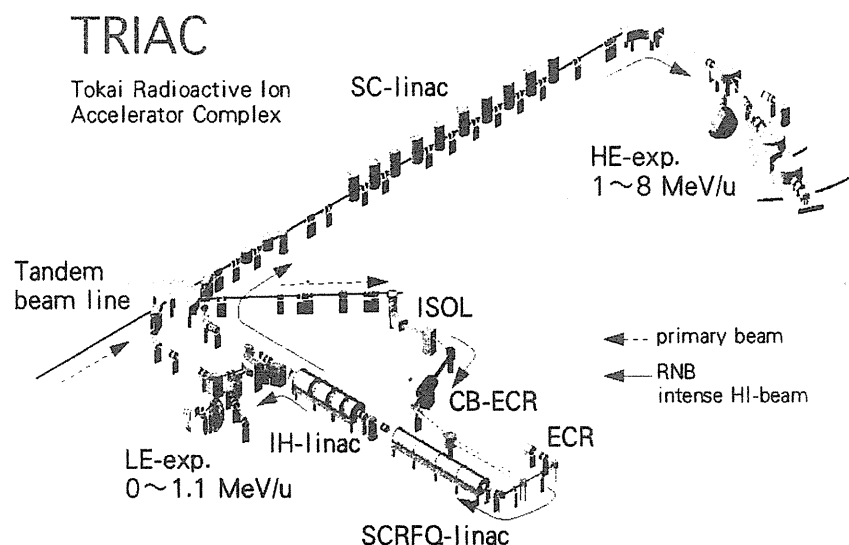
Fig. 1 The layout of the TRIAC. The dotted and solid lines indicate the primary beam and RNB (or HI-beam from ECR), respectively.

A charge-breeding time was also measured with Xe-ions. This quantity is characterized as a delay time and a time constant of a growth curve of the charged-bred q^+-ion beam from the

---

[1] Institute of Particle and Nuclear Studies, KEK
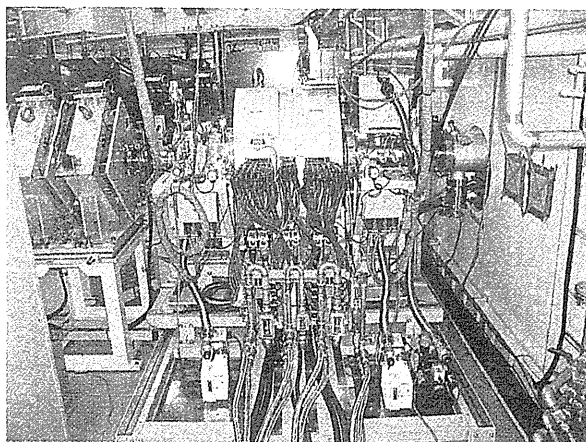
Fig. 2 A photo of CB-ECR .The 18 GHz ECR has been set at the RNB experimental room.
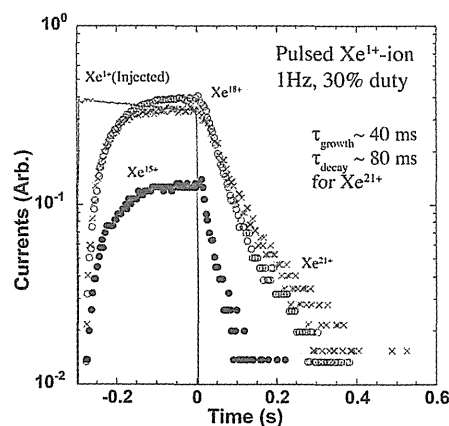
Fig. 3 The time spectrum of extracted Xe-ions from CB-ECR.

beginning of the injection of the pulsed 1^+-ion beam to the CB-ECR. The 1^+ Xe-ions were injected to the CB-ECR for 300 ms with repetition frequency of 1 Hz. Fig. 3 shows the time structures of extracted 15^+-, 18^+-, and 21^+-ions together with the profile of the injected 1^+-beam. From this figure, the charge-breeding time was as short as 60 ms for the process of 1^+ to $21+$.

The SCRFQ-linac and IH-linac were also installed in the RNB experimental room as shown in Fig. 4. The electric power line as well as cooling water system for TRIAC facility is operational and some electromagnetic devices together with those vacuum chambers and power sources were tested. After the installation of the control system and the careful check of each device, such as ISOL, CB-ECR, the low-energy beam line, linac accelerators, and the beam line to the experimental apparatus in the experimental hall, the first beam will be delivered in the end of FY2004.
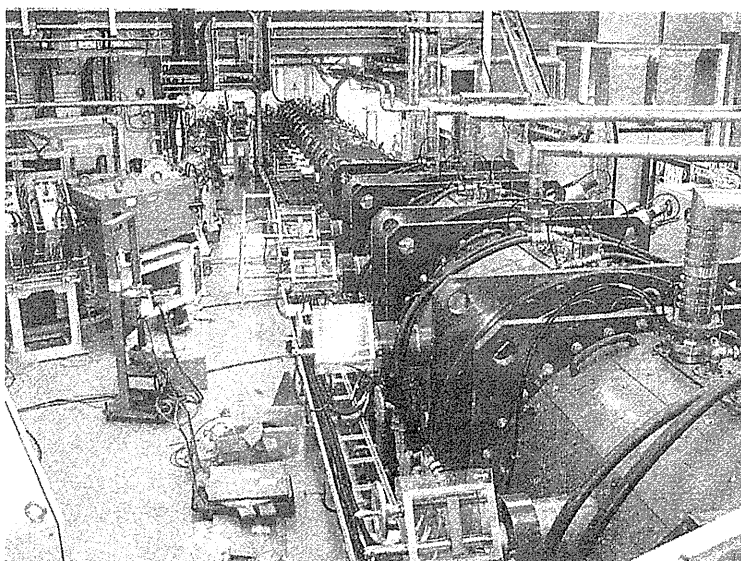
Fig. 4 Photograph of TRIAC. The mass-separated radioactive ions with appropriate charge state after CB-ECR are transported through the low-energy beam line and are accelerated by KEK linacs from back to forward direction in this picture.

References
[1] H. Miyatake et al., Nucl. Instrum. Meths B204(2003)746.

1. 4 ION SOURCE DEVELOPMENT FOR THE JAERI-KEK JOINT RNB PROJECT

T.SATO, A. OSA, M. MATSUDA, K.TSUKADA, M.ASAI, S.C. JEONG[1)],
I. KATAYAMA[1)], and S.ICHIKAWA

Online tests of a uranium carbide target coupled with a surface ionization type ion source at a temperature of 2700K have been performed to produce radioactive nuclear beams (RNBs) of alkali, alkaline earth isotopes produced in proton-induced fission of uranium. Overall efficiencies of neutron-rich Rb, Sr, Cs, and Ba isotopes from two types of graphite matrix used as the uranium carbide targets are obtained. Production yields of Rb, Sr, Cs, and Ba isotopes from the target-ion -source system were evaluated at 36 MeV proton beam with an intensity of 3 μA.

The experiments were carried out with the surface ionization type ion source which is shown in Fig. 1 schematically. The target container and the ionizer are heated by electron bombardment from tungsten filaments, which is at a potential of -300 V relative to the ionizer as well as target container. With this arrangement, the ionizer and the target container can be heated up to 2700 K.
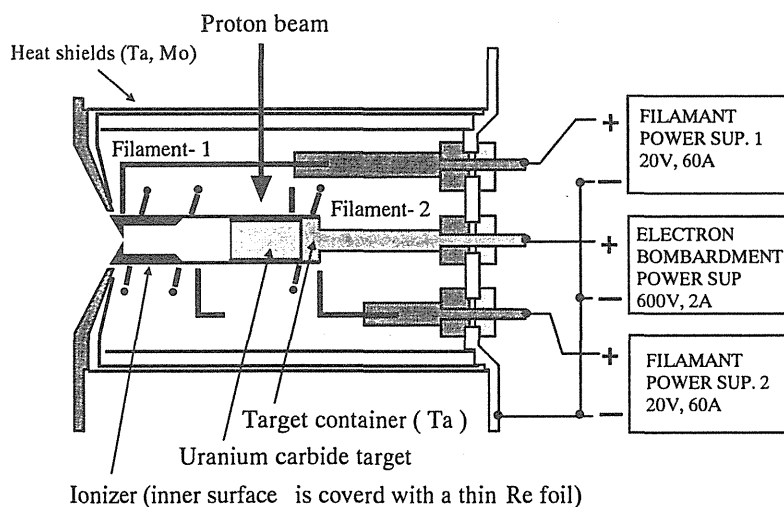
Fig. 1. Schematic drawing of the surface ionization type ion source.

Two kinds of target materials have been tested: a porous carbon (reticulated vitreous carbon, pore size 100 ppi, void volume 97%, ERG materials & Aerospace Co.) and a carbon fiber ((ϕ =11 μm, GC-20, Tokai Carbon Co.). Each uranium carbide target, about 300 mg/cm^2 thickness, was prepared by impregnating a graphite matrix with a solution of uranyl nitrate. The targets were dried in the atmosphere by IR radiation. Then, the targets were outgassed and converted to oxide form at 600 °C in argon atmosphere before insertion into the ion source.

In the measurement of yields of the RNBs, the targets were bombarded with a 30 MeV proton beam (20 MeV on target) with an intensity of about 100 nA. The ionized products were accelerated with 30 kV and mass-separated. The mass-separated products were implanted into an aluminized Mylar tape in a tape transport system and transported periodically to the measuring position where an HP-Ge detector was placed for γ rays measurements.

---

[1] High Energy Accelerator Research Organization

Figure 2 shows measured overall efficiencies of cesium isotopes from the porous carbon matrix (open circle), and from the carbon fiber matrix (closed circle) at the target-ion source temperature of 2500 K. This efficiency is defined as the collection rate at the tape divided by the production rate that is calculated on the basis of the independent cross section in the proton-induced fission of ^{238}U [1].
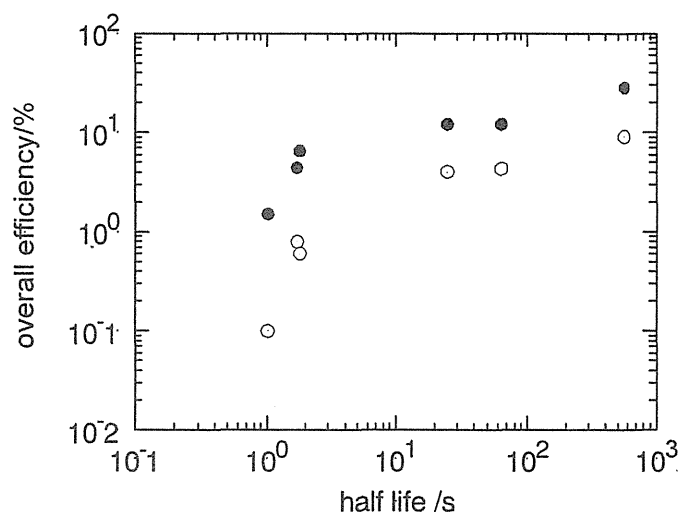
Fig.2. Observed halflife-dependence of the overall efficiency for Cs isotopes. The open and closed circles indicate porous carbon matrix and carbon fiber one, respectively.

As shown in figure 2, the carbon fiber matrix gave higher efficiency than the porous carbon one. However, there was strong dependence of overall efficiencies on the halflives. The overall efficiencies were 28.2% for long-lived ^{139}Cs ($T_{1/2}$=9.29 min) and 1.5% for short-lived ^{144}Cs ($T_{1/2}$=1.01 s). The same tendencies were observed for Rb, Sr, and Ba isotopes. Those were 17.2% for ^{91}Rb ($T_{1/2}$=58.4 s), 4.9% for ^{95}Rb ($T_{1/2}$=0.335 s), 4.2% for ^{93}Sr ($T_{1/2}$=7.423 min), 3.3% for ^{95}Sr ($T_{1/2}$=23.9 s), 5.6% for ^{142}Ba ($T_{1/2}$=10.6 min), 0.4% for ^{144}Ba ($T_{1/2}$=11.5 s), respectively. Although the delay times at the same experimental condition were not measured, we assumed that the difference in overall efficiency between the long-lived and short-lived isotopes was due to the slow diffusion and effusion-speeds of alkali and alkaline earth atom from the graphite matrix.

The evaluated production yields of Rb, Sr, Cs, and Ba isotopes are summarized in table 1. The yields are calculated under the following conditions; thickness of uranium target is 2.6 g/cm^2 ^{nat}U, irradiating proton beam is 36 MeV with the intensity of 3 μA, and taking into account of the overall efficiencies of each isotopes observed in this study. As shown in the table, we can provide RNB of neutron-rich Rb, Sr, Cs. and Ba isotopes with the intensity between around 10^5 and 10^8 atoms per second.

Table 1. Evaluated production yield of Cs, Ba, Rb and Sr isotopes.

Nuclides	Intensity (atoms/s)	Nuclides	Intensity (atoms/s)	Nuclides	Intensity (atoms/s)	Nuclides	Intensity (atoms/s)
^{139}Cs	3.4x10^8	^{139}Ba	6.0x10^7	^{91}Rb	1.6x10^8	^{91}Sr	4.7x10^8
^{140}Cs	1.5x10^8	^{141}Ba	4.6x10^7	^{92}Rb	1.9x10^7	^{92}Sr	1.1x10^9
^{141}Cs	9.6x10^7	^{142}Ba	6.6x10^7	^{93}Rb	7.5x10^7	^{93}Sr	4.9x10^7
^{142}Cs	1.9x10^7	^{143}Ba	2.5x10^6	^{94}Rb	3.0x10^7	^{94}Sr	6.2x10^7
^{143}Cs	8.6x10^6	^{144}Ba	1.8x10^6	^{95}Rb	3.1x10^6	^{95}Sr	4.7x10^7
^{144}Cs	4.6x10^5						

References

[1] H. Kawakami, KEK Report 2001-15 Oct. 2001

1. 5 SNB ION SOURCE
FOR THE RNB ACCELERATOR FACILITY

M. MATSUDA, T. NAKANOYA, S. HANASHIMA, S. C. JEONG[1] and E. TOJYO[1]

JAERI-Tokai and KEK-IPNS have been constructing an ISOL-based radioactive nuclear beam (RNB) facility (TRIAC: Tokai Radioactive Ion Accelerator Complex) in a tandem accelerator laboratory at Tokai [1]. The TRIAC consists of heavy-ion linacs [2, 3] for the RNB acceleration with energy up to 1.1MeV/u. In near future, TRIAC will be connected to the existing JAERI superconducting booster linac [4] in order to increase the beam energy up to 5-7MeV/u.

In the beginning of the RNB operation, a stable nuclear beam (SNB) is needed as a pilot beam to obtain the setting parameters of the linac system. For this purpose, we have installed a permanent magnet type ECR ion source of 10GHz, 200W. Highly charged ion beams of tens-of microampere are available from this source. This ion source also supplies ion beams of noble gas, alkali metal and alkaline earth metal, which are difficult to be generated by the negative ion source for the tandem accelerator. This means the TRIAC allows to use almost all elements of the periodic table as the beams with 10-100 times intensity compared to the present tandem facility.
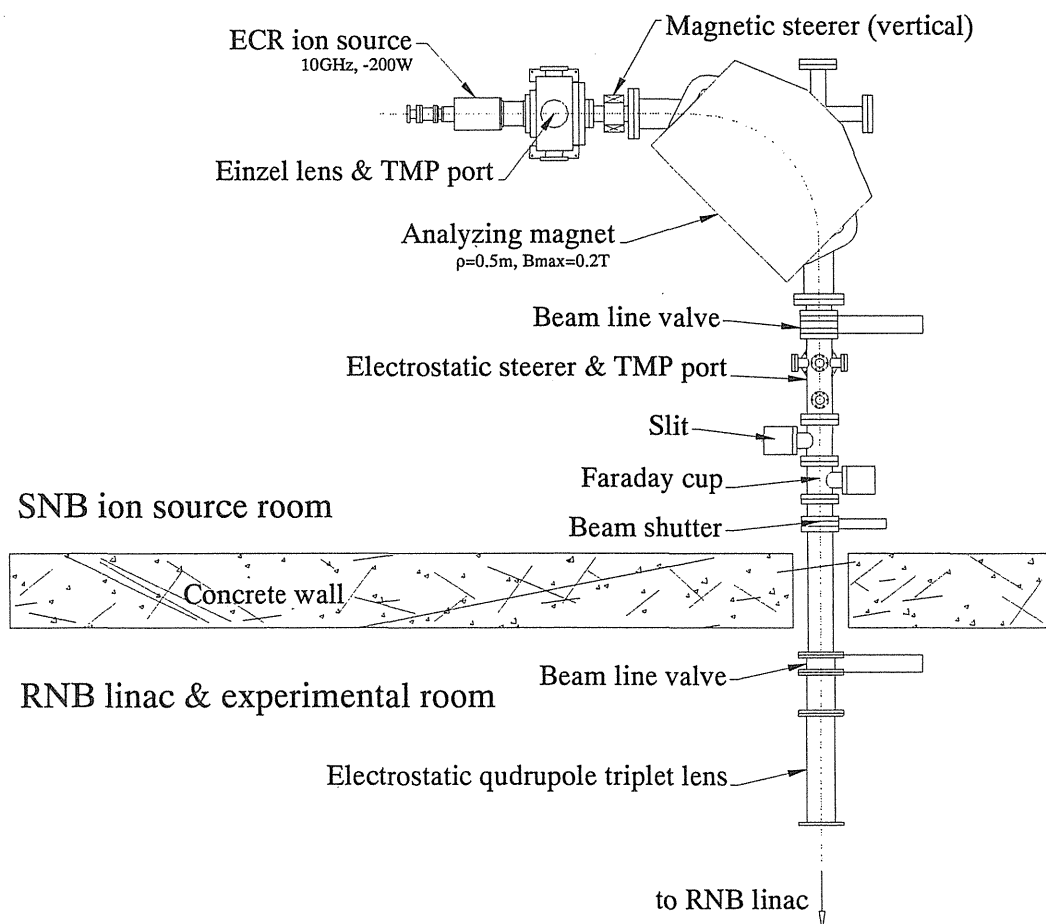
Figure 1. The layout of SNB injector system.

[1] Institute of Particle and Nuclear Studies, KEK

The layout of the SNB injector system is shown in Figure 1. The ion beams are extracted by 20kV potential gap from the ion source and focused by an Einzel lens. The mass and charge of the ion are selected by a $9.0°$ analyzing magnet. The beam direction is tuned by magnetic and electrostatic steerer placed upstream and downstream of the analyzing magnet, respectively. A variable slit is used to set change the beam shape and beam current at a faraday cup. Finally, ion beams are focused by an electrostatic quadrupole triplet lens, and injected into the RNB linac.

The control system of the SNB injector was developed based on the personal computer by the PCI-bus interface. A general control module by the optical digital communications was newly developed to control devices on the high-voltage platform of the injector. This control module has functions of two DAC channels, eight ADC channels, four status control channels and six status read channels. It was designed for the Q lens or steerer to be controlled by one module. The SNB control system is developed as the subsystem of the distributed control system to operate the SNB injector in cooperation with the tandem control system or independently.
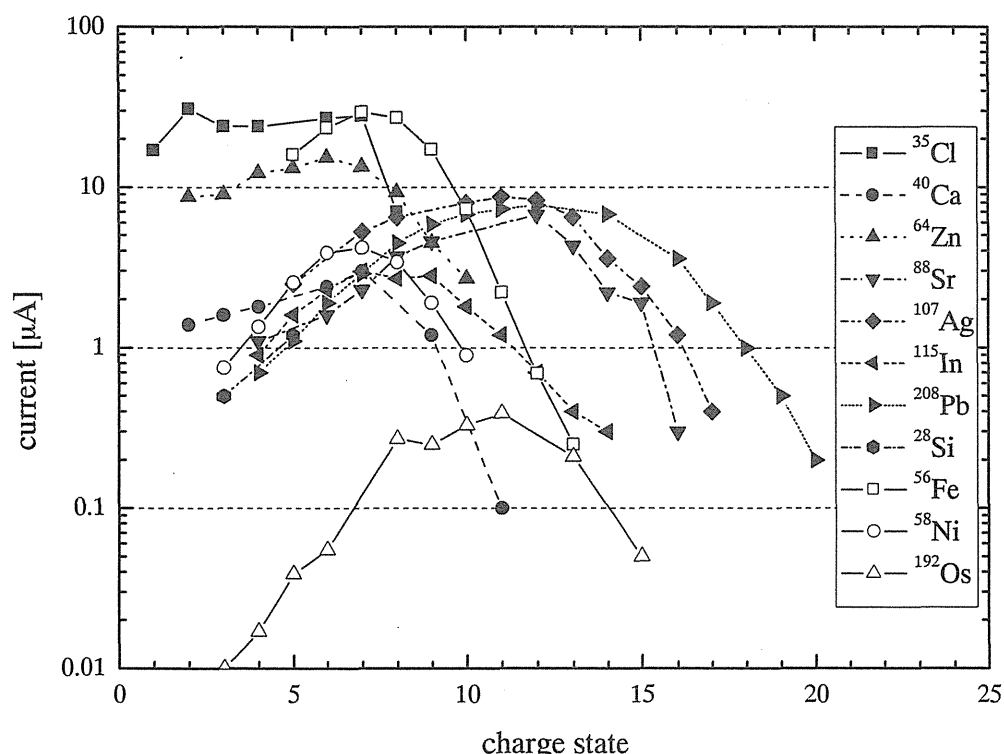
Figure 2. Measured charge distribution and beam current of the metallic ion beam from the ion source.

The beam current of several ions was measured as shown in Figure 2. These metallic ions have been generated by the oven method and the metal ions from volatile compounds (MIVOC) method. The open and close symbols in Figure 2 are for the ions extracted by using the oven method and the MIVOC method, respectively.

References

[1] H.Miyatake et al., Nucl. Instrum. Method B204(2003)746-751.
[2] S. Arai et al., Nucl. Instrum. Method A390(1997)9-24.
[3] M. Tomizawa et al., Proc. Of the Heavy Ion Accelerator Technology: Eighth International Conference, AIP 1-56396-806-1/99, pp451-465.
[4] S. Takeuchi et al., Nucl. Instrum. Method A382(1996)153-160.

1. 6 DEVELOPMENT OF SUPERCONDUCTING TWIN QUARTER WAVE RESONATOR FOR ACCELERATION OF LOW VELOCITY HEAVY IONS

H.KABUMOTO, S.TAKEUCHI, M.MATSUDA, T.NAKANOYA

JAERI and KEK have been constructing a Tokai Radioactive Ion Accelerator Complex (TRIAC) in the tandem accelerator laboratory since 2001. We will start acceleration of stable ion beam (SNB) from ECR Ion source and radioactive nuclear beam (RNB) from ISOL in 2004. SNB and RNB are accelerated by split coaxial RFQ (SCRFQ) and interdigital-H (IH) linac up to the energy of 1.1MeV/u. We were planning to re-accelerate the beams in the near future by superconducting booster up to an energy of 5~8MeV/u, that is, beyond the Coulomb barrier energy for almost all of the beams and species. In order to inject the beams into superconducting booster, we need a pre-booster capable of acceleration from 1.1MeV/u to 2.0MeV/u.

Even for the present acceleration system of the tandem and superconducting booster, a pre-booster was wanted in order to improve beam intensities and energies of very heavy ions. For these reasons, we started to develop a twin quarter wave resonator (twin-QWR).

The present superconducting booster consists of forty acceleration cavities and ten cryostat vessels. The cavities are a coaxial quarter wave resonator (QWR) of which frequency is 130MHz, and optimum beam velocity (β_{opt}) is 10% of the light velocity. We were planning to replace the eight QWRs in the front end two cryostat vessels of the superconducting booster with eight twin-QWRs, and add one cryostat vessel with four of the removed QWRs to the rear end of the superconducting booster. We will be able to get SNB and RNB of 5~8MeV/u by using eight twin-QWRs and thirty-six QWRs.
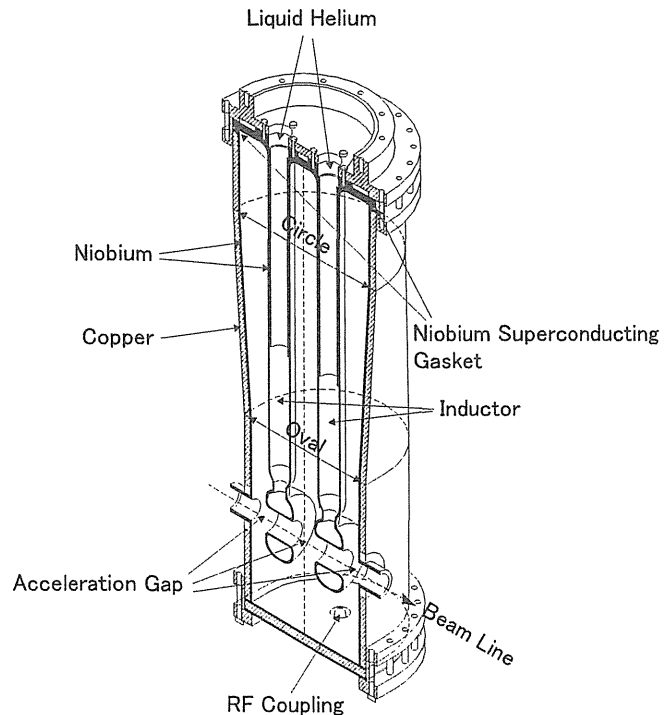
(Size : 0.6m × 0.24m × 0.26m)

Fig. 1 : Outline of twin-QWR

Figure 1 shows an outline of the twin-QWR to develop. The cavity has two inductors and three acceleration gaps. The resonant frequency is designed for 130MHz same as for QWR, and the optimum beam velocity (β_{opt}) is 6% of the light velocity. The outer conductor is made of niobium plate clad in copper, and its upper section becomes widespread and circular. We constructed normal conducting model cavity made of aluminum. We measured distribution of electromagnetic fields in the cavity by perturbation method. The transit time factor is shown in Figure 2. Table 1 shows the main parameters obtained from the model cavity (twin-QWR) and those for the QWR. After carrying out a beam optics calculation, electromagnetic calculation of cavity, and a mechanical examination, we were planning to fabricate a prototype superconducting twin-QWR in FY2004.
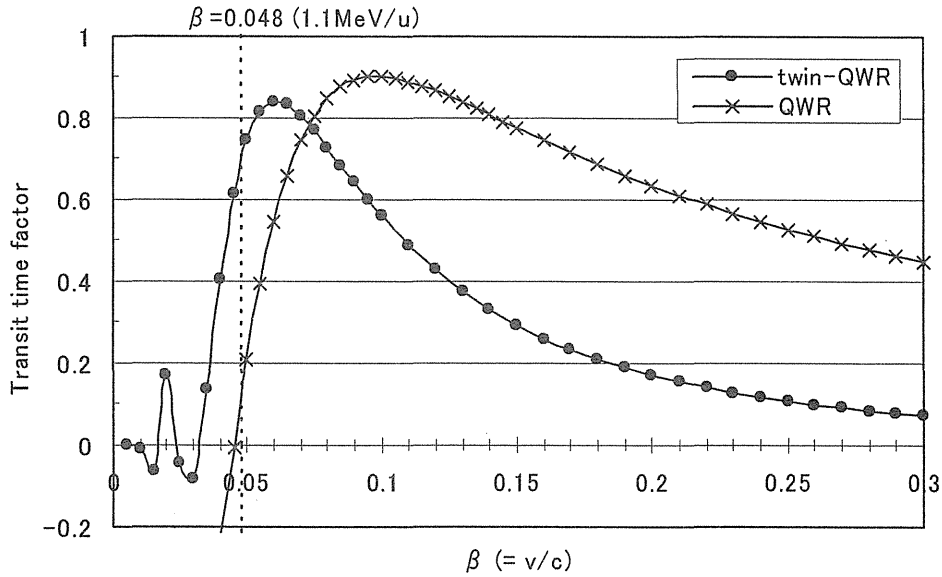
Fig. 2 : Transit time factor

Table 1 : Main parameters of model twin-QWR and QWR

Resonator		model twin-QWR	QWR
Optimum beam velocity	β_{opt}	0.06 × c (light velocity)	0.10 × c (light velocity)
Frequency [MHz]	f_0	129.34	129.80
RF stored energy [Joule/(MV/m)^2]	$U_0/E_{acc}{}^2$	0.039	0.046
Peak surface electric field [MV/m/(MV/m)]	E_p/E_{acc}	3.1	4.6
Peak surface magnetic field [mT/(MV/m)]	H_p/E_{acc}	12.5	7.5
Reference acceleration length [m]	L	0.15	0.15
Acceleration gap length [m]	L_g	0.0175 0.035 0.0175	0.04 0.04
Drift tube length [m]	L_D	0.04 × 2	0.07 × 1
Inductor length [m]	ℓ	0.443	0.453

2. Nuclear Structure

This is a blank page.

2. 1 HIGH-SPIN STATES IN ^{43}Sc

T. MORIKAWA[1], M. NAKAMURA[1], T. SUGIMITSU[1], H. KUSAKARI[2],
M. OSHIMA, Y. TOH, M. KOIZUMI, A. KIMURA, J. GOTO,
Y. HATSUKAWA, J. KATAKURA and M. SUGAWARA[3]

^{43}Sc nucleus has a relatively simple configuration; only one proton and two neutrons are coupled to the doubly magic ^{40}Ca inert core. In this simple 3-particle structure, the terminating $J^{\pi} = 19/2^{-}$ state has been known to show up as a high-spin isomer [1]. Since this high-spin isomer possesses a sizeable oblate deformation of $\beta_2 \sim -0.07$ [2], it is interesting to search for excited states lying at low excitation energy above the isomer, which may originate from the large deformation. In the mean time, a positive parity band-like structure based on the low-lying $K^{\pi} = 3/2^{+}$ state also has been known up to the $J^{\pi} = 15/2^{+}$ level [3]. These positive parity levels can be interpreted as having a predominant $\{sd\}^{-1} \otimes \{fp\}^{4}$ configuration, and show an enhanced $E2$ collectivity of > 10 w.u. [4] It is also interesting to search the higher-spin members of this band up to the terminating $J^{\pi} = 27/2^{+}$ state which is theoretically expected in the $\{sd\}^{-1} \otimes \{fp\}^{4}$ configuration. Other positive parity levels of $J^{\pi} = (19/2^{+}), (23/2^{+})$ and $(25/2)^{+}$ at 5517, 6429 and 7355 keV, respectively, have been reported [5] as being the precursors of the $J^{\pi} = 19/2^{-}$ high-spin isomer. However, the γ-ray transitions from these levels to the lower-lying positive parity levels have not been known.

Motivated by the above mentioned interests, we carried out an experiment to investigate the high-spin states in ^{43}Sc nucleus using the ^{27}Al(^{19}F,$p2n$)^{43}Sc reaction. The ^{19}F beam of 50 MeV was delivered from the JAERI Tandem Accelerator. The target was an 0.92 mg/cm^2 thick metallic foil of ^{27}Al with a 10 mg/cm^2 ^{nat}Pb backing. Prompt- and delayed-γ-γ coincidence events were measured by the γ-ray detector array GEMINI-II [6] consisting of 16 HPGe detectors with BGO anti-Compton shields. The data were off-line sorted into $4k \times 4k$ γ-γ correlation matrices. Standard γ-ray sources of ^{152}Eu, ^{133}Ba and ^{56}Co were used for the detector calibration. Based on γ-γ coincidence relationships, γ-ray energy sums, relative intensities, angular distribution ratio [7] and amount of the Doppler shift, a partial level scheme has been proposed as shown in Fig. 1.

Most of the observed negative parity states in yrast region were quantitatively well reproduced by a shell model calculation by using a realistic two-body interaction FPD6 [8]; the jj-coupled shell model code jjSMQ [9] has been used in the calculation. The observed 1259 keV and 1395 keV transitions were interpreted as being γ-rays deexciting the newly identified $J^{\pi} = (17/2^{-})$ state which is a member of the $\{0f_{7/2}\}^{3}$ multiplet. However, the calculation failed to reproduce the $J^{\pi} = (17/2^{-}, 21/2^{-})$ state at 4633 keV. The largeness of the spin value (17/2 or 21/2) and the lowness of the level energy for this 4633 keV state suggest some contribution of the higher-lying $0g_{9/2}$ orbital caused by a large deformation and/or some collective excitation of the ^{40}Ca core.

---

[1]Department of Physics, Kyushu University
[2]Faculty of Education, Chiba University
[3]Chiba Institute of Technology

The positive parity band-like structure was extended up to the terminating $J^\pi = (27/2^+)$ state at 8829 keV. A relatively enhanced (> 7.6 w.u.) $E2$ transition connecting between the $J^\pi = (19/2^+)$ state and the $J^\pi = 15/2^+$ state was newly identified. A shell model calculation by using the SDI [10, 11] with strength parameters $A_0 = 0.90$ and $A_1 = 0.56$ [12] in the $\{0d_{3/2}0f_{7/2}1p_{3/2}\}$ model space was found to give a good reproduction of the observed levels. An investigation of the calculated wave functions suggests that the levels above the $J^\pi = 17/2^+$ state consist of the dominant seniority $\nu = 5$ configurations, while the lower-spin members are formed by a mixture of $\nu = 3$ ($40 \sim 50\%$) and $\nu = 5$ ($50 \sim 60\%$) components.
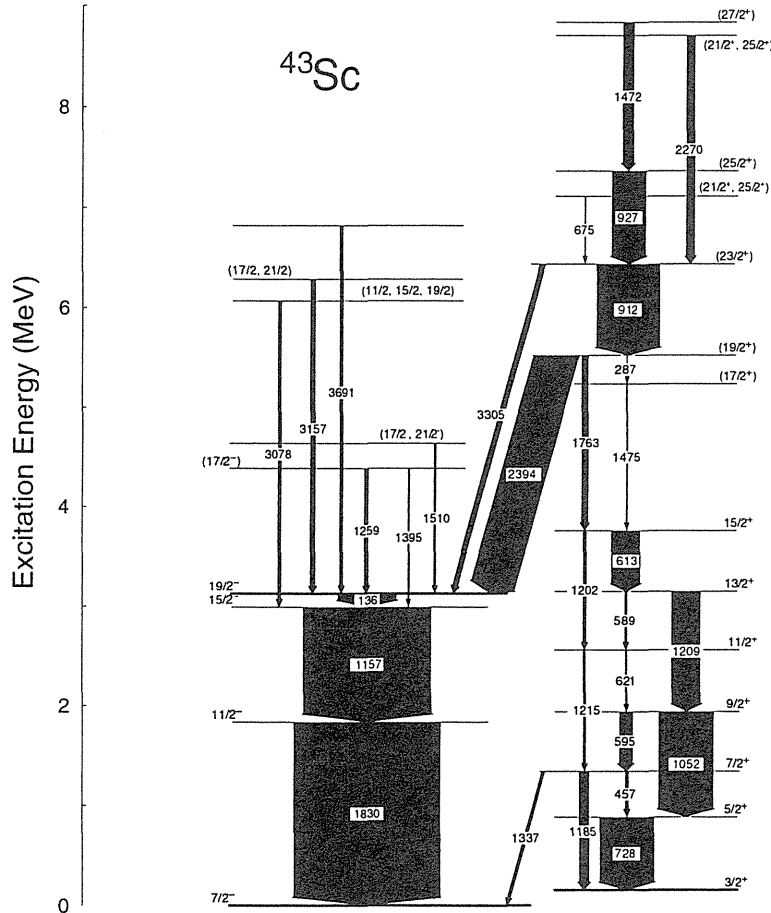
Fig. 1. Partial level scheme of ^{43}Sc proposed in the present work.

References

[1] Z. Sawa et al., Phys. Scr. **2** (1970) 261.

[2] E. Dafni et al., Phys. Rev. C **23** (1981) 1612.

[3] A. R. Poletti et al., Phys. Rev. C **13** (1976) 1180, and references therein.

[4] L. Meyer-Schutzmeister et al., Phys. Rev. C **18** (1987) 1148, and references therein.

[5] H. M. Sheppard et al., J. Phys. G **6** (1980) 511.

[6] K. Furuno et al., Nucl. Instrum. Methods **A421** (1999) 211.

[7] M. Piiparinen et al., Nucl. Phys. **A605** (1996) 191.

[8] W. A. Richter et al., Nucl. Phys. **A523** (1991) 325.

[9] K. Takada et al., ftp://ftp.kutl.kyushu-u.ac.jp/pub/takada/jjSMQ.

[10] R. Arivieu and S. A. Mozkowski, Phys. Rev. **145** (1966) 830.

[11] A. Plastino et al., Phys. Rev. **145** (1966) 837.

[12] C. K. Davis et al., J. Phys. A **6** (1973) 844.

2. 2 GAMMA-RAYS IN ONE-PROTON-HOLE NUCLEUS ^{47}K

T. ISHII, M. ASAI, M. MATSUDA, S. ICHIKAWA, A. MAKISHIMA[1], T. KOHNO[2] and M. OGAWA[2]

We have measured γ-rays emitted by nano-second isomers in ^{47}K produced by deep-inelastic collisions, ^{48}Ca(8.5 MeV/nucleon)+^{198}Pt, using an isomer-scope [1,2]. This is the first γ-ray measurement in $^{47}_{19}$K$_{28}$, one-proton-hole nucleus of the doubly-magic ^{48}Ca. Figure 1 (left) shows a γ-ray spectrum of potassium isotopes selected by Si ΔE-E detectors of the isomer-scope. The $7/2^-$ state at 2020 keV is isomeric with $T_{1/2} = 6.3(4)$ ns and its decay scheme is shown in Fig. 1 (right). The $3/2^+$ state at 360 keV was also found to be isomeric to be $T_{1/2} = 1.1(3)$ ns; this lifetime was derived from the intensity ratio of the stopped and flight peaks of the 360 keV γ-ray.

The lifetime of the first excited state corresponds to $B(M1; 3/2^+ \to 1/2^+) < 9 \times 10^{-4} \mu_N^2$. This transition can be interpreted as an l forbidden $M1$ transition between the $\pi d_{3/2}^{-1}$ and $\pi s_{1/2}^{-1}$ states. This hindrance indicates that a single particle picture is well realized in ^{47}K. Furthermore, this large hindrance may be given as the cancellation of the $[Y^{(2)} \times s]$ component arising from the core polarization and that from the meson exchange [3]. On the other hand, the $B(M2; 7/2^- \to 3/2^+)$ value of 0.62(4) $\mu_N^2 fm^2$ in ^{47}K$_{28}$ is much smaller than that of 6.1(3) $\mu_N^2 fm^2$ in another one-proton-hole nucleus ^{39}K$_{20}$. This small $B(M2)$ value would be attributable to the configuration of the $7/2^-$ state. The $\pi d_{3/2}^{-1}$ single hole energy increases with the neutron number as compared to the $\pi s_{1/2}^{-1}$ single energy; the $3/2^+$ level in ^{47}K becomes higher than the $1/2^+$ level. Since these levels are close in ^{47}K, the $7/2^-$ state may include a large $\pi f_{7/2}(s_{1/2}^{-2})_{0+}$ component as well as $\pi f_{7/2}(d_{3/2}^{-2})_{0+}$; the former does not induce an $M2$ transition to the $\pi d_{3/2}^{-1}$ states.
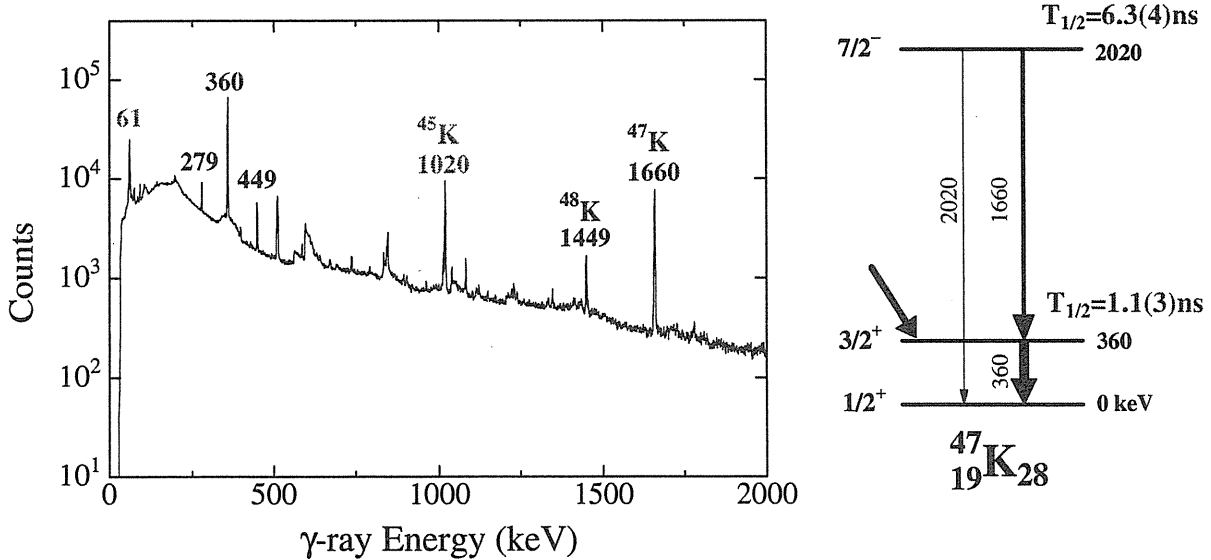
Fig. 1. A γ-ray spectrum of potassium isotopes measured with the isomer-scope (left). A decay scheme of the $7/2^-$ isomer in ^{47}K.

References

[1] T. Ishii et al., Nucl. Instrum. Methods Phys. Res. **A395** (1997) 210.
[2] T. Ishii et al., Phys. Rev. Lett. **84** (2000) 39.
[3] A. Arima and L.J. Huang-Lin, Phys. Lett. **41B** (1972) 429.

[1]Department of Liberal Arts and Sciences, National Defense Medical College
[2]Tokyo Institute of Technology

2.3 COULOMB EXCITATION EXPERIMENT OF ^{68}Zn

M. KOIZUMI, A. SEKI[1], Y. TOH, A. OSA, Y. UTSUNO, A. KIMURA, M. OSHIMA, T. HAYAKAWA, Y. HATSUKAWA, J. KATAKURA, M. MATSUDA, T. SHIZUMA, T. CZOSNYKA[2], M. SUGAWARA[3], T. MORIKAWA[4] and H. KUSAKARI[5]

Zn nuclei have two extra protons outside the $Z=28$ closed shell. The structure of stable even-even Zn nuclei is generally interpreted as the collective vibration, showing a typical pattern characterized by a 2_1^+ state and a triplet of 0_2^+, 2_2^+ and 4_1^+ states at about twice the energy of the 2_1^+ state. On the other hand, enhancements of the $E2$ transition probabilities in the ground state band and in the 2_2^+ band are found in ^{62,64,66}Zn isotopes, while inter-band transitions are weak. These enhancements can be interpreted as the quasi-rotational bands [1,2]. It is, therefore, interesting to experimentally confirm the $B(E2)$ values and quadrupole moments of Zn isotopes for understanding the low-lying structures. In this study, we carried out a projectile multiple Coulomb excitation experiment of ^{68}Zn to measure $E2$ transition matrix elements and the quadrupole moment of the 2_1^+ state.

The Coulomb excitation is a useful technique for measurements of $B(E2)$'s and quadrupole moments of low-lying levels. Because its excitation process is purely electromagnetic, those quantities can be derived model independently [3,4]. The multiple Coulomb excitation with heavy ion beams enables us to study nuclear structure up to about 2 MeV. Recently, a 4π γ-ray detector array coupled with position-sensitive particle detectors covering a wide range of scattering angle has been proven to be useful to get necessary information of particle-γ correlations [5-10].

A multiple Coulomb excitation experiment of ^{68}Zn was carried out using a γ-ray detector array, GEMINI [11] and a position-sensitive particle detector system, LUNA [12]. The projectile nuclei were Coulomb excited on a 1.8-mg/cm^2-thick self-supporting ^{nat}Pb target. The energy of ^{68}Zn beam was 4.06 MeV/u (276 MeV) which does not exceed the Coulomb barrier against the target nucleus. De-excitation γ-rays and scattered projectiles were detected by GEMINI and LUNA, respectively. Particle-γ coincidence events were recorded. The experimental data were analyzed with the least-squares search code GOSIA [13, 14]. Details of the analysis and the results are given in Ref. [15]. The resultant quadrupole moment of the 2_1^+ sate of ^{68}Zn is +0.09±0.03 eb, showing a small quadrupole moment.

In order to investigate the deformation, the potential energy surface (PES) was calculated with the Nilsson-Strutinsky model [16], in which a harmonic oscillator was used for the single-particle energy calculation. The result of the calculation is given in Fig. 1. As seen in Fig. 1, shallow two minima were found; the first minimum is located at $\beta_2 \sim 0.1$ and $\gamma = 60°$, and the second minimum is located at $\beta_2 \sim 0.2$ and $\gamma \sim 40°$. The energy difference between the two minima is less than 500 keV, which is lower than the excitation energy of the 2_1^+ state. The

---

[1] Ibaraki University
[2] Warsaw University
[3] Chiba Institute of Technology
[4] Kyushu University
[5] Chiba University

shallowness of the potential minimum can be interpreted as an unstable nuclear shape, which is consistent with the small quadrupole moment of the 2_1^+ state.

We also examined how the Nilsson orbits influence the PES. At the neutron number of $N=38$, low-spin orbits of $2p_{3/2}$, $1f_{5/2}$ and $2p_{1/2}$ mainly contribute to the nuclear structure. A shell model (SM) calculation with the ^{56}Ni inert core and particles occupying those orbits reproduced the character of the low-lying states of ^{68}Zn quite well, except for the 0_2^+ and 2_3^+ states [15,17]. The first minimum of the PES contains those orbits. At the deformation of the second minimum ($\beta_2 \sim 0.18$), the single-particle energy of a high-spin orbit of $1g_{9/2}$ comes down below the Fermi surface. Therefore, the second minimum is strongly influenced by the $1g_{9/2}$ orbit, while the first minimum is not. Since the SM calculation within the $2p_{3/2}$, $1f_{5/2}$, and $2p_{1/2}$ space suggests that the 0_2^+ and 2_3^+ states have an intruder character which may be strongly influenced by the $1g_{9/2}$ orbit [17], those states whould be constructed on the second minimum of the PES.
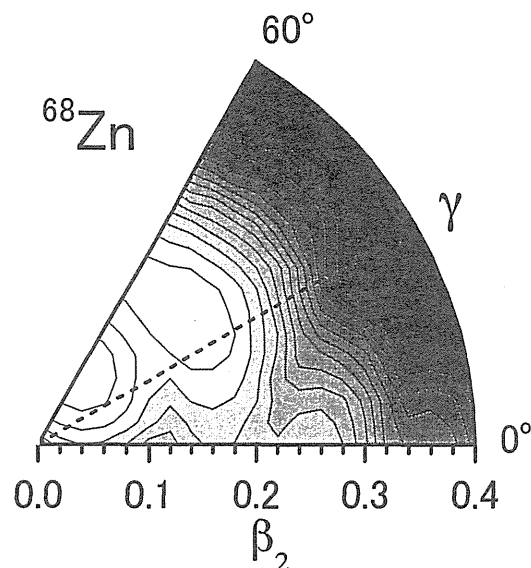
Fig. 1. Potential energy surface of ^{68}Zn calculated with the Nilsson-Strutinsky model [16]. Energy difference between two contour lines is 250 keV. The dashed line indicates $\gamma = 30°$.

References

[1] D.N. Simister et al., J. Phys. G 4 (1978) 1127.
[2] B. Crowell et al., Phys. Rev. C 50 (1994) 1321.
[3] K. Alder and A. Winther, Coulomb Excitation (Academic, NewYork, 1966).
[4] K. Alder and A. Winther, Electromagnetic Excitation (North Holland, Amsterdam, 1975).
[5] Y. Toh et al., J. Phys. G 27 (2001) 1475.
[6] Y. Toh et al., Eur. Phys. J. A 9 (2000) 353.
[7] A. Osa, T. Czosnyka, et al., Phys. Lett. B 546 (2002) 48.
[8] M. Zielinska, T. Czosnyka, et al., Nucl. Phys. A 712 (2002) 3.
[9] M. Koizumi, A. Seki, Y. Toh, et al., Eur. Phys. J. A 18 (2003) 87.
[10] M.Sugawara et al., Eur. Phys. J. A 16 (2003) 409.
[11] K. Furuno et al., Nucl. Instrum. Methods Phys. Res. A 421 (1999) 211.
[12] Y. Toh et al., Rev. Sci. Instrum. 73 (2002) 47.
[13] T. Czosnyka, D. Cline, L. Hasselgren, and C.Y. Wu, Nucl. Phys. A 458 (1986) 123.
[14] T. Czosnyka, C.Y. Wu, and D. Cline, Bull. Am. Phys. Soc. 28 (1983) 745.
[15] M. Koizumi, A. Seki, Y. Toh, A. Osa, et al., Nucl. Phys. A 736 (2003) 46.
[16] T. Bengtsson et al., Computational Nuclear Physics vol. 1, ed. K. Langanke et al.
    (Springer-Verlag, Berlin, 1991) p. 51.
[17] J.F.A. Van Hienen, W. Chung and B. H. Wildenthal, Nucl. Phys. A 269 (1976) 159.

2. 4 IN-BEAM γ-RAY STUDY OF ^{70}Ge

M. SUGAWARA[1], Y. TOH, M. OSHIMA, M. KOIZUMI, A. KIMURA,
A. OSA, J. GOTO, Y. HATSUKAWA and H. KUSAKARI[2]

It has been well known for many years that even Ge isotopes have a low-lying second 0^+ state of different shape from that of the ground state. Our systematic studies in recent years through multiple Coulomb excitation have revealed that the 0_2^+ state of ^{70}Ge is interpreted as a deformed intruder state differently from the fact that those of heavier Ge isotopes are considered to be spherical intruders[1-3]. Therefore it is desirable to identify members of the rotational band based on the 0_2^+ state in ^{70}Ge which should exist if it is really a deformed intruder state.

In-beam γ-ray spectroscopy was made on ^{70}Ge through the reaction of ^{60}Ni(^{12}C, 2p). A ^{12}C beam of 45 MeV was bombarded on a enriched ^{60}Ni foil of 10 mg/cm^2 thickness. Emitted γ-rays were detected with an array of 16 HPGe detectors with BGO Compton suppressors and 3 LOAX detectors without BGO shields (GEMINI-II). Total events of 6.0×10^8 were collected for 3 days of beam time.

Prior to this work, there had been an in-beam γ-ray study on ^{70}Ge through the reaction of ^{46}Ti(^{28}Si, 4p) [4], where no members of the rotational band based on the 0_2^+ state were reported although the negative-parity yrast states were tentatively assigned up to (21$^-$) state. Although the data analysis is still in progress, the present results from our data are summarized as follows. Rotational members of the band based on the 0_2^+ state may be seen up to (8$^+$) state, above which only the γ-rays within the negative-parity yrast band are observed. However the ordering of γ-rays are different from the results of the previous experiment[4].

References
[1] Y. Toh, T. Czosnyka, M. Oshima, T. Hayakawa, H. Kusakari, M. Sugawara, Y. Hatsukawa, J. Katakura, N. Shinohara, M. Matsuda, Eur. Phys. J. A9(2000)353.
[2] Y. Toh, T. Czosnyka, M. Oshima, T. Hayakawa, H. Kusakari, M. Sugawara, Y. Hatsukawa, J. Katakura, N. Shinohara, M. Matsuda, J. Phys. G27(2001)1475.
[3] M. Sugawara, Y. Toh, T. Czosnyka, M. Oshima, T. Hayakawa, H. Kusakari, Y. Hatsukawa, J. Katakura, N. Shinohara, M. Matsuda, T. Morikawa, A. Seki and F. Sakata, Eur. Phys. J. A16(2003)409.
[4] B. Mukherjee, S. Muralithar, G. Mukherjee, R. P. Singh, R. Kumar, J. J. Das, P. Sugathan, N. Madhavan, P. V. M. Rao, A. K.Sinha, A. K. Pande, L. Chaturvedi, S. C. Pancholi, R. K. Bhowmik, Acta. Phys. Hung. N.S. 11(2000)189, Erratum Acta Phys. Hung. N.S. 13(2001)253.

[1]Chiba Institute of Technology
[2]Chiba University

2. 5 METASTABLE STATE POPULATION DISTRIBUTION OF NEODYMIUM ATOMS IN A LASER ABLATION PLUME

H. WANG[1], H. OHBA, M. SAEKI, M. MIYABE, H. MIYATAKE[1], and H. IIMURA

Laser ablation has attracted much attention as a promising technique for application to novel element-selective ion source systems. Such laser ion source is strongly desired for studying the properties of radioactive isotopes produced in nuclear reactions. On the other hand, ablation-initiated atomic beam provides a unique source for high-resolution laser spectroscopy of refractory elements which are not accessible via normal resistance heating method. For these purposes, it is indispensable to know the characteristics of ablated species. In particular, the knowledge of metastable state population distribution is important to excite the atoms effectively from highly populated metastable state.

Neodymium has been used as a first sample in this work because it has a number of low-lying metastable levels near the ground state, which makes the transitions easily accessible without complicated non-linear optics. A pulsed beam from a Q-switched Nd:YAG laser was focused onto a rotating neodymium metallic target. The plume generated from the target by laser ablation was irradiated perpendicularly by a XeCl-pumped dye laser beam with a proper time delay. The laser-induced fluorescence of Nd atoms was collected to an optical fiber through a lens system and transferred to a photomultiplier tube. Flux of the atoms was calibrated by monitoring ions with a Langmuir probe. The measurements were performed under vacuum condition.

The neodymium atom has four low-lying metastable levels close to the ground level: 1128 cm^{-1} (J=5), 2367 cm^{-1} (J=6), 3682 cm^{-1} (J=7), and 5049 cm^{-1} (J=8). By exciting the atoms in a plume from two different lower levels to a common upper level, and measuring the induced fluorescence intensities, one can determine the population ratio of the lower levels. Here, it is crucial to saturate the transitions with a high enough laser fluence so that the oscillator strength does not play a role and hence relative photon intensities directly reflect the population of the involved metastable states. Figure 1 shows the measured relative population distributions of the states as a function of their energy. The uncertainty arises mainly from the fluctuation of the atomic beam intensity.
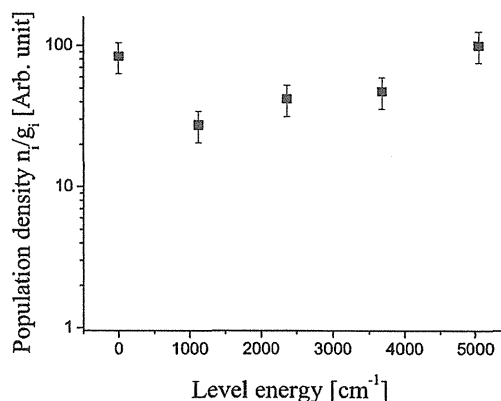
Fig. 1. Dependence of reduced population ratio of metastable states on level energy in Nd atoms produced by laser ablation under vacuum condition.

In the case of electron beam heating experiment, the atomic excitation temperature of about 1400–1600 K can be obtained from the slope of the Boltzmann plot [1]. However, laser ablated Nd atoms show a completely different character. The three upmost metastable states are more heavily populated than is predicted by a Boltzmann-type distribution. The reason for this is not yet known, but it is partly due to the fact that there exist much less electrons in laser ablation as compared to the case in electron beam heating. Indeed, relaxation of low-lying metastable states is frequently caused by atom-electron collision in the latter case. The acquired data provide useful parameters for the design of a resonance photo-ionization laser ion source and for the laser spectroscopy. The excitation scheme can be optimized to start from a densely populated metastable state in the laser ablation plume.

Reference
[1] H. Chen et al., J. Appl. Phys. 49, 6136 (1978).

[1]Institute of Particle and Nuclear Studies, KEK

2. 6 STUDIES ON HIGH-K ISOMERS IN HF-W-OS REGION BY DEEP INELASTIC COLLISIONS

T. SHIZUMA, T. HAYAKAWA, S. MITARAI[1],
T. MORIKAWA[1], T. ISHII and H. UTSUNOMIYA[2]

Nuclei with $A \approx 180$ lie at the region where many high-Ω orbitals are close to both the proton and neutron Fermi surfaces [1]. High-$K (= \sum \Omega)$ multi-quasiparticle states formed by stretched coupling of these high-Ω quasiparticles therefore can compete with collectively excited states near a yrast line. Transitions depopulating such states often require large K changes, low transition energies, parity change, or combination of these, making the initial state to be an isomer with a comparatively long half-life.

However, high-spin studies of the heavier Hf-W-Os nuclei have been limited due to inaccessibility by a fusion-evaporation reaction in combination of stable projectile and target material. In order to populate excited states of these nuclei, we employed a reaction of deep inelastic collisions (DIC). The experiment was carried out by use of the JAERI tandem and booster accelerator. A self-supporting target stacked by two ^{186}W (enriched to 98.2 %) metallic foils with a thickness of 450 μg/cm^2 each was bombarded by a 630 MeV ^{82}Se beam. Projectile fragments were detected by a silicon detector, while delayed γ rays emitted by target fragments were measured with four HP Ge detectors using the so-called recoil shadow method. Events were recorded on magnetic tapes when the silicon detector and one or more Ge detectors were fired in coincidence.

Figure 1 shows a γ-ray spectrum gated on DIC events of the silicon detector. In this spectrum, known γ-ray peaks from the $E_x = 2124$ keV isomer in ^{185}Re [2] and the $E_x = 1682$ keV isomer in ^{187}Re [3] with half-lives of a range of 100 ns can be seen. Further analysis of delayed γ-ray transitions is in progress.
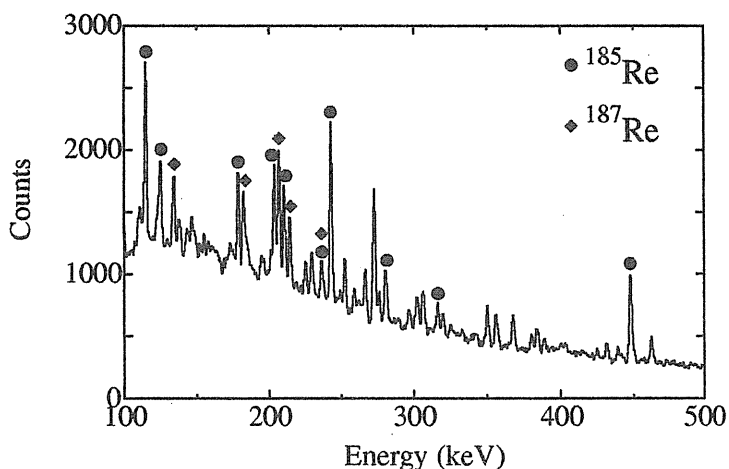
Fig.1 A projected γ-ray spectrum

References

[1] P.M. Walker and G.D. Dracoulis, Nature (London) **399**, 35 (1999).

[2] T. Shizuma et al., Zeit. Phys. **A359**, 229 (1997).

[3] T. Shizuma et al., Euro. Phys. J. **A17**, 159 (2003).

[1]Kyushu University
[2]Konan University

2. 7 ROTATIONAL BANDS BUILT ON THE 1/2[660]($i_{13/2}$) CONFIGURATION IN ^{179}Au

L. T. SONG,[1] X. H. ZHOU,[1] Y. H. ZHANG,[1] Y. X. GUO,[1] Z. Y. SUN,[1] M. OSHIMA, T. TOH, A. OSA, M. KOIZUMI, J. KATAKURA, Y. HATSUKAWA, and M. SUGAWARA[2]

Gold nuclei with Z=79 have provided rich information on the shape coexistence and shape transition along the yrast line. For the heavier odd-A Au nuclei with A>187, the low-energy level structure shows typical character of single-particle excitations [1-3]. The level structures in ^{181,183,185,187}Au consist mainly of prolate rotational bands, and the intruder 1/2[541]($h_{9/2}$) and 1/2[660]($i_{13/2}$) bands dominate the yrast line [4-6]. Recently, excited states in the proton-unbound ^{173,175,177}Au nuclei were identified [5]. While the yrast lines of ^{175}Au and ^{177}Au undergo a shape transition from oblate or spherical to prolate at low spin and are dominated at high spin by a prolate band built upon the intruder 1/2[660]($i_{13/2}$) proton orbital, no sign of collectivity was observed in ^{173}Au isotope [5]. The purpose of the present work is to search for the decoupled bands based on the 1/2[541]($h_{9/2}$) and 1/2[660]($i_{13/2}$) intruder orbitals in ^{179}Au, and complete the evolution of bandhead energies and deformations of these intruder bands while changing neutron number in odd-A Au isotopes.

The excited states in ^{179}Au were populated via the ^{149}Sm (^{35}Cl, 5n) ^{179}Au reaction. The ^{35}Cl beam was provided by the tandem accelerator at the Japan Atomic Energy Research Institute (JAERI). The target is an isotopically enriched ^{149}Sm metallic foil of 1.5 mg/cm^2 thickness with a 5.0 mg/cm^2 Pb backing. A γ-ray detector array, GEMINI-II, comprising 16 HPGe's with BGO anti-Compton shields and 3 LOAX detectors was used. The beam energy of 180 MeV was chosen to populate the high-spin states in ^{179}Au. γ-γ-t and X-γ-t coincidence measurements were performed. The level scheme of ^{179}Au, including eight γ rays, is proposed and shown in Fig. 1. The ordering of transitions in the band is determined according to the γ -
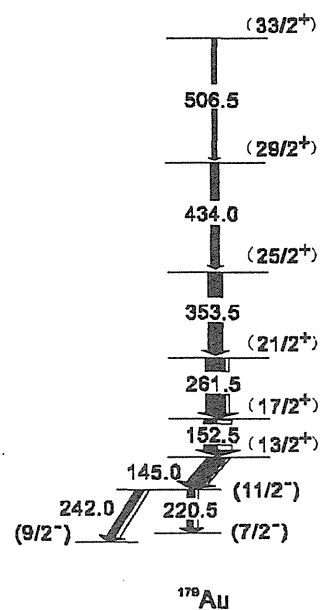
Fig. 1. Level scheme for ^{179}Au

---

[1]Institute of Modern Physics, P. R. China

[2]Chiba Institute of Technology

ray relative intensities. The relative transition intensities were extracted from gated spectra. Figure 2 compares partial level schemes of ^{179,181,183,185}Au, strongly suggesting that the band of ^{179}Au fits well into the systematics of the $1/2[660](i_{13/2})$ intruder bands observed in the heavier odd-A Au isotopes. Based on the similarity as shown in Fig. 2, spins and parities are proposed tentatively to the levels in ^{179}Au. The transition multipolarities derived from DCO ratios are consistent with the results deduced from the intensity balances.
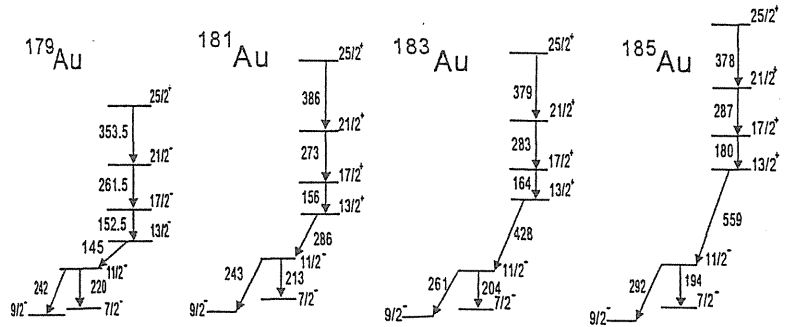
Fig. 2. Partial level schemes of ^{179,181,183,185}Au.

Comparing the level spaces of the $1/2[660]$ bands in the odd-A Au nuclei, one can see that the level space at ^{179}Au is smaller than the other isotopes, indicating the largest deformation in ^{179}Au among the four nuclei shown in Fig. 2. In Ref. 5, a variable moment of inertia fit was carried out for the $1/2[660]$ bands in the odd-A Au nuclei, and empirical values of the deformation were subsequently deduced. The extracted deformations were maximized at neutron numbers of 98 and 100. This result is contradictory to the total Routhian surface (TRS) prediction, which placed the maximum in deformation near mid-shell [5]. Such a difference may be due in part to the existence of a deformed sub-shell gap at N=98 as suggested in the Nilsson diagram. This sub-shell gap might enhance the occupation probabilities of the low-Ω $i_{13/2}$ neutron orbitals and the low-Ω $h_{9/2}$ proton orbitals at N~ 98, which is responsible for the magnitude of the deformation of the intruder bands.

References

[1] E. F. Zganjar et al., Phys. Lett. B58, 159 (1975).

[2] Ts. Venkova et al., Z. phys . A344, 232 (1992).

[3] N. Perrin et al., Z. Phys. A347, 81 (1993).

[4] A. J. Larabee et al., Phys. Lett. 169B, 21 (1986).

[5] F. G. Kondev, et al., Phys. Lett. B 512, 268 (2001).

[6] J. K. Johansson et al., Phys. Rev. C40, 132 (1989).

[7] U. J. Schrewe, et al., Phys. Lett. 91B, 46 (1980).

2.8 GAMMA TRANSITIONS IN THE α DECAY OF ^{257}No

M. ASAI, M. SAKAMA[1], K. TSUKADA, T. ISHII, Y. NAGAME, I. NISHINAKA,
K. AKIYAMA, S. ICHIKAWA, K. SUEKI[2], Y. OURA[3] and M. SHIBATA[4]

The stability of superheavy nuclei is one of the most interesting subjects in nuclear physics. This stabilization is caused by nuclear shell effects. Many theoretical studies have predicted shell structure of superheavy nuclei, while the experimental information is very scarce. In particular, little is known about level energies, spin-parities and single-particle configurations of ground states as well as excited states, and γ transitions between them. The aim of this study is to establish Nilsson single-particle states in odd-mass $Z > 100$ and $N > 152$ nuclei through experimental spin-parity assignments by means of α-γ and α-e (internal conversion electron) coincidence spectroscopy. In this report, we present the α-γ coincidence result for the α decay of ^{257}No.

The nucleus ^{257}No was produced by the ^{248}Cm(^{13}C, $4n$) reaction. Reaction products recoiling out of the target were transported to a rotating wheel α-γ detection system by a He/KCl aerosol jet, and deposited on a 120 μg/cm^2 thick polyethylene terephthalate foil, forty of which were set on the periphery of the rotating wheel. The wheel periodically rotated 63° at 60 s intervals, and moved the deposited sources to two consecutive detector stations each of which was equipped with two Si PIN photodiodes and two Ge detectors. Gamma-ray singles, α singles and α-γ coincidence measurements were performed.

Figure 1 shows a γ-ray spectrum in coincidence with α particles of ^{257}No. Three γ transitions of 77.0, 101.8 and 124.1 keV and Fm L X rays were clearly observed. These γ rays were coincident with 8222 keV α transitions. In addition, we also performed an α-e coincidence measurement and assigned an $M1$ multipolarity to the 77.0 and 124.1 keV transitions through deduced internal conversion coefficients, whose details are described in Ref. [1].
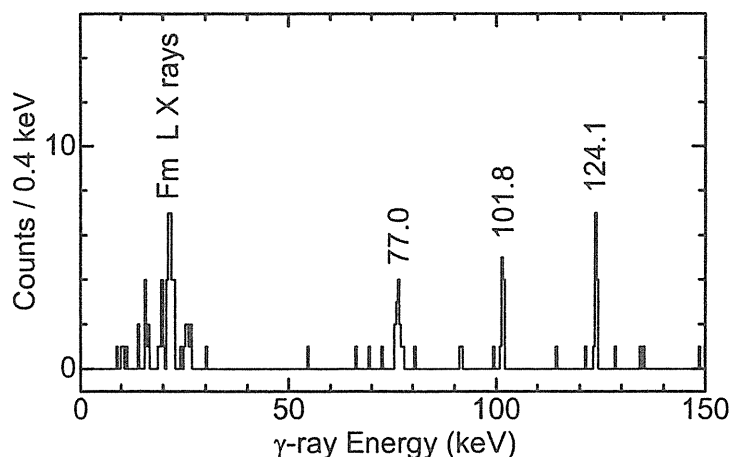
Fig. 1. Gamma-ray spectrum in coincidence with α particles of ^{257}No.

[1]Department of Radiologic Science and Engineering, The University of Tokushima
[2]Radioisotope Center, University of Tsukuba
[3]Department of Chemistry, Tokyo Metropolitan University
[4]Radioisotope Research Center, Nagoya University

Figure 2 shows a proposed decay scheme of ^{257}No compared with a previously evaluated one [2,3]. It has been revealed that the 8323 keV α transition populates the excited state of ^{253}Fm, not the ground state, and the 8270 keV α transition does not exist in the decay scheme; this α peak arises from the coincidence summing effect between the 8222 keV α particle and following 50 keV electron.

The spin-parity of the ground state of ^{253}Fm is known to be $1/2^+$ with the $\nu 1/2^+[620]$ configuration. Since the 124.1 keV transition has an $M1$ multipolarity, the spin-parity of the 124.1 keV level is either $1/2^+$ or $3/2^+$. On the other hand, the 124.1 keV level is populated by the favored α transition with a hindrance factor of 1.3, indicating that this level is a Nilsson single-particle state whose configuration is same as that of the ground state of ^{257}No. Among the Nilsson single-particle states with a spin $1/2^+$ or $3/2^+$, only the $3/2^+[622]$ state could lie at such low energy in ^{253}Fm. Therefore, we have assigned the $3/2^+[622]$ configuration to the 124.1 keV level as well as the ground state of ^{257}No. It was found that the ground state configuration of ^{257}No is different from that of lighter $N = 155$ isotones ^{255}Fm and ^{253}Cf whose configuration is the $7/2^+[613]$.
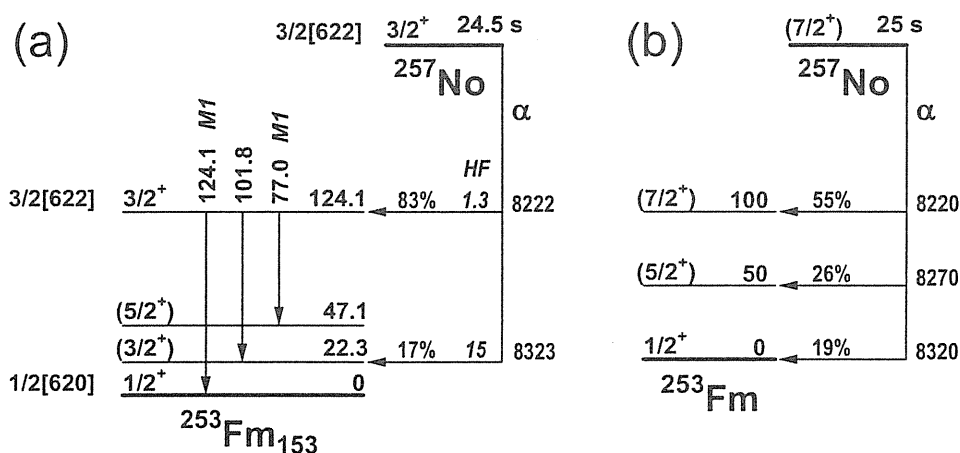
Fig. 2. (a) Decay scheme of ^{257}No established on the basis of the present result. (b) Previously evaluated one in Ref. [2,3].

References

[1] M. Asai, K. Tsukada, S. Ichikawa, Y. Nagame, T. Ishii, I. Nishinaka, K. Akiyama, A. Osa, M. Sakama, Y. Oura, K. Sueki and M. Shibata, *Extended Abstracts of the 2nd Int. Conf. on the Chemistry and Physics of the Transactinide Elements, Napa, November 16–20, 2003*, LBNL-53896 Abs. (2003) 20.

[2] *Table of Isotopes*, 8th ed., edited by R. B. Firestone and V. S. Shirley (John Wiley & Sons, New York, 1996).

[3] P. Eskola, K. Eskola, M. Nurmia and A. Ghiorso, Phys. Rev. C 2 (1970) 1058.

2. 9 PERFORMANCES OF AN HPGe TOTAL ABSORPTION DETECTOR FOR Q_β MEASUREMENTS

H. HAYASHI[1], I. MIYAZAKI[1], M. SHIBATA[2], K. KAWADE[1], M. ASAI, S. ICHIKAWA,
I. NISHINAKA, Y. NAGAME, A. OSA, K.TSUKADA, Y. KOJIMA[3] and A.TANIGUCHI[4]

Atomic masses are fundamental physical quantities in nuclear physics. The concern with atomic masses of nuclides far from the β stability has been growing, because they are strongly related to the stability of nuclei, nuclear models and nucleosynthesis. One of the precise ways for atomic mass determination is to measure beta-decay energies (Q_β-values). The total absorption method is powerful way to measure Q_β of low-yield unstable nuclei like new isotopes. A total absorption detector, which was composed of twin large volume BGO scintillators, was developed by Shibata *et al.* and measured Q_β within accuracy of 100 keV [1-3]. To realize Q_β measurements within accuracy of about 10 keV, we have developed a new HPGe total absorption detector [4]. First, we described analysis of γ-ray responses using Monte Carlo simulation code (EGS4). Second, we tested the detector performances experimentally by measuring nine β sources, whose Q_β are well evaluated.

Figure 1 shows our HPGe total absorption detector, which is composed of a true coaxial HPGe detector and an annular BGO detector. The HPGe detector has a through hole in the center, and radioactive sources can be put in the hole ($\Omega\approx4\pi$). The HPGe detector can absorb nearly all of β-ray energies, however sufficient efficiency of γ-rays is not provided. To detect Compton scattered γ-rays, the BGO detector was used. From geometrical restrictions of the HPGe detector, the HPGe detector could not be covered with BGO detector completely. In γ-ray spectra, only full energy peaks were obtained by subtracting the coincidence spectra multiplied a factor of $1/\varepsilon_c(E)$ from singles spectra. The energy dependent coincidence efficiency ($\varepsilon_c(E)$) was deduced by means of EGS4 code. In the subtracted spectrum as shown in Fig.2, a remaining part in the Compton scattering is less than 6%.

Nine β sources were prepared by a thermal neutron irradiation at KUR. Singles spectra and coincidence spectra were measured with the HPGe total absorption detector. As mentioned above, total absorption spectra were obtained from singles and coincidence spectra. To deduce Q_β-values from the total absorption spectra, the folding method was applied. Response functions for monoenergetic electrons were calculated for an energy range of 1-8 MeV using the EGS4 code. A typical result for ^{42}K is shown in Fig.3. A folded spectrum for assumed Q_β-value was calculated and the spectrum was compared with the experimental one. In the folding procedure, we preliminarily chose a range of 500 keV below the end-point in the experimental spectrum for the fitting range. The Q_β-value was determined so that the folded spectrum was in agreement with the experimental one in the fitting range

[1]Graduate School of Engineering, Nagoya University
[2]Radioisotope Research Center, Nagoya University
[3]Graduate School of Engineering, Hiroshima University
[4]Research Reactor Institute, Kyoto University

(Fig.3). Energy losses for electrons originated from an Al window and self-absorptions were corrected. The Q_β-values of nine nuclides were deduced as shown in Fig.4. For the nuclei having simple decay schemes, systematic uncertainty was evaluated to be about 10 keV from the differences between experimental values and evaluated ones [5]. More precise analysis is in progress.

In conclusion, this detector can deduce Q_β-values within accuracy of 10 keV. We will measure Q_β-values of neutron-rich rare-earth isotopes in the proton-induced fission product of ^{238}U using the JAERI on-line isotope separator (JAERI-ISOL).
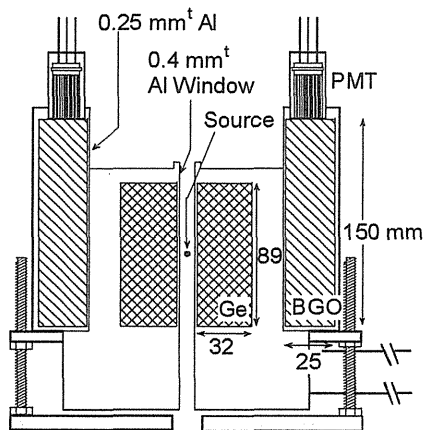
Fig.1 Schematic view of the HPGe total absorption detector.

Fig.2 Measured spectra for a 662 keV γ-ray. The subtracted spectrum is obtained by subtracting the coincidence spectrum multiplied a factor of 1/0.7 from singles spectrum.

Fig.3 A measured spectrum for ^{42}K decay compared with folded one.
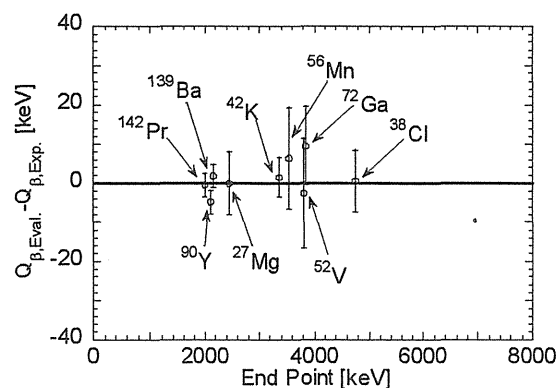
Fig.4 Comparisons between experimental values and evaluated ones. Each data is deviated within 10 keV.

References

[1] M. Shibata et al., Nucl. Instrum. Method. A 459, (2001) 581.

[2] M. Shibata et al., J. Phys. Soci. Jpn. 71, (2002) 1401.

[3] M. Shibata et al., JAERI-Review 2003-028, p.32.

[4] H. Hayashi et al., JAERI-Conf 2004-005, p.207.

[5] G. Audi et al., Nucl. Phys. A729, (2003) 337.

3. Nuclear Reactions

This is a blank page.

3. 1 DIRECT MEASUREMENT OF THE ^{8}Li (α, n) ^{11}B REACTION CROSS SECTION

H. ISHIYAMA[1], T. HASHIMOTO[1], T. ISHIKAWA[2], S. K. DAS[3], H. MIYATAKE[1], Y. X. WATANABE[1], Y. HIRAYAMA[1], M. H. TANAKA[1], Y. FUCHI[1], N. YOSHIKAWA[1], S. C. JEONG[1], H. KAWAKAMI[1], I. KATAYAMA[1], T. NOMURA[1], S. MITSUOKA, K. NISHIO, M. MATSUDA, S. ICHIKAWA, H. IKEZOE, T. FURUKAWA[4], H. IZUMI[4], Y. MIZOI[3], M. TERASAWA[5], P. K. SAHA[3], T. FUKUDA[3], K. NAKAI[2], T. SHIMODA[4]

Recently, it has been discussed that the r (rapid neutron capture)-process occurs in so-called "hot-bubble" under explosive conditions in the universe. In such conditions, nuclear reactions involving light neutron-rich nuclei play an important role as the r-process starting point [1]. We have tried to acquire directly systematical nuclear cross sections data of (α, n) reactions using low energy (E = 1-2 MeV/u) light neutron-rich radioactive nuclear beams (RNB). The excitation function of the ^{8}Li (α, n) ^{11}B reaction in the energy region of E_{cm} = 0.7 – 2.5 MeV has been measured successfully at the Tandem facility of JAERI.

The ^{8}Li-beam was produced via the ^{9}Be (^{7}Li, ^{8}Li) reaction. The produced ^{8}Li-beam was separated from the primary ^{7}Li-beam with the JAERI recoil mass separator. The obtained yield of ^{8}Li was 4.8 × 10^3 pps per 3.3 pnA ^{7}Li-beam at 24 MeV. For the exclusive measurement of the reaction cross section, a detector system consists of a Multi-Sampling and Tracking Proportional Chamber (MSTPC) and a large solid angle neutron detector array. As for experimental set up in detail, please see the reference [2].

The analysis of the measurement of ^{8}Li (α, n) ^{11}B reaction cross sections has been almost completed. Figure 1 shows the excitation function of ^{8}Li (α, n) ^{11}B reaction, indicated by black circles, in the energy region from 0.7 to 2.5 MeV. Open circles and squares indicate the data by Boyd et al. [3] and Gu et al.[4], respectively, based on inclusive measurements without neutron detection. Black triangles indicate the data by Mizoi et al. [5] based on the exclusive measurement using a detector system similar to that in the present work. The present data are consistent with ones of Mizoi et al. within their error bars and have at least ten-times better statistics than the previous ones.

[1] Institute of Particle and Nuclear Studies, KEK
[2] Tokyo University of Sciences
[3] Osaka Electro-Communication University
[4] Osaka University
[5] CNS
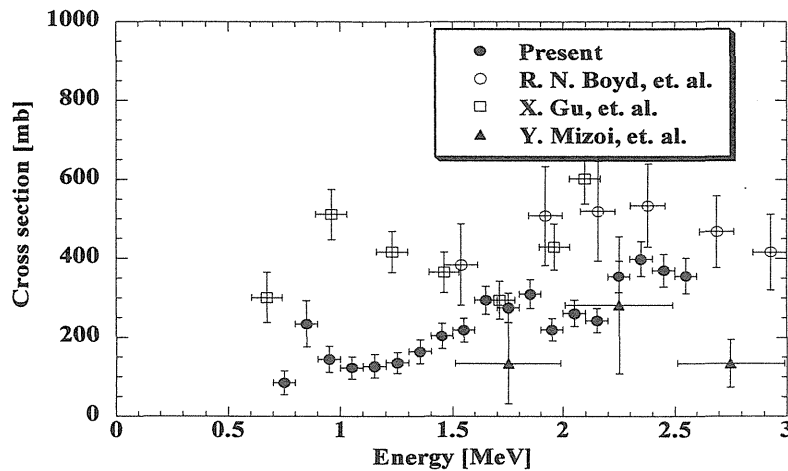
Fig. 1. The excitation function of ^{8}Li (α, n) ^{11}B reaction together with previous measurements.

In the energy region below 1.5 MeV, the present result is about three-times smaller than one of Gu et al. This result strongly suggests that the previous data included back-ground events, for example, elastic scattering events. The exclusive measurement has an advantage to distinguish the reaction events from elastic scattering events with taking account of the neutron information simultaneously obtained.
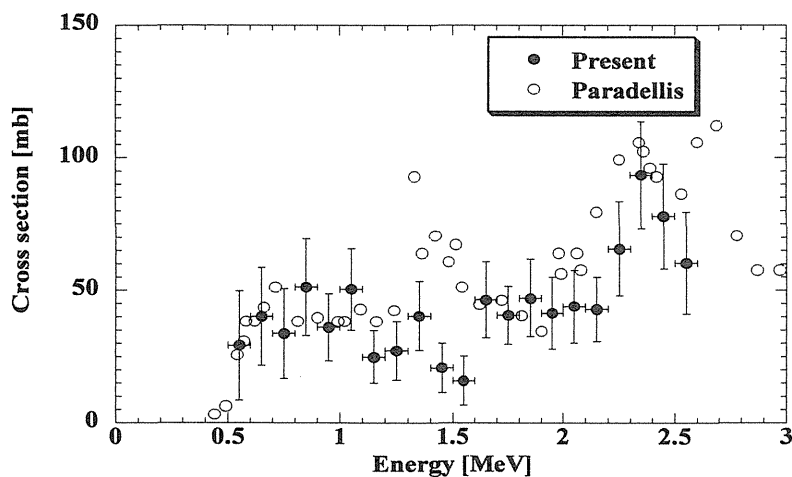
Fig. 2. The excitation function of ^{8}Li (α, n) ^{11}B$_{gnd}$ reaction together with the previous data.

From our measurement, the excitation function to each final state in ^{11}B was also deduced. Figure 2 shows the excitation function of ^{8}Li (α, n) ^{11}B$_{gnd}$, indicated by black circles. White

circles indicate reaction cross sections leading to $^{11}B_{gnd}$ by the inverse reaction (Paradellis et al. [6]). The present data are consistent with the previous ones in the energy region below 1.0 MeV. But in the energy region above 1.0 MeV, they do not agree with the previous ones. Especially, in our data the resonant structure around E_{cm} = 1.3 MeV does not exist. The previous data consist of only the transition to ^{8}Li-ground state in the energy region below 0.94 MeV, but in the above energy region, they may include the other transition to the 1st excited state (E_x = 0.94 MeV, 1^+) in ^{8}Li. The J^π of the corresponding ^{12}B excited state (E_x = 11.3 MeV) at E_{cm} = 1.3 MeV is not identified. But if it is, for example, $J^\pi = 1^+$, the transition probability to ^{8}Li-ground state (2^+) would be suppressed.

It is quite important to determine each final state transition in order to obtain an exact astrophysical reaction rate in the low energy region. And in order to obtain the excitation function of ^{8}Li (α, n) ^{11}B reaction in the lower energy region, the subsequent experiment has already been performed at the Tandem facility and its analysis is in progress.

References

[1] M. Terasawa, et. al., Nucl. Phys. A688(2001)581c.
[2] H. Ishiyama, et. al., America. Insti. Phys. 704(2003)453.
[3] R. N. Boyd, et. al., Phys. Rev. Lett. 68(1992)1283.
[4] X. Gu, et. al., Phys. Rev. Lett B343(1995)31.
[5] Y. Mizoi, et. al., Phys. Rev. C62(2000)065801.
[6] T. Paradellis, et al., Z. Phys. A337(1990)211.

3. 2 TOTAL FUSION CROSS SECTION MEASUREMENT IN ^{64}Ni+^{154}Sm

S. MITSUOKA, H. IKEZOE, K. NISHIO, K. TSURUTA, K. SATOU, C.J. LIN

We have studied the effect of nuclear deformation on fusion process by measuring the excitation functions of the evaporation residue cross sections at energies around the Coulomb barrier [1-4]. It was found that complete fusion was the dominant process above the Bass barrier energy region where near side collisions mainly contribute. On the other hand, in the lowest energy region where only near tip collisions are possible, the complete fusion was significantly hindered by almost three orders of magnitude in ^{64}Ni+^{154}Sm [2]. This means that two colliding nuclei not always fuse each other in the tip collisions and are likely to re-separate without forming a compound nucleus (referred as quasi-fission process). In order to see whether the hindered component really goes to quasi-fission, we planted to distinguish the fusion-fission and quasi-fission fragments by measuring the mass-energy distribution. These data also allows to obtain the total fusion cross section with a comparison of the evaporation residue cross section measured by using the RMS.

For this purpose, we developed a double-arm time-of-flight (TOF) fission fragment spectrometer put in a new large vacuum chamber at the entrance of the RMS. The arms can be rotated independently around the target in the horizontal plane in a rage of 20° - 110° and were positioned so that the center-of-mass angle between the detected fission fragments was around 180° . Each TOF detector includes a compact start (1.4 cmϕ) and a wide stop detectors (1×5 cm), both based on microchannel plate (MCP). The window of the start detector with an electrostatic mirror with negative high voltage was placed at a distance of 2.7 cm from the target, on which also a positive high voltage was applied to suppressed electron background from the target. The path length of TOF was 22 cm and the time resolution was typically 180 ps.

Beam of ^{64}Ni from the tandem-booster accelerator was used to bombard a target of ^{154}Sm (100 μ g/cm^2 in thickness, 99% enriched) sputtered onto carbon foil (50 μ g/cm^2). The beam energy was varied in a rage of $E_{c.m.}$ = 170 - 220 MeV ·corresponding to 2n - 6n evaporation channels. Time-coincident fission fragments were registered by the TOF spectrometer. The data were analyzed on the basis of the standard two-body kinematics with full momentum transfer. In the high energy region, normal fusion-fission of symmetric mass division was dominantly observed. In the low energy region where large fusion hindrance of fusion-evaporation residue have been observed, the statistic of the data was not enough to discuss whether the dominant process is quasi-fission where asymmetric fission is expected, so the further experiment is in progress.

Reference

[1] S. Mitsuoka, H. Ikezoe, K. Nishio, and J. Lu, Phys. Rev. C62, 54603 (2000).
[2] S. Mitsuoka, H. Ikezoe, K. Nishio, K. Satou, and J. Lu, Phys. Rev. C65, 54608 (2002).
[3] K. Nishio, H. Ikezoe, S. Mitsuoka, and J. Lu, Phys. Rev. C62, 14602 (2000).
[4] K. Nishio, H. Ikezoe, S. Mitsuoka, K. Satou, and S. Jeong, Phys. Rev. C63, 44610 (2000).

3.3 EVAPORATION RESIDUE MEASUREMENT FOR THE REACTION ^{16}O+^{204,206}Pb

K. SATOU[1], H. IKEZOE, S. MITSUOKA, K. NISHIO, K. TSURUTA, C. J. LIN[2] and S. C. JEONG[3]

We measured evaporation residue (ER) cross sections for the reactions ^{16}O+^{204,206}Pb to study the effect of the entrance-channel mass asymmetry on the heavy-ion fusion reaction. We used the ^{16}O beams from the JAERI-tandem accelerator. Targets were fabricated by sputtering lead on a thin aluminum foil in thickness of $1.3\,\mu$m. The thicknesses of the targets were from $50\,\mu$ g/cm^2 to 130 μ g/cm^2, and the enrichments of the ^{204}Pb and ^{206}Pb targets were 66.5% and 99.76%, respectively. The ^{204}Pb target contained the other lead isotopes 206, 207 and 208 with the percentage of 16.12, 7.49, and 9.89, respectively. A silicon surface barrier detector (SSD) was set at the angle 45° with respect to the beam direction to measure elastically scattered ^{16}O beams from the target. The measured elastic scattering events were used to obtain the absolute values of the ER cross sections. The aluminum catcher foil in thickness of 5 μ m was put just behind the target to collect all fusion products emitted from the target. After the beam irradiation of 70 to 80 min., we observed α decay events from the catcher foil by using an SSD. By measuring the α decay energies, the total decay events and the decay lifetimes, each ER cross section was determined. The results are listed in Table 1. The ER cross sections for the reaction ^{16}O+^{206}Pb were used to estimate the fusion products originated from the bombardment of ^{16}O on the lead isotope 206 in the ^{204}Pb target.

In order to compare the obtained ER cross sections with those for other reaction systems ^{40}Ar+^{180}Hf [1], ^{48}Ca+^{172}Yb [2], ^{82}Se+^{138}Ba [3], and ^{124}Sn+^{96}Zr [2], which produce the same compound nucleus ^{220}Th, we introduce here the same method used in the refs. [4, 5]. In this method, a reduced cross section which is the sum of the obtained xn channel cross sections divided by the factor $\pi\,(\hbar/p)^2$ was used, where $\hbar/p$ is the reduced de Broglie wavelength. The obtained reduced cross sections are shown in Figure 1 as a function of the excitation energy of the compound nucleus. As shown in Fig. 1, the reduced cross sections for the most asymmetric fusion reaction ^{16}O+^{204}Pb is about one order of magnitude larger than those from the other reactions. This result is consistent with the data reported by Hinde et al. [5], although their results show rather small value than ours. The present result indicates that the fusion probability depends strongly on the entrance-channel mass asymmetry.

[1]Tandem Accelerator Complex, Research Facility Center for Science and Technology, University of Tsukuba
[2]China Institute of Atomic Energy, Beijing, China
[3]Institute of Particle and Nuclear Studies, KEK

Table 1 Evaporation residue cross sections (mb) for the fusion reactions $^{16}O+^{204}Pb$ and $^{16}O+^{206}Pb$.

E_{cm} (MeV)	$^{16}O+^{204}Pb$			E_{cm} (MeV)	$^{16}O+^{206}Pb$			
	$^{217}Th+^{213}Ra$	$^{216}Th+^{212}Ra$	$^{216}Ac+^{212}Fr$		$^{220}Th+^{216}Ra$	$^{217}Th+^{213}Ra$	$^{216}Th+^{212}Ra$	$^{216}Ac+^{212}Fr$
74	5.0			79	18.1			
79	8.9	4.7	3.8	97		18.1	0.9	
83	5.6	4.3	3.2	102		26.9	9.1	2.6
88	4.6	7.7	1.2	111		6.3	5.4	3.0
93	16.5	9.5	2.2					
96	9.2	2.5	1.6					
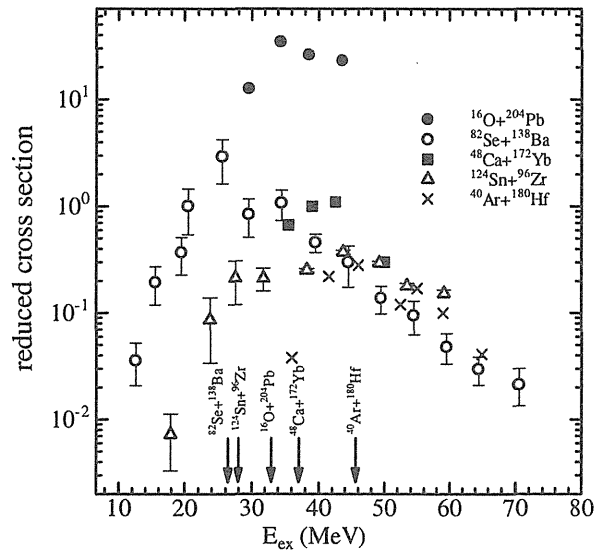
Fig. 1 Obtained reduced cross sections for the various reaction systems which produce the same compound nucleus ^{220}Th. The abscissa is the excitation energy of the compound nucleus. The present data are shown as the solid dotted points. The fusion barriers for these reaction systems are shown by arrows.

References

[1] H.-G. Clerc, J. G. Keller, C.-C. Sahm, K.-H. Schmidt, H. Schulte, and D. Vermeulen, Nucl. Phys. A419, 571 (1984).

[2] C. C. Sahm and H. G. ClercK. -H. Schmidt, W. Reisdorf, P. Armbruster, F. P. Hessberger, J. G. Keller, G. Münzenberg and D. Vermeulen, Nucl. Phys. A441, 316 (1985).

[3] K. Satou, H. Ikezoe, S. Mitsuoka, K. Nishio, and S. C. Jeong, Phys. Rev. C 65, 054602 (2002).

[4] H. Ikezoe, K. Satou, S. Mitsuoka, K. Nishio, and S. C. Jeong, Phys. Atom. Nucl. 66, 1053 (2003).

[5] D. J. Hinde, M. Dasgupta, and A. Mukherjee, Phys. Rev. Lett, 89, 282701 (2002).

3. 4 EVIDENCE OF COMPLETE FUSION IN THE SUB-BARRIER $^{16}O + ^{238}U$ REACTION

K. NISHIO, H. IKEZOE, Y. NAGAME M. ASAI, K. TSUKADA, S. MITSUOKA, K. TSURUTA, K. SATOU[1], C.J. LIN[2], and T. OHSAWA[3]

Recently, there has been much interest in the fission fragment angular distribution in sub-barrier heavy ion reactions using actinide targets [1,2]. This is because of the observation that the angular anisotropies in the sub-barrier region shows much larger values than the prediction of the standard transition state model [3]. By assuming the quasi-fission to be dominated in the sub-barrier region, where the interaction of the projectile is restricted to the tips of the prolately deformed target, Hinde et al. [1] explained the energy dependence of the anisotropy for the $^{16}O+^{238}U$ reaction. In this orientation-dependent quasi-fission model, the fusion-fission and quasi-fission was separated by the critical angle $35\pm5°$. To determine the presence (or absence) of complete fusion in the $^{16}O+^{238}U$ reaction we measured the evaporation residue (ER) cross sections in the sub-barrier region.

Experiment was carried out by using the ^{16}O beams supplied by the JAERI-tandem accelerator. The natural uranium target of $320\,\mu g/cm^2$ was prepared by electrodeposition on the Be backing of 1.7 mg/cm^2. We employed an aerosol-loaded He-gas jet system to transport ERs ($^{248,249,250}Fm$), and their α decays are detected to determine the production rates. The ERs recoiling out of the target were stopped in He gas loaded with KCl aerosol clusters. The ERs attached to the clusters were continuously swept out of the target chamber with a He-gas flow, and transported through a Teflon capillary to a rotating wheel apparatus MAMON [4]. The α-particles from the deposit were detected by a series of 18 silicon PIN photodiodes ($18\times18mm^2$). The transport efficiency for the ERs was determined to be 0.369 ± 0.019 at 36 pnA.

We show in Fig.1 the results of ER cross sections for three fermium isotopes. We also show the fission cross sections from Ref.[1]. The thin solid curve is the fusion cross section determined by a coupled channel calculation using the CCDEGEN code [5]. Because of the highly fissile compound nucleus ^{254}Fm formed in the present reaction, the fusion cross section is well approximated to the fission cross section, in so far as the system fuses completely. In this calculation, we adopted the quadruple and hexadecapole deformation parameters of (β_2, β_4)=(0.275, 0.05) for ^{238}U as in Ref. [1]. Up to two phonon states are included for the octupole vibration in ^{238}U with the first excitation energy 0.73 MeV [6], and the deformation parameter β_3 of 0.086 [7] was used. The partial wave cross sections from the CCDEGEN code were used as input to a statistical model code (HIVAP [8]) to calculate the ER cross sections. The calculation (thick solid curves) reproduces the measured ER cross sections from above- to extreme sub-barrier region. This indicates that the collision of the projectile with the tips of ^{238}U also results in complete fusion without any significant fusion hindrance. We tried to calculate the ER cross sections within the constraint that the collision of the projectile with the tips of ^{238}U does not form the compound nucleus as is discussed in Ref.[1]. The results are shown by bold dashed curves in Fig.1.

---

[1] Tsukuba University
[2] China Institute of Atomic Energy
[3] Kinki University

In the sub-barrier region, the calculation is about two orders of magnitude smaller than the experimental data. We conclude that in the sub-barrier region, complete fusion is the main process after the projectile is captured to the target and the orientation-dependent quasi-fission is not a reason for the anomalously large fission fragment angular anisotropy.

Figure 2 shows the fusion probability determined by using the present data. The coupled-channel calculation (solid curve) taking into account the deformation of ^{238}U reproduces the data, whereas the calculation ignoring the deformation (dotted curve) underestimates the data in the sub-barrier region.
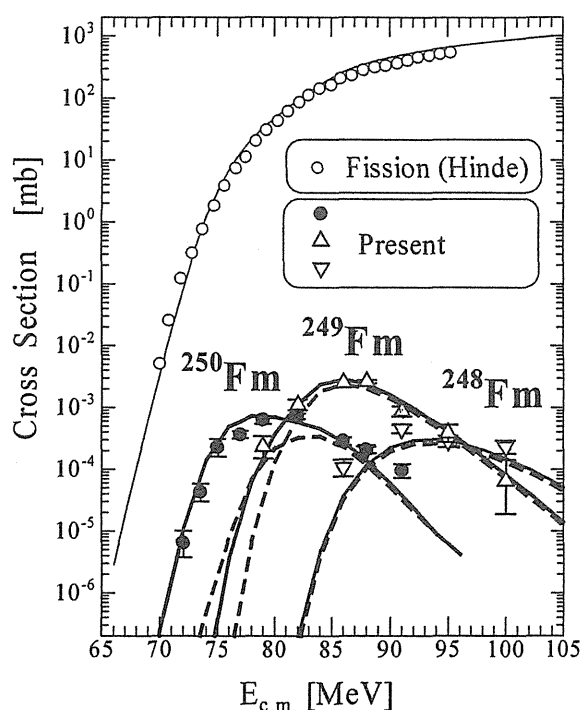
Fig.1 Evaporation residue and fission cross sections as function of center-of-mass energy.
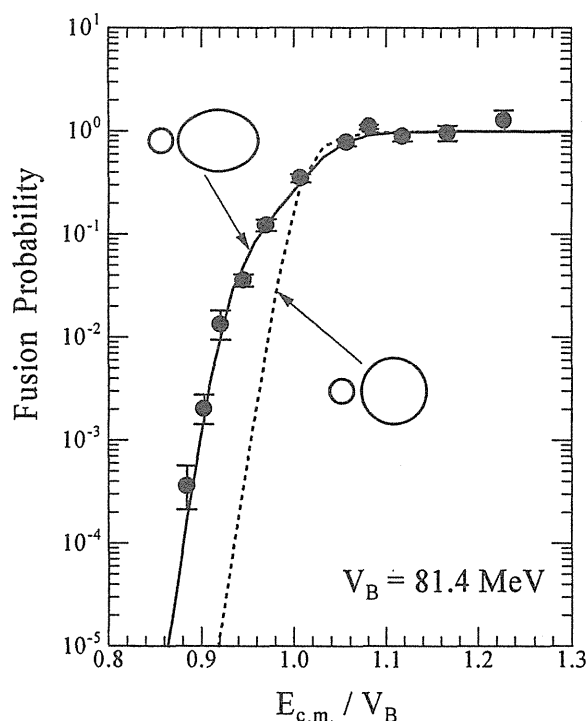
Fig.2 Fusion probability. V_B is the Coulomb barrier when ^{238}U is assumed to be spherical.

References

[1] D.J. Hinde *et al.*, Phys. Rev. Lett. 74 (1995) 1295.

[2] J.C. Mein *et al.*, Phys. Rev. C, 55 (1997) R995., H. Zhang *et al.*, Phys. Rev. C, 49 (1994) 926., N. Majumdar *et al.*, Phys. Rev. C, 51, (1995) 3109. A. Karnik *et al.*, Z. Phys. A, 351 (1995) 195., Z. Liu *et al.*, Phys. Lett. B, 353 (1995) 173., J.P. Lestone *et al.*, Phys. Rev. C, 56 (1997) R2907., B.K. Nayak *et al.*, Phys. Rev. C, 62 (2000) R031601.

[1] R. Vandenbosch and J.R. Huizenga, *Nuclear Fisson* (Academic Press, New York, 1973).

[4] Y. Nagame *et al.*, J. Nucl. Radiochem. Sci. 3 (2002) 85.

[5] K. Hagino (unpublished).

[6] R.B. Firestone, Table of Isotopes, edited by V.S. Shirley (Wiley, New York, 1996)

[7] R.H. Spear, At. Data and Nucl. Data Tables 42 (1989) 55.

[8] W. Reisdorf and M. Schaedel, Z. Phys. A 343 (1992) 47.

—41—

4. Nuclear Chemistry

This is a blank page.

4. 1 FLUORIDE COMPLEXATION OF Rf

H. HABA,[1] K. TSUKADA, M. ASAI, A. TOYOSHIMA,[2] K. AKIYAMA, I. NISHINAKA,
M. HIRATA, T. YAITA, S. ICHIKAWA, Y. NAGAME, K. YASUDA, Y. MIYAMOTO, T. KANEKO,
S. GOTO,[3] S. ONO,[3] T. HIRAI,[3] H. KUDO,[3] M. SHIGEKAWA,[2] A. SHINOHARA,[2] Y. OURA,[4]
H. NAKAHARA,[4] K. SUEKI,[5] H. KIKUNAGA,[6] N. KINOSHITA,[6] N. TSURUGA,[6]
A. YOKOYAMA,[6] M. SAKAMA,[7] S. ENOMOTO,[1] W. BRÜCHLE,[8] M. SCHÄDEL,[8]
and J. V. KRATZ[9]

The first transactinide element, rutherfordium (Rf), is considered to be a group-4 member with the ground-state electronic configuration of $[Rn]5f^{14}6d^27s^2$, though relativistic calculations have predicted different configurations such as $6d^27s^2$, $7s^27p^2$, and $6d7s^27p$ [1]. Previously, we investigated the anion-exchange behavior of Rf together with those of lighter homologues of group-4 elements Zr and Hf in 4.0–11.5 M HCl and 8.0 M HNO_3 solutions [2]. It was found that the adsorption trends of Rf in HCl and HNO_3 are very similar to those of Zr and Hf, indicating that Rf is a typical group-4 member. Reported in this paper is our recent result of the successive anion-exchange study of Rf in 1.9–13.9 M HF solutions.

Isotope ^{261}Rf was produced in the ^{248}Cm(^{18}O,$5n$) reaction using a 94-MeV ^{18}O beam delivered from the JAERI tandem accelerator. A ^{248}Cm target of 610 µg cm^{-2} thickness was prepared by electrodeposition onto a 2.4 mg cm^{-2} thick Be foil. Beam intensity was approximately 0.3 particle µA. Reaction products recoiling out of the target were transported by a He/KCl gas-jet system to the Automated Ion-exchange separation apparatus coupled with the Detection system for Alpha spectroscopy (AIDA) [2]. Two different microcolumns, 1.6 i.d. × 7.0 mm and 1.0 i.d. × 3.5 mm, were filled with the CA08Y resin. After the aerosol collection for 125 s, Rf was dissolved in 240 (260) µL of 13.9, 11.6, 7.7, 5.8, 4.8, and 3.9 (3.0, 2.4, and 1.9) M HF and fed into the column at a flow rate of 0.74 (1.0) mL min^{-1} [3]. The effluent was collected on a Ta dish as Fraction 1 and evaporated to dryness using hot He gas and a halogen heat lamp. The remaining Rf in the column was eluted with 210 (200) µL of 4.0 M HCl. This effluent was collected on another Ta dish and evaporated to dryness as Fraction 2. The pair of Ta dishes, Fractions 1 and 2, was automatically transferred to an α spectrometry station equipped with eight 600 mm^2 PIPS detectors. All events were registered event by event. To investigate the on-line anion-exchange behavior of Zr and Hf, isotopes ^{85}Zr and ^{169}Hf were simultaneously produced in the ^{nat}Ge(^{18}O,xn) and ^{nat}Gd(^{18}O,xn) reactions,

[1] Cyclotron Center, RIKEN

[2] Department of Chemistry, Graduate School of Science, Osaka University

[3] Department of Chemistry, Faculty of Science, Niigata University

[4] Department of Chemistry, Graduate School of Science, Tokyo Metropolitan University

[5] Department of Chemistry, University of Tsukuba

[6] Department of Chemistry, Faculty of Science, Kanazawa University

[7] Department of Radiologic Science and Engineering, School of Health Sciences, University of Tokushima

[8] Gesellschaft für Schwerionenforschung

[9] Institut für Kernchemie, Universität Mainz

respectively. The anion-exchange experiments were performed with AIDA at 3.9–17.4 M HF under the same experimental conditions as those with ^{261}Rf. The effluents were assayed by γ-ray spectrometry with Ge detectors.

From ion-exchange experiments performed 4226 times at 1.9–13.9 M HF, a total of 266 α events from 78-s ^{261}Rf (8.28 MeV) and its daughter 25-s ^{257}No (8.22, 8.27, and 8.32 MeV) were registered in the energy range of 8.00–8.36 MeV, including 25-time-correlated α pairs. From the activities A_1 and A_2 observed in Fractions 1 and 2, respectively, the percent adsorption (%ads) on CA08Y was evaluated using %ads = $100A_2/(A_1 + A_2)$. Then, the %ads values of Rf were transformed into K_d values based on the smooth relationship between the %ads values of ^{85}Zr and ^{169}Hf and the K_d values of ^{89}Zr and ^{175}Hf measured by the batch method [4]. In Fig. 1, the variation of the K_d value of Rf is shown by closed diamonds as a function of HF concentration, [HF], together with those of ^{89}Zr and ^{175}Hf shown by open squares and open circles, respectively. As shown in Fig. 1, the K_d values of Zr and Hf are identical with each other and both decrease with an increase of [HF]. A linear relationship with a slope of –3.0±0.1 was found in the log K_d-log [HF] plot shown by a dashed line. As HF is a weak acid, equilibrations among HF, H^+, F^-, and HF_2^- in the solution are established following the two chemical relations: $H^+ + F^- \rightleftharpoons HF$ and $HF + F^- \rightleftharpoons HF_2^-$ [5]. Above 1 M, $[HF_2^-]$ is more than one order of magnitude higher than $[F^-]$, and the decrease of K_d with [HF] is explained as displacement of the metal complexes from the binding sites of

the resin with HF_2^-. Although the K_d values of Rf also decrease linearly with [HF], they are apparently smaller than those of Zr and Hf. Also noted is that the slope of –2.0±0.3 of the plot of log K_d vs. log [HF] for Rf differs from that for Zr and Hf, implying that different anionic species are formed. The relativistic molecular density functional calculations on the fluoride complexes of Rf, Zr, and Hf are under study in our group to interpret the remarkable difference in the anion-exchange behavior and to discuss the influence of relativistic effects on the fluoride complexation of Rf.
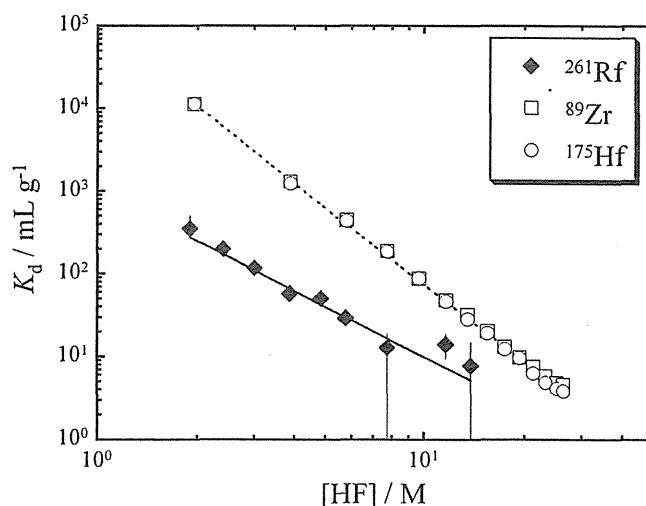
Fig. 1. Variations of the distribution coefficient values (K_d) of ^{261}Rf, ^{89}Zr, and ^{175}Hf on CA08Y as a function of HF concentration, [HF].

References

[1] M. Schädel (Ed.), *The Chemistry of Superheavy Elements* (Kluwer Academic Publishers, Dordrecht, 2003).

[2] H. Haba *et al.*, J. Nucl. Radiochem. Sci. **3**(2002)143.

[3] The values given in parenthesis refer to the condition when the 1.0 i.d. × 3.5 mm column was used.

[4] H. Haba *et al.*, J. Am. Chem. Soc. **126**(2004)5219.

[5] P. M. Plaisance and R. Guillaumont, Radiochim. Acta **12**(1969)32.

4. 2 ANION-EXCHANGE CHROMATOGRAPHIC BEHAVIOR OF RUTHERFORDIUM (RF) IN HYDROFLUORIC ACID

K. TSUKADA, A. TOYOSHIMA[1], M. ASAI, H. HABA[2], K. AKIYAMA, I. NISHINAKA, Y. NAGAME, D. SAIKA[1], K. MATSUO[1], W. SATO[1], A. SHINOHARA[1], H. ISHIZU[3], M. ITO[3], J. SAITO[3], S. GOTO[3], H. KUDO[3], H. KIKUNAGA[4], N. KINOSHITA[7], C. KATO[4], A. YOKOYAMA[4] AND K. SUEKI[5]

Recently, the anion-exchange behavior of Rf in 1.9-13.9 M hydrofluoric acid (HF) solution was studied together with its homologues, Zr and Hf [1]. It was suggested that the different anionic fluoride complexes between Rf and the homologues are formed. The K_d values of Rf were derived from the transformation of the percent adsorption (%ads) values, that represent the percentage of the activity adsorbed on the anion-exchange column when a constant volume of solution was fed into the column, with the help of the relationship between K_d and %ads of the homologues. The purpose of this study is to directly measure the K_d value of Rf from its elution curve on the anion-exchange chromatography with HF solution by using the modified AIDA (the Automated Ion-exchange separation apparatus coupled with the Detection system for Alpha spectroscopy) [2].

The isotope ^{261}Rf was produced in the ^{248}Cm(^{18}O,5n) reaction with the 94-MeV ^{18}O projectiles delivered from the JAERI tandem accelerator. The target included 39.3%-enriched ^{152}Gd to simultaneously produce the short-lived ^{169}Hf isotope. The reaction products recoiling out of the target were transported to the collection site of AIDA by a He/KCl gas-jet system. After the collection, the site was moved onto a micro-column packed with an anion exchange resin (MCI GEL, CA08Y, 1.6 mm i.d. x 7 mm). Hydrofluoric acid solution of 5.4 M was then fed to the column with a flow rate of 0.82 mL/min. The effluent was consecutively collected on three separate Ta disks. Each fraction was evaporated to dryness with hot He gas and halogen heat lamps. 4.0 M HCl solution was thereafter fed to the column to elute the ^{261}Rf and ^{169}Hf remaining in the column. The effluent was collected on a Ta disk as the 4th fraction and evaporated to dryness. The 4 disks were in turn transferred to the α-spectrometry station equipped with eight 600 mm^2 PIPS detectors, followed by γ-spectroscopy with Ge detectors to monitor the isotope ^{169}Hf.

[1]Graduate School of Science, Osaka University

[2]Cyclotron Center, RIKEN

[3]Faculty of Science, Niigata University

[4]Graduate School of Science, Kanazawa University

[5]Department of Chemistry, Tsukuba University

The anion-exchange experiments were performed 511 times and 8, 20, 12, and 8 α-events of 78-s ^{261}Rf and its daughter "25-s ^{257}No" were registered in the energy range of 8.0-8.3 MeV in the 1st to 4th fractions, respectively. The peak volume of the elution curve of ^{261}Rf was observed around 200 μL while ^{169}Hf was eluted only in the 4th fraction. In the dynamic column method, the K_d value is described as

$$K_d = \frac{v}{m_r},$$

where m_r is the mass of the dry resin and v is the peak volume corrected for the dead volume of the columns. The preliminary K_d value of Rf was evaluated to be 20-40 mL/g. The present K_d value plotted in Fig. 1 is consistent with the previous result [1].
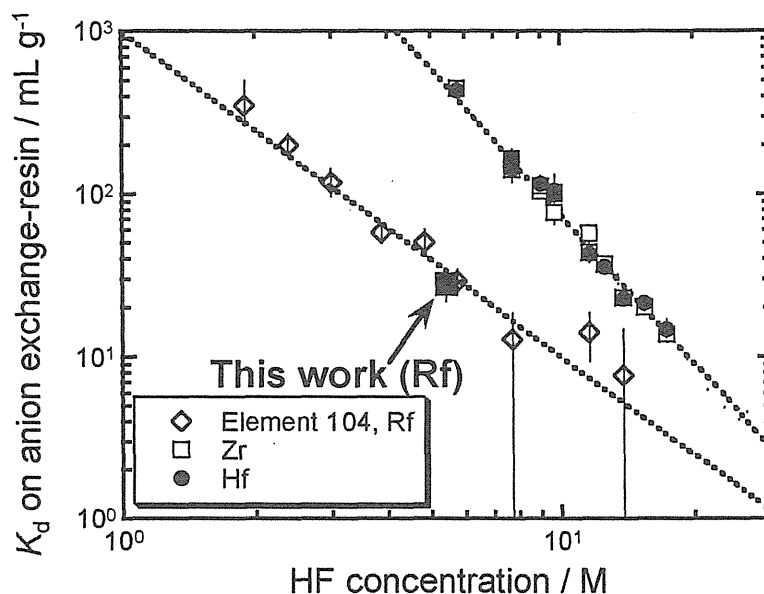
Fig. 1 Variation of the distribution coefficient, K_d, of Rf, Zr, and Hf on the anion-exchange resin CA08Y as a function of the HF concentration.

References

[1] H. Haba, K. Tsukada, M. Asai, A. Toyoshima, K. Akiyama, I. Nishinaka, M. Hirata, T. Yaita, S. Ichikawa, Y. Nagame, K. Yasuda, Y. Miyamoto, T. Kaneko, S. Goto, S. Ono, T. Hirai, H. Kudo, M. Shigekawa, A. Shinohara, Y. Oura, H. Nakahara, K. Sueki, H. Kikunaga, N. Kinoshita, N. Tsuruga, A. Yokoyama, M. Sakama, S. Enomoto, M. Schädel, W. Brüchle, J. V. Kratz, J. Am. Chem. Soc. 126 (2004) 5219.

[2] Y. Nagame, H. Haba, K. Tsukada, K. Akiyama, M. Hirata, I. Nishinaka, S. Ichikawa, H. Nakahara, S. Goto, T. Kaneko, H. Kudo, A. Toyoshima, A. Shinohara M. Schädel J. V. Kratz, H. W. Gäggeler, and A. Türler, Czech. J. Phys. Suppl. A 299 (2002) 143.

5. Nuclear Theory

This is a blank page.

5.1 DEFORMATION OF NEUTRON-RICH MG ISOTOPES

Y. UTSUNO, T. OTSUKA[1], T. MIZUSAKI[2] and M. HONMA[3]

Owing to recent experiments of in-beam γ-ray spectroscopy for neutron-rich Mg isotopes ^{32,34}Mg [1,2] the structure of these nuclei can be discussed in the direction other than the disappearance of the magic structure. Although both of them are regarded as well deformed nuclei from the measured low 2^+_1 energy levels, the ratios of $E_x(4^+_1)$ to $E_x(2^+_1)$ are rather different, i.e., 2.6 and 3.2 for, ^{32,34}Mg, respectively [1,2]. The latter is very close to the value of the rigid axially symmetric rotor, whereas the former is not. The Monte Carlo shell model (MCSM) is a useful tool to examine the nuclear structure in this region, but it is not easy to draw an intuitive picture from its wave function. In the present study, we interpret the result by the MCSM in terms of the intrinsic frame of view, making use of the potential energy surface (PES).

We first perform a shell-model calculation for ^{32,34}Mg by the MCSM. The shell-model Hamiltonian used in this study is the same as that of our previous works [3]. Figure 1 compares the energy levels and the B(E2) values between the experiment and the MCSM. The observed difference in $E_x(4^+_1)/E_x(2^+_1)$ is well reproduced, similarly to the excitation energies and the B(E2) values. We also calculate the non-yrast states, and find a difference between those nuclei: the 2^+_2 level of ^{32}Mg drops closely to the 4^+_1 level, and is connected to the 2^+_1 level with a moderately large B(E2) value.

In order to examine the deviation from the rigid axially symmetric rotor, the PES is calculated within the shell-model space and using the same Hamiltonian as illustrated in Fig. 2. Here, the quadrupole deformation of a nucleus is constrained as $<Q_{20}>=q \cos \gamma$ and $<Q_{22}>=(1/\sqrt{2})q \sin \gamma$. The intrinsic shape of ^{32}Mg is more γ-unstable than that of ^{34}Mg, and after the angular-momentum projection, the energy minimum moves to $\gamma=20°$. By comparing with the asymmetric rigid rotor model, it turns out that this γ value accounts for the shell-model result in Fig. 1. On the other hand, ^{34}Mg appears to be a rather good symmetric rotor with $\gamma \sim 10°$ and its deformation is more stable than that of ^{32}Mg (see, e.g. the region with E<3 MeV where E denotes the energy measured from the lowest energy). The present result demonstrates that our shell-model calculation is capable of describing not only the shell structure but also the deformation which is a severe test for the nuclear-structure calculation.

[1] Department of Physics, University of Tokyo
[2] Institute of Natural Sciences, Senshu university
[3] Center for Mathematical Sciences, University of Aizu
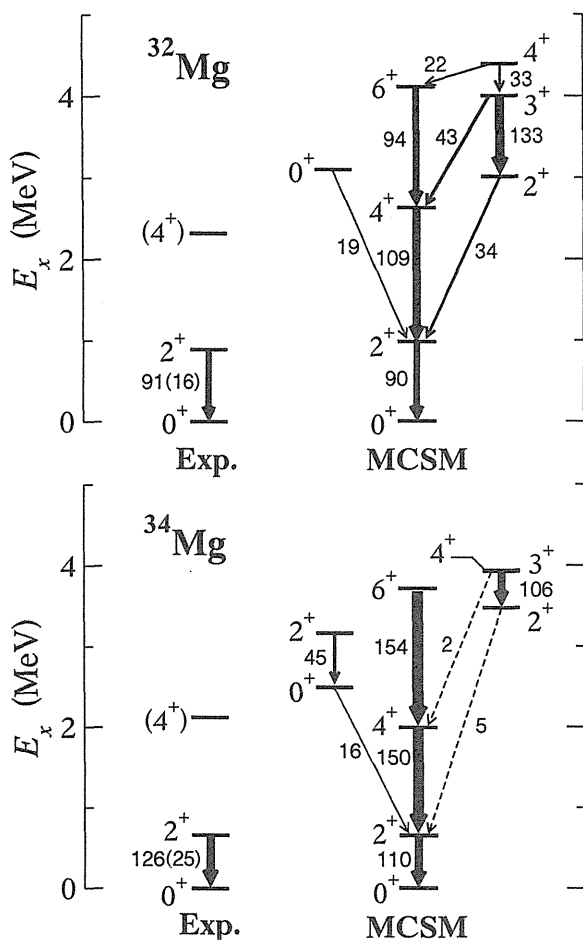
Fig. 1. Experimental energy levels and B(E2) values of ^{32,34}Mg (Exp.) compared with those of the MCSM calculation (MCSM). The numbers near the arrows denote the B(E2) in e^2fm^4.
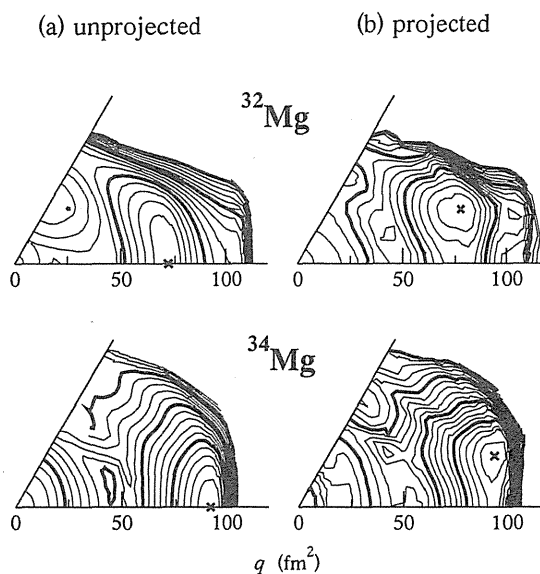
Fig. 2. Comparison of the potential energy surfaces of ^{32,34}Mg (a) without and (b) with the angular momentum projection onto I=0. The thin and thick lines are drawn at intervals of 0.3 and 1.5 MeV, respectively.

References

[1] K. Yoneda et al., Phys. Lett. B 499 (2001) 233.

[2] F. Azaiez et al., in Proceedings of Nuclear Structure '98, edited by C. Baktash, AIP Conference Proceedings Vol. 481, p. 243 (1998).

[3] Y. Utsuno, T. Otsuka, T. Mizusaki, M. Honma, Phys. Rev. C 60 (1999) 054315; ibid., 64 (2001) 011301(R).

5.2 ESTIMATION OF EFFECTIVE FUSION BARRIER FOR COLD FUSION REACTIONS WITH ^{208}Pb TARGET

T. ICHIKAWA, A. IWAMOTO, P. MÖLLER[1], A. J. SIERK[1]

We calculate effective fusion barriers at the entrance channel for cold fusion reactions leading to the production of superheavy elements (SHEs). So far the GSI group was successful in synthesizing SHEs up to Z=112 by using cold fusion reactions with ^{208}Pb and ^{209}Bi targets [1]. The excitation energy of the compound nucleus produced with the cold fusion reaction becomes relatively low due to the large negative reaction Q-values. This method has an advantage of the enhancement of the survival probability at the de-excitation stage. On the other hand, when we synthesize much heavier elements, the formation probability of the compound nucleus becomes low. It is very important to determine the optimum bombarding energy and the optimum target and projectile combinations. Thus, the theoretical estimation of the height of the fusion barrier at the entrance channel is required. The Bass model [2] is often used for the estimation of the fusion barrier. However, this model is a phenomenological one and some adjustable parameters are determined from experimental data of reactions between light nuclei. In addition, despite the importance of projectile deformations in heavy systems, these effects are not taken into account. The aim of this study is to propose a more realistic model where projectile deformations and zero-point vibrations are taken into account.

On the basis of the macroscopic-microscopic model, we calculate the effective fusion potential where projectile deformations are taken into account. In our calculations, we assume that the deformation of ^{208}Pb can be neglected during the approach of the projectile due to its double-magic nature. It is also assumed that the target and projectile energetically favor the tip-to-tip configuration having the axial symmetry. Thus, the effective fusion potential is a function of the center separation r and the projectile deformation ϵ_2. The effective fusion potential is the sum of the interaction energy between the target and projectile and the self energy of the projectile. The interaction energy consists of the Coulomb repulsion energy and the surface energy calculated with Yukawa-plus-exponential macroscopic model [3]. The self energy is calculated with the macroscopic-microscopic model, where for the macroscopic part, the FRLDM is used and for the microscopic part, the shell and pairing correction energies in terms of the Strutinsky method are used [4,5].

We calculate the effective fusion potential for each center separation decreasing from $r=15$ fm with small step $\Delta r=0.01$ fm and analyze the obtained potential energy surface. When the projectile approaches the target, the local saddle point against prolate deformations appears in the deformation energy surface of the projectile. We expect that the zero-point energy level of the projectile vibration exists between energies at this saddle point and at the local minimum. We calculate the zero-point energy level by using the WKB approximation with the irrotational flow mass. The height of the saddle point becomes low with the decrease of the center separation. Thus, the zero-point energy level vanishes at a certain center separation. Then, we expect that the system becomes unstable due to the vanishing of the

---

[1]Los Alamos National Laboratory
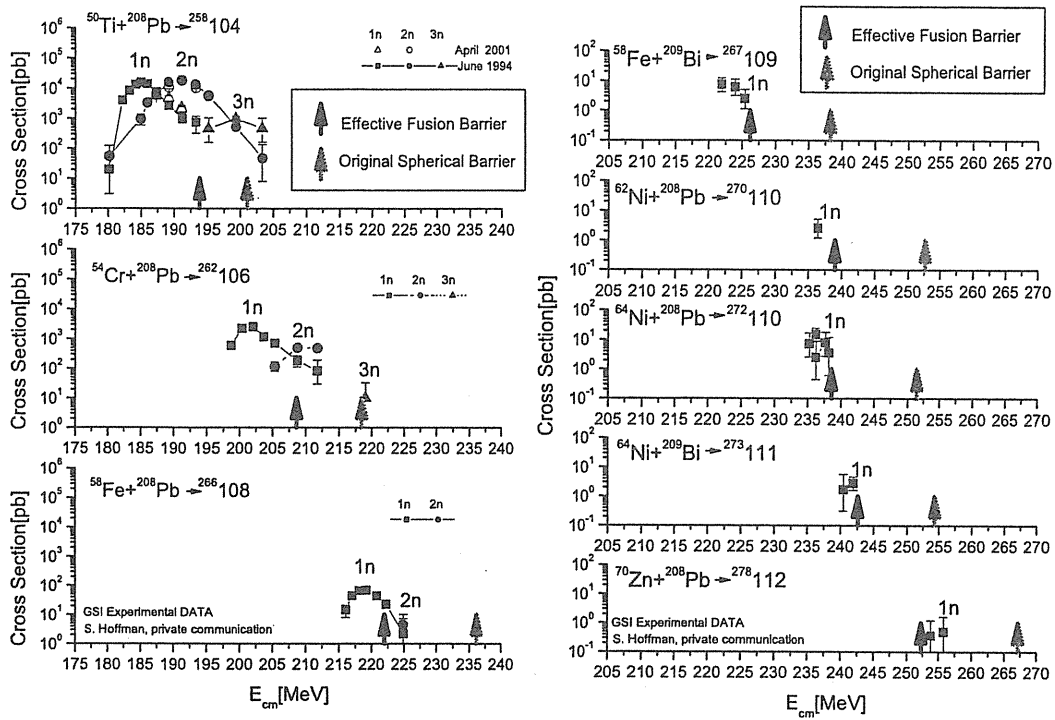
Figure 1: Comparison of the present calculations with the experimental data.

eigen-state and that the overlaps of both surfaces occur immediately. Thus, we define the effective fusion barrier as the total energy of the system where this instability occurs. We also take account of the energy transfer from the zero-point energy to the kinetic energy of the projectile.

We estimate effective fusion barriers for the eight cold-fusion reactions with projectiles from ^{50}Ti to ^{70}Zn. The difference between our results and Bass barriers is within ± 3.5 MeV. We compare our results with peak energies for the 1n-reactions measured in the experiments. This is because we expect that the 1n-reaction occurs in the vicinity of the fusion barrier. In Fig. 1, black arrows denote the effective fusion barriers and solid points denote the measured evaporation-residue cross-sections. We also show the spherical barrier where projectile deformations are not taken into account. For ^{50}Ti and ^{54}Cr+^{208}Pb reactions, we seem to overestimate the effective fusion barriers. However, with the increase of the mass number of the projectile, it appears that effective fusion barriers are in good agreement with the peak energy of the 1n-reaction. The overestimations for ^{50}Ti and ^{54}Cr come from the persistence of the zero-point vibrations due to the double magic nature and its neighbor. The development of our model in order to explain these reactions is now under progress.

References

[1] S. Hofmann and G. Münzenberg, Rev. Mod. Phys. **27**, (2000) 733

[2] R. Bass, *Nuclear Reactions with Heavy Ions* (Springer-Verlag, Berlin, 1980).

[3] P. Möller and A. Iwamoto, Nucl. Phys. **A575**, (1994) 381

[4] P. Möller, J. R. Nix, W. D. Myers, and W. J. Swiatecki, At. Data Nucl. Data Tables **59**, (1995) 185

[5] P. Möller, A. J. Sierk, and A. Iwamoto, Phys. Rev. Lett. **92**, (2004) 072501

5.3 $^1S_0$ PROTON SUPERFLUIDITY IN NEUTRON STAR MATTER WITHIN A RELATIVISTIC MANY-BODY MODEL

T. TANIGAWA[1] M. MATSUZAKI[2] and S. CHIBA

Superfluidity in neutron star matter has been drawing much attention because of its influence on properties of neutron stars, such as their heat capacity and neutrino emissivity [1]. They consequently affect their thermal evolution. Neutron star matter is infinite matter, which is composed of nucleons (n, p), hyperons, and leptons (e^-, μ^-), under the chemical equilibrium and the charge neutrality. Recent studies often use relativistic many-body models to calculate the composition of neutron star matter since they are suited to treat dense matter in accord with the special relativity.

Here we report an impact of bulk properties, especially the Dirac effective mass of protons and the symmetry energy, on $^1S_0$ proton superfluidity in (n, p, e^-, μ^-) neutron star matter. To approach the subject, we employ the relativistic Hartree-Bogoliubov (RHB) model, which is an extended model of the well-known relativistic mean field (RMF) model, with capability of handling the pairing correlation. Unlike the $^1S_0$ neutron superfluidity, $^1S_0$ proton superfluidity are realized in dense region of neutron stars with supra-nuclear density because of the proton density much smaller than the neutron one. Thus protons and neutrons see qualitatively different environmental properties from each other; one of the properties is the Dirac effective mass that is a consequence of a covariant description inherent in the relativistic models. In addition, the symmetry energy is also a determinant of the environmental properties since it controls the proton fraction, namely the ratio of protons in neutron star matter. We also use an additional interaction Lagrangian proposed by Horowitz and Piekarewicz [2], which includes an isovector nonlinear coupling with its strength specified by Λ_ω, to investigate a relation between the pairing gap and the density dependence of the proton fraction. It makes difference in the proton fraction particularly at high density. To avoid ambiguity in choosing the particle-particle channel interaction, we adopt the Bonn-B potential in the BCS gap equation.

First, we investigate the impact of the Dirac effective mass on the pairing gap. Figure 1 displays the $^1S_0$ proton pairing gaps and the Dirac effective masses of protons without the isovector nonlinear coupling. The RMF parameter sets used here,
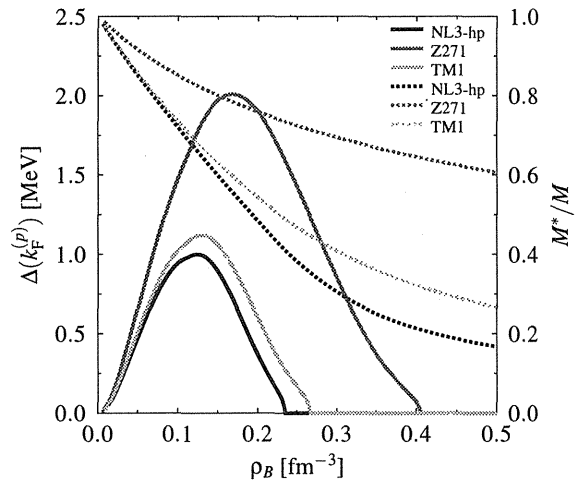
Figure 1: $^1S_0$ proton pairing gaps (left scale, solid curves) and Dirac effective masses (right scale, dashed curves) as functions of baryon density in neutron star matter using the standard RHB model with the NL3-hp, Z271, and TM1 parameter sets.

---

[1] Japan Society for the Promotion of Science and Advanced Science Research Center, JAERI
[2] Department of Physics, Fukuoka University of Education
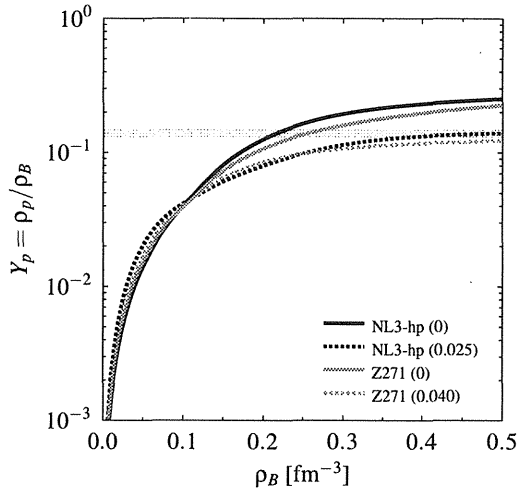
Figure 2: Proton fractions of the four distinct models of neutron star matter as functions of baryon density. The thin region hatched in gray represents a threshold of the proton fraction for the direct URCA process, about 13–15%. The number in parenthesis in the legend indicates the value of Λ_ω.
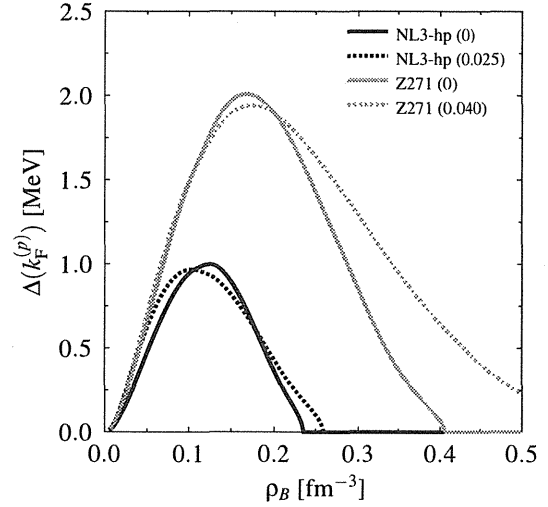
Figure 3: $^1S_0$ proton pairing gaps as functions of baryon density in neutron star matter using the RHB models with the NL3-hp and Z271 parameter sets with and without Λ_ω. The legend is the same as in Fig. 2.

NL3-hp, Z271 [2], and TM1 [3], are adjusted to give almost the same properties of symmetric nuclear matter and finite nuclei. The result apparently shows a strong correlation between the gap and the Dirac effective mass; the smaller the mass, the smaller the gap. This was also shown in a nonrelativistic framework [1]. The fact hence suggests that we can utilize the strong correlation to narrow down the parameter sets suitable for the study of interior proton superfluidity. Second, we examine the relation between the pairing gap and the proton fraction. Figure 2 shows the proton fractions obtained by the NL3-hp and Z271 set with and without the isovector nonlinear coupling. The solid curves that cross the URCA threshold exhibit a typical behavior of the proton fraction in the standard RMF/RHB model. Under the four compositions of neutron star matter, we calculate the $^1S_0$ proton pairing gaps shown in Fig. 3. We have found that the moderate increase of the proton fraction in the core region of neutron stars, $\rho_B \gtrsim 0.1$ fm^{-1}, with the finite Λ_ω widens the density range under the superfluid state and slightly lowers the peak of the gap. Again, the difference of the obtained gaps between the parameter sets reflects that of the Dirac effective masses, which are already shown in Fig. 1.

In summary, we have clarified the impact of the bulk properties to $^1S_0$ proton superfluidity in neutron star matter. Since proton Cooper pairs immerse themselves in dense surroundings inside neutron stars, the bulk properties at high density—which are not much known—should be cared about. Study of $^1S_0$ hyperon superfluidity with such care is under progress using the RHB model.

References

[1] T. Takatsuka and R. Tamagaki, Prog. Theor. Phys. 97 (1997) 345.

[2] C. J. Horowitz and J. Piekarewicz, Phys. Rev. Lett. 86 (2001) 5647.

[3] Y. Sugahara and H. Toki, Nucl. Phys. A579 (1994) 557.

—55—

6. Atomic Physics and Solid State Physics

This is a blank page.

6. 1 CHARGE STATE DISTRIBUTION OF SULFUR IONS
AFTER PENETRATION OF C–FOIL TARGETS

M. IMAI[1], M. SATAKA, K. NISHIO, Y. SUGIYAMA,

K. KAWATSURA[2], K. TAKAHIRO[2], K. KOMAKI[3] and H. SHIBATA[1]

Charge state evolution is one of the most important aspects in ion-solid interactions. Various processes, such as electron capture, ionization, excitation and the consequent phenomena like energy loss and stopping, are closely related with the projectile charge state evolution in the target. Equilibrium charge state distributions for many collision systems after passing gaseous or solid target have been widely investigated [1], although the charge state distribution somewhat changes upon exiting the target foil. Charge state distributions before its equilibrium have also been studied experimentally as well as theoretically. We have been devoted to measuring Coster-Kronig (C-K) electrons from S^{12+} [2] and Si^{5+} [3] ions excited through penetration of He or C-foil target, to study ion-solid interaction from another viewpoint, and succeeded in reproducing the experimental spectra with C-K electron energies calculated by perturbation theory of Z-expansion method (MZ code), weighed by assumed ion charge distributions "inside" foil [4]. For the progress of our study, we started a separate experiment to derive the charge state distributions "after" the foil penetration for 2.0 MeV/u S^{q+} (q = 6, 8, 10, 12) ions with thin carbon foils of $0.9 - 10$ $\mu g/cm^2$, which cover the non-equilibrium region.

The present experiments were performed at the LIR1–3 beam line of the 20UR Tandem Accelerator Facility. A beam of 2.0 MeV/u (64 MeV) S^{6+} or S^{8+} ions was provided from the tandem accelerator within 0.1% of energy accuracy, using a calibrated energy analyzing magnet. A post-stripper C-foil of ~20 $\mu g/cm^2$ in thickness was placed after the energy analyzing magnet to produce higher charge state fractions. The energy loss values at the post-stripper foil were estimated to be at most 0.7% by our separate measurement of cusp electron energies with zero-degree electron spectroscopy [2,4]. The primary S^{6+}, S^{8+} or post-stripped S^{10+} and S^{12+} ion beam was directed by a switching magnet to self-support carbon target foils of 0.9, 1.1, 1.5, 2.0, 3.0, 4.7, 6.9 and 10 $\mu g/cm^2$ in thickness. The charge state distributions after foil penetration were measured using the heavy ion magnetic spectrometer ENMA [5] and position-sensitive gas chamber detector. The vacuum condition inside the spectrometer was maintained below 10^{-6} Pa to eliminate the background charge exchange collisions with residual gas, which was confirmed by measurements without target foil.

Charge state fractions for 2.0 MeV/u S^{6+}, S^{8+}, S^{10+} and S^{12+} ions incident on the carbon foil targets of $0.9 - 10$ $\mu g/cm^2$ are shown in fig. 1. Typical error values for the charge fractions are estimated as 20% for the smallest fractions around 1.0_10^{-5} and less than 0.5% for the largest fractions around 0.3. The fractions in the figure do not flat off in the measured foil thickness range, but from the viewpoint of the

---

[1] Department of Nuclear Engineering, Kyoto University
[2] Department of Chemistry and Materials Technology, Kyoto Institute of Technology
[3] Institute of Physics, Graduate School of Arts and Sciences, University of Tokyo
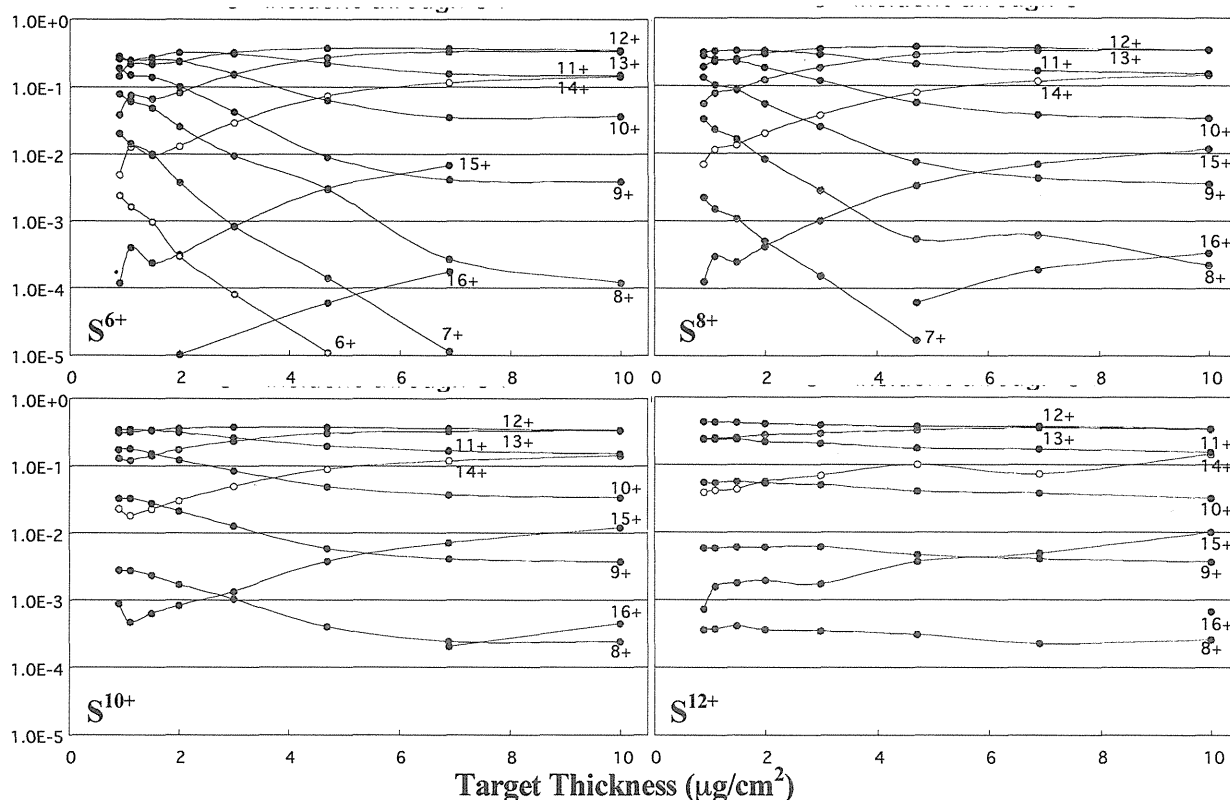
Fig. 1 Charge state distribution of 2.0 MeV/u S^{6+}, S^{8+}, S^{10+} and S^{12+} ions incident through carbon foil targets of 0.9, 1.1, 1.5, 2.0, 3.0, 4.7, 6.9 and 10 $\mu g/cm^2$.

mean charge, it almost reaches its equilibrium value of 12.4. The equilibrium mean charge states of ions in carbon foils have been estimated to follow semi-empirical or empirical formulas by Nikolaev and Dmitriev (ND) [6], To and Drouin (TD) [7], and Shima et al. [8]. For the present collision system, they give a value of 12.7 (ND and TD) or 12.8 (Shima et al.). Recently, Schiwietz and Grande proposed a pair of "improved" fit formulas for mean equilibrium charge states for gaseous and solid targets [9], which gives a better value of 12.6 for the present experiment.

References

[1] A. B. Wittkower and H. D. Betz, At. Data Nucl. Data Tables 5, 5 (1973); K. Shima et al., At. Data Nucl. Data Tables 34, 357 (1986); K. Shima et al., At. Data Nucl. Data Tables 51, 173 (1992).

[2] K. Kawatsura et al., Nucl. Instrum. Method B48, 103 (1990); Nucl. Instrum. Method B53, 421 (1991); M. Imai et al., Nucl. Instrum. Method B67, 142 (1992); K. Kawatsura et al., Nucl. Instrum. Method B124, 381 (1997); M. Imai et al., Nucl. Instrum. Method B193, 674 (2002).

[3] M. Imai et al., Physica Scripta T73, 93 (1997).

[4] M. Sataka et al., J. Phys. B35, 267 (2002); Phys. Rev. A65, 052704 (2002).

[5] Y. Sugiyama et al.,Nucl. Instrum. Method A281, 512 (1989).

[6] V. S. Nikolaev and I. S. Dmitriev, Phys. Lett. A28, 277 (1968).

[7] K. X. To and R. Drouin, Physica Scripta 14, 277 (1976).

[8] K. Shima, T. Ishihara, T. Mikumo, Nucl. Instrum. Method 200, 605 (1982).

[9] G. Schiwietz and P. L. Grande, Nucl. Instrum. Method B175_177, 125 (2001).

6. 2 MEASUREMENT OF DIFFUSION COEFFICIENTS
IN SOLIDS BY USING SHORT-LIVED RADIOTRACER OF ^{8}Li

S.C. JEONG[1], I. KATAYAMA[1], H. KAWAKAMI[1], H. ISHIYAMA[1], Y. WATANABE[1],
H. MIYATAKE[1], M. SATAKA, S. OKAYASU, H. SUGAI, S. ICHIKAWA, K. NISHIO,
T. NAKANOYA, N. ISHIKAWA, Y. CHIMI, Y. SUGIYAMA[2], T. HASHIMOTO[3],
M. YAHAGI[3], K. TAKADA[4], M. WATANABE[4], T. HASHIMOTO[5], T. ISHIKAWA[5]and
A. IWASE[6]

As an effort to effectively use the short-lived radioactive beams for materials science, we have developed a radiotracer method for diffusion studies in solids. The test experiment has been performed to measure the diffusion coefficients of Li in the sample of LiAl compound, by using a α-emitting radiotracer of ^{8}Li ($T_{1/2}$=0.838s). We have found that the time-dependent yields of the α-particles from diffusing ^{8}Li, primarily implanted in the sample, could be used as a measure of the diffusivity of the tracer in a non-destructive way. The method has been applied to measure the Li diffusion coefficients in one of the electrode materials of secondary Li-ion batteries.

The ^{8}Li beam of ~2MeV/amu was produced by using the JAERI-RMS and implanted to an appropriate depth of the sample after being energy-degraded. The beam was pulsed; beam-on for 1.5s and beam-off for 4.5s. The implanted ^{8}Li decays into two α-particles. One of them was measured as a function of time by an annular solid-state detector located close to the sample surface.

In Fig.1 are shown the time spectra of α-particle yields normalized by the time-dependent radioactivity of ^{8}Li-nuclei implanted in LiAl. The experimental spectra measured at different temperatures (20°C, 150°C, and 300°C) shows a clear diffusion effect: If ^{8}Li does not diffuse at all, the spectra should be constant over time. In Fig.1, the spectra are also compared with those from the simulations comprehensively described in [1].

Using the present method, we have measured the diffusivity of Li in the mixture of LiCoO$_2$ and SiS$_2$ based glass (SiS$_2$-glass), which is one of the electrode materials of solid Li-ion batteries.

---

[1] Institute of Particle and Nuclear Studies, KEK
[2] Nihon Advanced Technology
[3] Aomori University
[4] National Institute of Materials Science (NIMS)
[5] Tokyo University of Science
[6] Osaka Prefecture Unversity
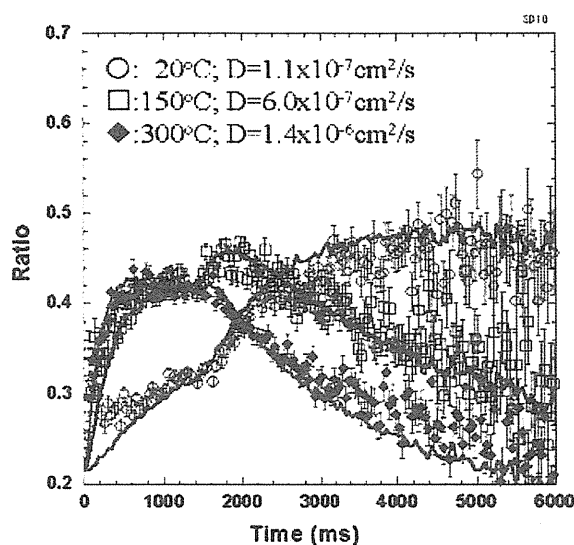
Fig.1 Normalized time spectra of α-yields at the temperature as indicated. The results from the simulation are also shown with most probable diffusion coefficients.
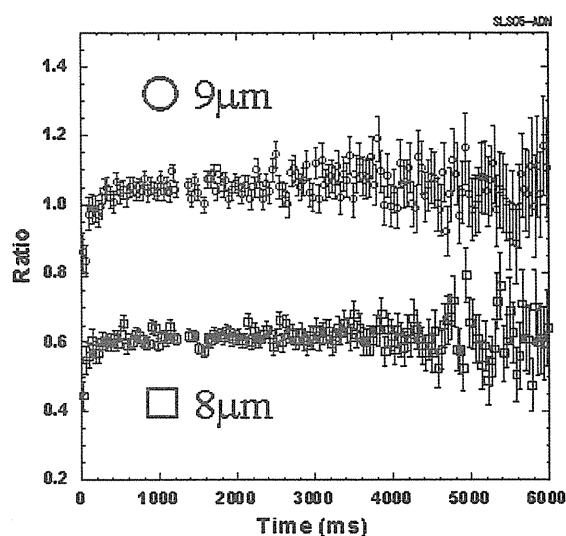
Fig.2 Normalized time spectra of α-yields measured at different depths of implantation as indicated. The temperature of the sample is the room temperature.

Although LiCoO$_2$ has been used as the positive electrode in the commercial secondary Li-ion batteries, the diffusion coefficient of Li has not been well known as yet. The SiS$_2$-glass (Li$_3$Po$_4$(0.01):Li$_2$S(0.63):SiS$_2$(0.36)) has been developed as a solid electrolyte of solid Li-ion batteries. The powder of LiCoO$_2$ and SiS$_2$-galss with the molar ratios of 6:4, intermixed at the grain sizes of several μm and pressed into the form of a thin disk, was used as the sample for the measurement at room temperature in order to investigate the surface resistance against Li diffusion on the grain boundaries of the constituents in the mixture. No significant diffusion effect was observed, as shown in Fig.2. The diffusion coefficients accessible by the present method are considered to be larger than 10^{-9}cm^2/s, implying that the diffusion coefficient of Li in the present sample is unexpectedly small. The electrode material, prepared in the way mentioned above, seems to be highly resistive to the Li diffusion at the beginning of charge-discharge processes in the solid batteries. Further investigation will be done in this respect.

References
[1] S.C. Jeong et al., Jpn. J. Appl. Phys., 42 (2003) 4576.

6. 3   VORTEX IMAGE OF TlBa$_2$Ca$_2$Cu$_3$O$_y$ CUPRATE SUPERCONDUCTOR FILM AND IRRADIATION EFFECT ON IT

Y. TANAKA[1], A. SUNDARESAN[1], A. IYO[1], T. NISHIO[2] and S. OKAYASU[2]

TlBa$_2$Ca$_2$Cu$_3$O$_y$ (Tl-1223) is a novel cuprate superconductor having high superconducting transition temperature (Tc) being more than 133 K [1]. Recently we established a fabrication method of this film having Tc of 108 K [2]. This film has very high critical current density (Jc > 1MA/cm^2) at 77 K and a strong pinning center. Comparing vortex image of as-prepared films and irradiated films, we found there is no drastic change in both of vortex image and its arrangements. It means that there are already strong pinning centers in the film before irradiation. Moreover we found a lot of vortex-anti-vortex pairs in Tl-1223 as-prepared films. We explained that the strong pinning center and anti-ferromagnetism hidden in superconductivity stabilize these pairs.

Heavy ion beams of 200 MeV Au are bombarded on Tl-1223 film of which thickness is 500 nm. Dose is 0.51 x 10^{10} ions/cm^2 corresponding to matching field of 0.2 T. Half of the film is covered by aluminum foil not to be bombarded. We scanned an image of trapped vortices in this film by a scanning SQUID microscope. The film was cooled to about 4 K under 0.5 μ T.

Figure 1 shows the scanning SQUID microscope image of Tl-1223 film. Left hand side is a part not being bombarded and right hand side is that being bombarded. There is a distorted vortex image indicated by (BD), and it is due to scratched hole in the film which we marked at the boundary between bombarded part and un-bombarded one. There were no drastic differences in image and arrangements between two parts. Large vortex image is typical one for film in which the magnetic flux is rapidly dispersing over the film surface. The local hexagonal arrangement was not seen either. Individual pinning by pinning centers destroys the hexagonal arrangement. Vortex-anti-vortex pair can also induce disordered arrangement of regular vortices.

We found a lot of pairs of dark spot and bright one in the scanning SQUID images of the as-prepared film as shown in Fig. 2. These are due to vortex-anti-vortex pair. Ordinarily an attractive force between vortex and anti-vortex is strong enough to annihilate the pair. The vortex-anti-vortex pair being created just below Tc tends to annihilate promptly. In ordinary high-Tc films, the pair can seldom be observed. The pairs were found in the irradiated films too.

Pairs can survive by the anti-ferromagnetism hindered by superconductivity. In the superconductivity in the cuprate superconductor, there is a competition between anti-ferromagnetic order and superconductivity. When superconductivity is the major order, there is reentrant anti-ferromagnetism near the vortex [3]. One of the CuO$_2$ plane is an ideal among three CuO$_2$ planes in a unit cell Tl-1223. It is free

[1]Nanoelectronics Research Institute, AIST
[2]Advanced Science Research Center, Japan Atomic Energy Research Institute
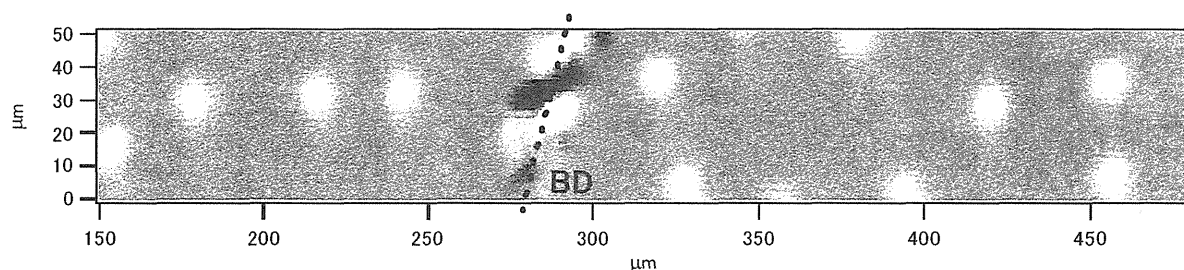
Fig. 1 Image of vortices in Tl-1223 film taken by a scanning SQUID microscope. Bright spots correspond to vortices. Right hand side was not irradiated part and left hand side was irradiated part. BD indicates boundary of these parts.
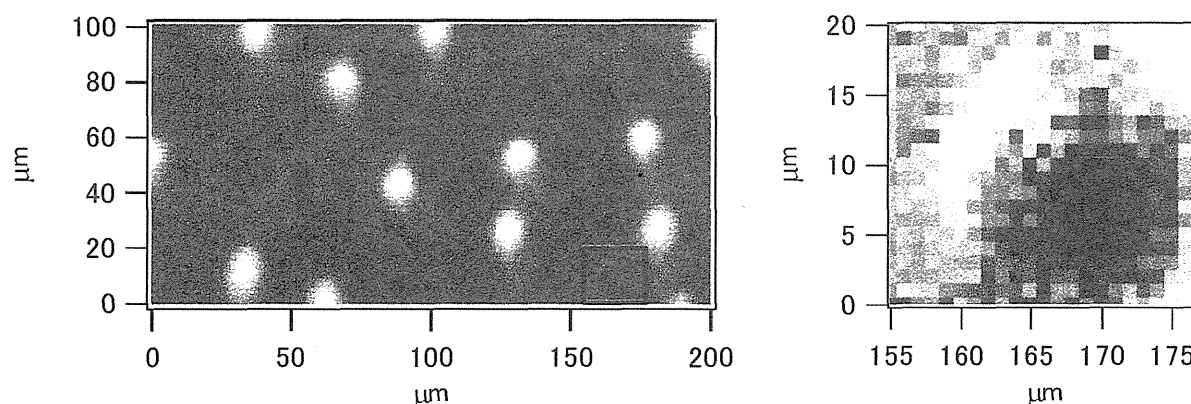
Fig. 2 Image of vortex and anti-vortex pairs (Left panel). There are more than 10 pairs. The right panel shows a high-contrast image of the expansion at the location indicated by a square in the left panel.

from disorder coming from the charge reservoir layer. This perfect CuO_2 plane can assist the coexistence of superconductivity and reentrant anti-ferromagnetism near the vortex. This situation is similar to that realized in the magnetic superconductor, in which there is a trap center for the anti-vortex due to inversion of polarity of magnetic field distribution created by a single vortex [4]. It disturbs the annihilation of the pair.

We are developing Tl-1223 film for a microwave device. The internal motion of vortex-anti-vortex pair should be frozen. The internal motion leads the loss of the microwave power. Further investigation of the pinning technology of Tl-1223 film using combination of heavy ion irradiation and scanning SQUID microscope technique is required.

References

[1] A. Iyo, Y. Tanaka, Y. Ishiura, M. Tokumoto, K. Tokiwa, T. Watanabe, H. Ihara, Supercond. Sci. Tech. 14 (2001)504.

[2] A. Sundaresan, Y. Tanaka, A. Iyo, M. Kusunoki, S. Ohshima, Supercond. Sci. Technol. 16(2003)L23.

[3] B.Lake B, H. M. Ronnow, N. B. Christensen, G. Aeppli, K. Lefmann, D. F. McMorrow, P. Vorderwisch, P. Smeibidl, N. Mangkorntong, T. Sasagawa, M. Nohara, H. Takagi, T. E. Mason, Nature 415(2002)299.

[4] M. Tachiki, H. Matsumoto, H. Umezawa, Phys. Rev. B 20(1979)1915.

7. Radiation Effects in Materials

This is a blank page.

7.1 STRUCTURE OF DISPLACEMENT CASCADES IN HEAVY IONS-IRRADIATED NICKEL BY X-RAY DIFFUSE SCATTERING

H.MAETA[1], N.MATSUMOTO, T.KATO, H.OTSUKA, H.SUGAI and M.SATAKA

The displacement cascades are one of the most important problems in the fusion reactor materials. In order to retain the defects in the original configuration after irradiations, it is necessary to irradiate at low temperature that the defects can not migrate. And after the irradiation the specimens have to be transferred to the measurement cryostat at low temperature, without any warming up. The x-ray diffuse scattering (XDS) is a powerful method to observe the defects [1]. The XDS has been used widely for the investigation of atomic point defects and smaller sized defect agglomerates [2, 3, 4]. We used these methods for an investigation of the displacement cascades after the heavy ions-irradiation at low temperature.

We report the measurements of the XDS close to Bragg reflections from low temperature heavy ions-irradiated Ni crystals. High purity Ni single-crystal specimens were spark-cut from a large single crystal grown by the Czochoralski method. The size of used all specimens is about 10 x 4 x 1 mm^3. The specimens were irradiated below 13K with 137 MeV xenon ions (Xe^{10+}) by the Tandem accelerator. After the irradiation the specimens were transferred to the x-ray cryostat at below 22K. The XDS experiments on the irradiated specimens were performed below 20K with four circle diffractometer using an 18kW rotating X-ray anode with a wave length of CuKα_1. The scattering intensities were measured close to Bragg (111) reflection in the [111] direction. The diffuse scattering intensity was obtained by taking a difference between the intensity from an irradiated and that from a non-irradiated region of the same specimen.

Fig. 1 shows a typical result for the x-ray scattering from nickel specimen irradiated with Xe. ions of 2.3×10^{13} ions/cm^2 close to the (111) reflection in the [111] direction measured at 22K, and annealed at 40 K, 93K and 300K. We can see a diffuse scattering over a large area of reciprocal lattice after the irradiation. After the annealing at 40K, this scattering disappeared. It is said that the recovery of this temperature is corresponding to the recovery stage I_A which the Frenkel defect of a closed interstitial and vacancy pair rearranges. To obtain the diffuse intensity, the scattered intensity before the irradiation was subtracted in each case. The diffuse scattering intensities were plotted on a double logarithmic scale versus q (deviation from the Bragg point). The results show that the typical $1/q^2$ dependence of Huang diffuse scattering [1] and the $1/q^4$ dependence of the Stokes and Williams [1] are clearly demonstrated. This fact indicates that the cascades are formed by the ion irradiated nickel metal [3] and amorphous like defect clusters are present inside the cascades.

---

[1] Hiroshima Kokusai Gakuin University
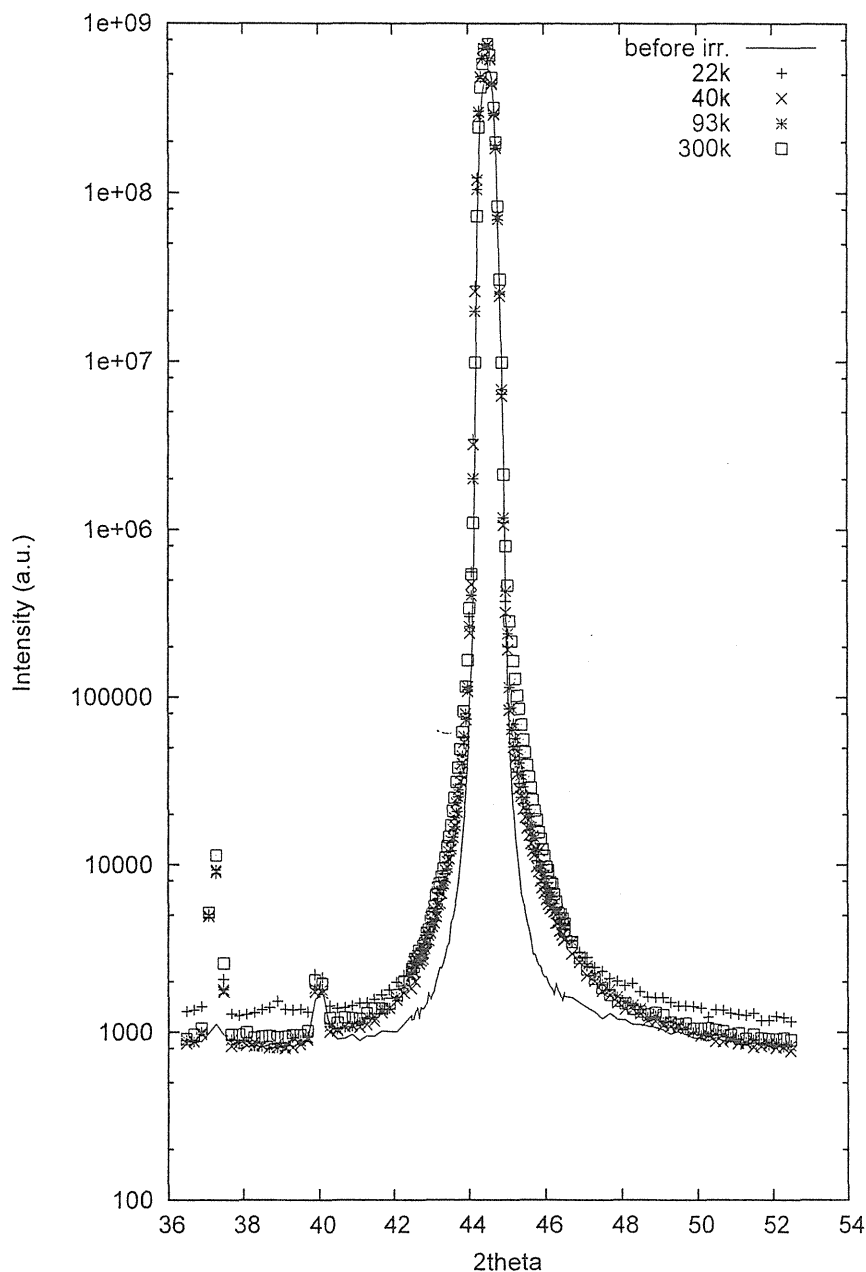
Fig. 1 Intensity of x-ray scattering from the nickel specimen irradiated with Xe ions of 2.3×10^{13} ions/cm^2 close to the (111) reflection in the [111] direction. The specimens were measured at 22K(+)after the irradiation, and annealed at 40 K ($\times$), 93K(*) and 300K($\square$).

References

[1] P.Ehrhart, J. Nucl. Mater. **216** (1994) 170.

[2] R.S.Averback and P.Ehrhart, J. Phys. F; Met. Phys. **14** (1984) 1374.

[3] B.v. Guerard, D.Grasse and J. Peisl, Phys. Rev. Lett. **44**(1980) 262.

[4] H.Yuya, T. Matsui, H. Maeta, H.Ohtsuka and H. Sugai, Nucl. Instrum.Methods, Phys. Res. B **148** (1999) 891.

7. 2 ELECTRONIC SPUTTERING OF OXIDES BY HIGH ENERGY HEAVY IONS: EXAMINATION OF SOME MODELS

N. MATSUNAMI[1], O. FUKUOKA[1], M. SATAKA, S. OKAYASU

We have been investigating the electronic sputtering yields of various oxides by high energy heavy ions [1-2], in order to understand the energy transfer mechanism from the electronic system to lattice, which has not been established yet. An objective of the present study is to examine models such as Coulomb explosion [3], thermal spike [4] and excitonic models [5]. Applying a carbon (C)-film collector method [1,2,6], we have performed measurements for ten kinds of oxides, i.e., amorphous (a)-SiO_2, crystalline (c)-SiO_2, $SrCe_{0.95}Yb_{0.05}O_{3-\delta}$(SCO), $SrTiO_3$ (STO), CeO_2, Al_2O_3, MgO, TiO_2, ZnO and $MgAl_2O_4$. These samples were subjected to irradiation with Xe, I, Ni, Ar and S ions with the energy of ~1 MeV/u. Sputtered atoms were accumulated in the C-films and analyzed by 1.8 MeV He Rutherford backscattering spectroscopy. The linear relationships were observed between the amount of atoms in the C-film collector and the ion dose (less than $10^{14}/cm^2$), and these were used to derive the sputtering yield of each component, with the calibrated collection-efficiency of the C-films [2].

Experimental results of the electronic sputtering are summarized as follows.
(1) The sputtering yields Y (atoms per ion), i.e., sum of sputtering yield of each component, are larger by 30 - 2000 times than the calculated yields of the elastic collision cascades.
(2) The electronic sputtering yields increase super-linearly with the electronic stopping power Se: $Y=(BSe)^n$. The exponent n varies from 1.4 (Al_2O_3) to 4 (CeO_2).
(3) Sputtering yield of each component is roughly proportional to the composition.
(4) The sputtering yields follow neither the mean charge of ions after transmission through the C-film nor the nuclear stopping power.

Based on the above results, we have suggested that the band gap is one of the relevant factors for the electronic sputtering [2]. Because it is reasonably assumed that the relaxation time from the highly excited states just after the ion impact to the lower excited states is very short, thus the available energy to the atomic displacement is due to the transition of electrons at lower excited states to the ground states (recombination). The available energy is proportional to or comparable with the band gap. Another factor is the conversion efficiency of the available energy into lattice or atomic displacement. The electron mobility thought to be a candidate for the electron-lattice coupling but it appears that this is not the case [2]. The second factor is under investigation. These results favor the excitonic model, if the band scheme holds. Anti-correlation between the electronic sputtering and luminescence yields also favor the excitonic model [7]. However, the existence of self-trapped exciton (STX: localized excited state coupled with lattice), which decays leading to atomic displacement, light emission or phonon generation, is known for a-SiO_2, c-SiO_2, Al_2O_3 and MgO, and is unknown for ZnO. Existence of STX is unclear for SCO, $SrTiO_3$, CeO_2, TiO_2 and $MgAl_2O_4$. Hence, a simple STX model is not applicable to the electronic sputtering. Furthermore, super-linear dependence of the electronic sputtering yields on the band gap indicates that the multiple excited states play an important role. A speculation is that self-trapping is easier for multi-excitons.

---

[1] Division of Energy Science, EcoTopia Science Institute, Nagoya University

Now, Coulomb explosion model is examined. Charge states should be kept for ions be ejected and thus considerable charged fraction should be observed in the sputtered particles, if this model is valid. We have measured the positive ion yields by using a double-cylindrical Faraday-cup which was negatively biased, with and without ions transmitted through a C-film. A few kV positive-bias was applied to the C-film to minimize the effects due to electrons emitted from the C-film. A typical result is shown in Fig. 1 for 100 MeV Xe on SiO_2 film. The positive ion yields are ~33, 25, 15 and 8 for 200 MeV Xe, 100 MeV Xe, 90 MeV Ni and 60 MeV Ar on SiO_2 film on Si, taking into account that the mean charge of these ions after C-film transmission is 30, 25, 19 and 13, respectively. The sputtering yields are 410, 360, 120 and 32. Thus the positive ion fraction is much less than unity and is roughly 10 % for Xe and Ni. For Ar, the fraction is somewhat large, but less than unity. Similar situation is found for SCO film on Si. The positive ion yields are ~50 and ~30 for 100 MeV Xe and 90 MeV Ni. The corresponding sputtering yields are 400 and 230. The positive ion fraction will be much reduced, when the corrections is made for the electron emission from the Faraday cup [8]. Hence, the charged fraction is very small and neutral components are dominant in the electronic sputtering. This result indicates that the Coulomb explosion model is unsound. A possibility is suggested that neutralization occurs during separation of ions with each other [9]. It is very hard to find a reason that separation force operates after neutralization because this is not the free space case and this model is too sensitive to the neutralization probability. Thus, the possibility is unrealistic.

Next, thermal spike model is examined. In this model, a region along an ion becomes hot or melted, generating a modified region. If this model were valid, a hot or melted region is reasonably assumed to follow rapid quenching, resulting in "amorphous track" for crystalline samples. Then it is anticipated that overlap of tracks eventually leads to crystal into amorphous transformation. According to preliminary results of X-ray diffraction of c-SiO_2, no amorphisation was observed for 90 MeV at $3x10^{12}/cm^2$ and $0.37x10^{14}/cm^2$, and 100 MeV Xe at 0.2 to $0.9x10^{14}/cm^2$. Track radius by these ions is deduced to be 2.9 and 4.5 nm [4] and dose required for overlap of tracks is estimated as 3.8 and $1.2x10^{12}/cm^2$, respectively. Hence, overlap of tracks does not lead to crystal into amorphous transformation. A possibility is re-crystallization of amorphous region by ion impact. However, XRD results of a-SiO_2 shows no indication of re-crystallization for 100 MeV Xe at $1x10^{14}/cm^2$. These results do not favor the thermal spike model. There seems to be no evidence for generation of hot or melted zone by high energy heavy ions.

Furthermore, an interesting result is that the electronic sputtering yields of a-SiO_2 and c-SiO_2 are the same for the same electronic stopping power, when a small difference in their densities (2.2 and 2.635 g/cm^3 for a-SiO_2 and c-SiO_2) is taken into account in the calculation of the stopping powers. This result, again, is unfavorable with the thermal process for the electronic-excitation-induced atomic-displacement, because the thermal conductivity of c-SiO_2 is much larger than that of a-SiO_2 [10], the heat capacity of both SiO_2 are reasonably assumed to be comparable, and no clear evidence for melting is found as described above.
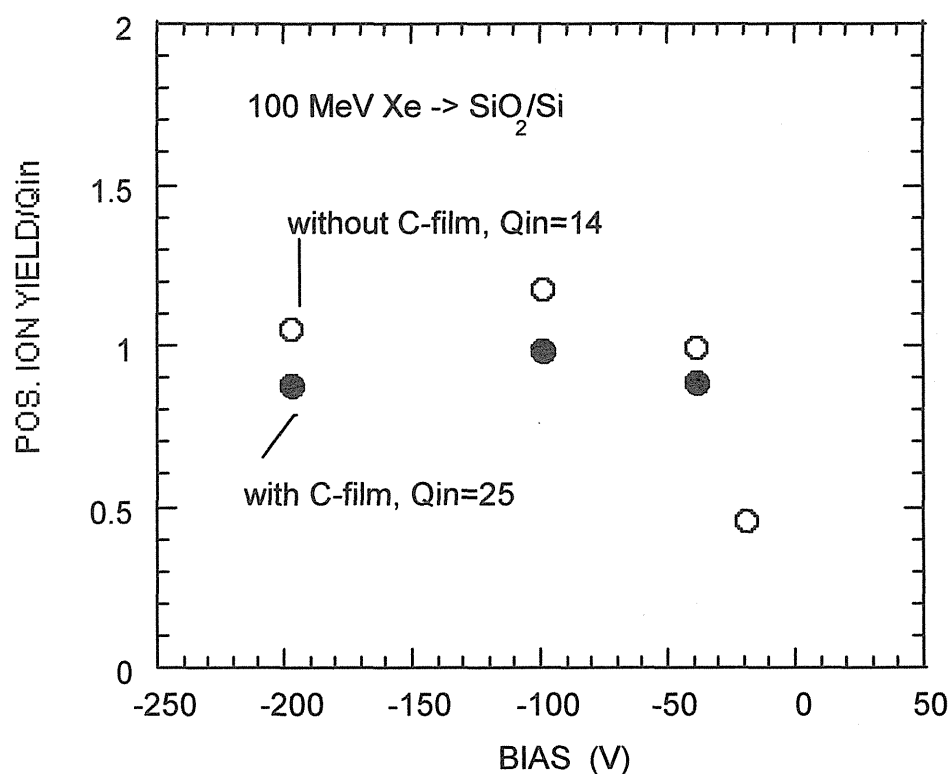
Fig. 1 Bias dependence of positive ion yields per incident charge for 100 MeV Xe
on SiO_2/Si without and with C-film. Qin with or without C-film means the mean charge of
Xe ions after C-film transmission or the incident charge of Xe ions.

REFERENCES

[1] N. Matsunami, M. Sataka, A. Iwase, Nucl. Instrum. Meth. B193(2002)830.

[2] N. Matsunami, M. Sataka, A. Iwase, S. Okayasu, Nucl. Instrum. Meth. B209(2003)282.

[3] R. L. Fleischer, Tracks to Innovation, Springer-Verlag, 1998.

[4] M. Toulemonde, C.H. Dufour, A. Meftah, E. Paumier, Nucl. Instrum. Meth. B166-167
    (2000)903.

[5] N. Itoh, A. M. Stoneham, Materials Modification by Electronic Excitation, Cambridge
    2001.

[6] N. Matsunami, M. Sataka, A. Iwase, T. Inami, M. Kobiyama, J. Nucl. Mater.
    302(2002)206.

[7] K. Kimura, Nucl. Instrum. Meth. B212(2003)123.

[8] N. Matsunami, E. Hatanaka, J. Kondoh, H. Hosaka, K. Tsumori, H. Sakaue, H. Tawara,
    Phys. Scripta 65(2002)278.

[9] E. M. Bringa, Nucl. Instrum. Meth. B209(2003)1.

[10] D. R. Lide, CRC Handbook of Chemistry and Physics, 84th ed. CRC Press, 2003.

7.3 ION-VELOCITY EFFECT IN OXIDE SUPERCONDUCTORS IRRADIATED WITH HIGH-ENERGY HEAVY IONS

N. ISHIKAWA, Y. CHIMI, O. MICHIKAMI[1], T. HASHIMOTO[1],
T. KAMBARA[2], R.NEUMANN[3], A. IWASE[4]

In $EuBa_2Cu_3O_y$ oxide superconductors irradiated with high-energy heavy ions, it is well established that the c-axis lattice parameter increases linearly as a function of ion-fluence, reflecting that each ion creates lattice defects[1,2]. In this case, most of the defect creation is attributed to the high-density electronic energy deposition. The characteristic of this irradiation-induced lattice expansion is that, when ion-velocity is sufficiently high ($v \geq 2.6 \times 10^9$cm/s), the lattice expansion per unit-fluence varies as a function of the electronic stopping power, S_e, and follows the power law ($\sim S_e^n$ (n=4)) [2]. However, as ion-velocity is lowered down to $v \leq 1.7 \times 10^9$cm/s, the lattice expansion per unit fluence becomes greater and deviates from the power law. Therefore, it is expected that even if the value of S_e is the same, the lattice expansion is expected to become greater for lower ion-velocity. However, the velocity dependence appeared in the low velocity region (known as the velocity effect[3]) is not quantitatively clarified yet. In this work, the velocity effect is investigated by performing the irradiations having same S_e value but different ion-velocity.

The $EuBa_2Cu_3O_y$ (EBCO) thin films with the thickness of 300nm were prepared by sputtering method. The irradiations with 80MeV I, 125MeV Br, 1.09GeV Mo, and 3.54GeV Xe ions were performed at room temperature. All of the irradiations have almost the same S_e (S_e=26-28 (MeV/(mg/cm^2))). The energy (velocity) ranges from 0.6-26MeV/nucleon(1.1×10^9cm/s~7.1×10^9cm/s). The fluence dependence of c-axis lattice parameter was measured for each irradiation. The irradiations with 80MeV I and 125MeV Br ions were performed by using the tandem accelerator at JAERI-Tokai. The irradiations with 1.09GeV Mo and 3.54GeV Xe ions were performed by using the UNILAC accelerator at GSI and the ring cyclotron at RIKEN, respectively.

The recent result of irradiation-induced lattice expansion for 1.09GeV Mo irradiation is shown in Fig.1. Here $\Delta c/c_o$ is the change in c-axis lattice parameter, Δc, normalized by the c-axis lattice parameter before irradiation, c_o. Linear increase in c-axis lattice parameter is observed as has been observed also for irradiations with 80MeV I, 125MeV Br, and 3.54GeV Xe ions. The slope of the lattice expansion, $(\Delta c/c_o)/\Phi$, is plotted as a function of energy in the unit of MeV/nucleon in Fig.1, where Φ represents ion-fluence. Although S_e is almost the
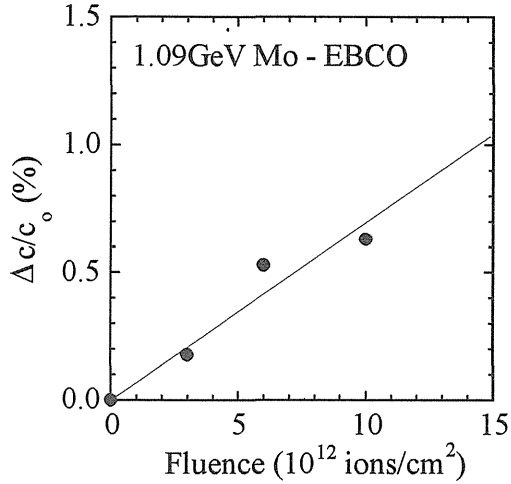
Fig.1. Fluence dependence of c-axis lattice parameter for EBCO films irradiated with 1.09GeV Mo ions.
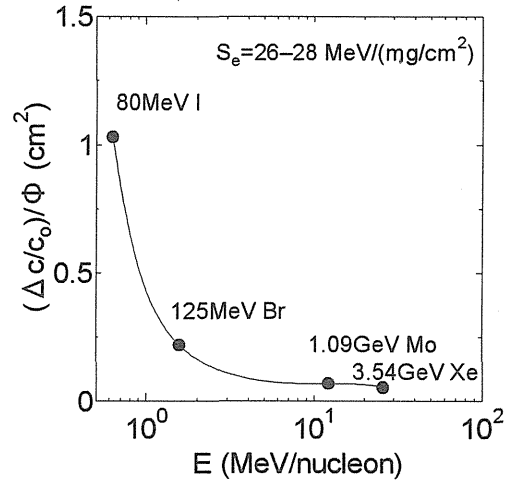
Fig.2. Energy dependence of change in c-axis lattice parameter per unit fluence for the irradiations with ions having almost same S_e.

same, the lattice expansion per unit fluence changes rapidly especially in the low velocity region of around v~1.4×10^9cm/s. In the high-velocity region of around v~4.7×10^9cm/s, it is found that the velocity effect still exist, but is very small.

We have already demonstrated that the electronic excitation effects in oxide superconductors is scaled by the primary ionization rate and proposed that the primary ionization causes Coulomb repulsion between ionized atoms leading to atomic displacements[2,4]. The velocity dependence of the electronic excitation effect shown in Fig.2 exhibits similar behavior to the velocity dependence of the fraction of S_e covering thermal energy which contributes to local melting of lattice system[5]. This result supports the thermalized ion explosion model[6]. The thermalized ion explosion model assumes that the ionization of target atoms triggers Coulomb repulsion of target atoms, and successively the kinetic energy of atoms is converted to thermal energy which contributes to local temperature increase.

References

[1] N. Ishikawa et al. Physica C 259 (1996) 54.

[2] N. Ishikawa et al. Nucl. Instr. Meth. B 193 (2002) 278.

[3] A. Meftah et al., Phys. Rev. B48 (1993) 920.

[4] N. Ishikawa et al., J. Phys. Soc. Jpn. 69 (2000) 3563.

[5] G. Szenes, Phys. Rev. B60 (1999) 3140.

[6] L.E. Seiberling et al. Radiat. Eff. 126 (1993) 201.

7. 4 QUANTITATIVE ANALYSIS OF RADIATION-INDUCED ATOMIC DISORDERING IN MAGNESIUM ALUMINATE SPINEL

M. SHIMADA[1], K. YASUDA[1], S. MATSUMURA[1], C. KINOSHITA[1], Y. CHIMI and N. ISHIKAWA

Magnesium aluminate spinel $MgO \cdot nAl_2O_3$ has excellent radiation resistance, and this is attributed to its crystallographic feature. The spinel structure are formed by oxygen fcc sublattice, and cations locate on only 1/8 of tetrahedral (IV) sites and 1/2 of octahedral (VI) sites in ideal spinel. Therefore significant numbers of IV and VI sites are empty. It is expected that the formation of defect clusters is suppressed by atomic disordering and/or interstitial-vacancy recombination through the empty sites. So it is very important to investigate radiation-induced atomic disordering. In the present study, the local atomic disordering around ion tracks are investigated in spinel subjected to high-density electronic excitation.

TEM specimens of single crystal $MgO \cdot nAl_2O_3$ ($n = 1.1$) were prepared by mechanical polishing and ion milling, followed by the annealing at 1673 K for 2 hours. The annealed specimens were irradiated with 200 MeV Xe ions at ambient temperature up to a fluence of 2.0×10^{16} ions $/m^2$. An analytical TEM, FEI tecnai-20 equipped with EDX analyzer at High Voltage electron Microscopy Laboratory of Kyushu University, was operated at 200 kV to perform HARECXS (*High Angular Resolution Electron Channeling X-ray Spectroscopy* [1,2]) experiments. HARECXS profiles were obtained by rocking the incident electron beam between $-4g$ and $+4g$ ($g = 400$) Bragg conditions. The atomic configurations were evaluated by fitting the experimental and calculation profiles with a parameter of occupation probability.

In a plan view, ion tracks were observed as sharp dot contrasts, and they changed their contrast from black dot under overfocus condition to white dot under underfocus condition in bright field images. The ion tracks have columnar dark contrasts with 5 nm in diameter in an inclined view, and the black and white dot contrasts were observed at the incident surface of the specimen. This suggests that tiny pits were formed by the atom sublimation at the irradiation surface. Fig.1 shows experimental HARECXS profiles of unirradiated specimen (a) and irradiated ones up to 3.0×10^{15} ions/m^2 (b), 5.0×10^{15} ions/m^2 (c) and 2.0×10^{16} ions/m^2 (d). Ion-irradiation is seen to induce weak dependence in HARECXS profiles against incident beam direction. The change in atomic configurations at IV and VI/fcc sites are summarized in Table 1. Ion-irradiation is clearly seen to induce atomic exchange between Mg^{2+} on IV sites and Al^{3+} on VI sites. O^{2+} is also found to move to IV sites. The size of disordered regions around ion tracks were evaluated to be 10–14 nm in diameter with an assumption that the inside of the region is random atomic configuration. The evaluated disordered zone is considerably larger than that of 5 nm in diameter observed in bright field images.

---

[1]Kyushu University
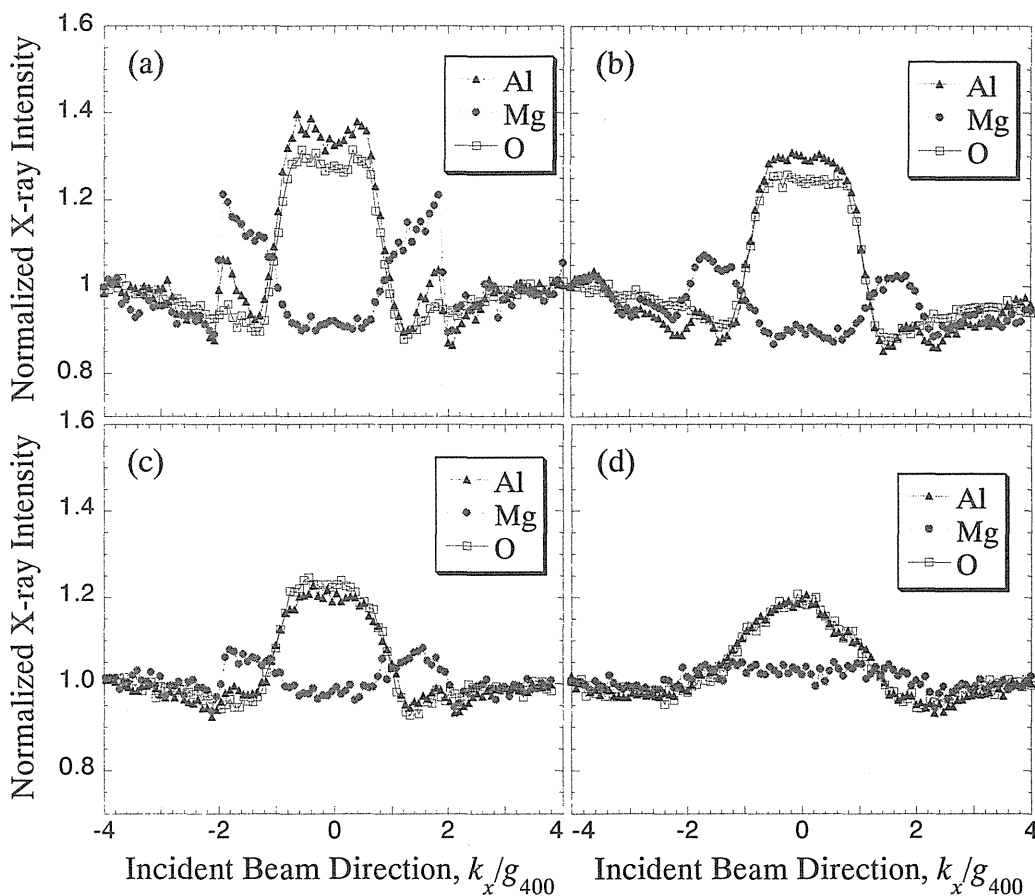
Fig. 1 HARECXS profiles of (a) unirradiated specimen and irradiated ones with 200 MeV Xe^{14+} up to (b) 3.0×10^{15} ions/m^2, (c) 5.0×10^{15} ions/m^2 and (d) 2.0×10^{15} ions/m^2.

Table 1. Occupation probabilities of Mg^{2+}, Al^{3+} and O^{2-} on the IV-sites, the VI-sites and fcc sites in unirradiated $MgO \cdot 1.1Al_2O_3$ and irradiated ones with 200 MeV Xe^{14+} up to 3.0×10^{15} ions/m^2, 5.0×10^{15} ions/m^2 and 2.0×10^{16} ions/m^2.

	Mg^{2+}		Al^{3+}		O^{2-}	
	IV	VI/fcc	IV	VI/fcc	IV	VI/fcc
Unirradiated	0.72	0.28	0.15	0.85	0.00	1.00
3.0×10^{15} ions/m^2	0.68	0.32	0.17	0.83	0.01	0.99
5.0×10^{15} ions/m^2	0.62	0.38	0.26	0.74	0.02	0.98
2.0×10^{16} ions/m^2	0.52	0.48	0.26	0.74	0.04	0.96

References

[1] T. Soeda, M. Shimada, S. Matsumura, N.J. Zalusec, C. Kinoshita, *Proc. 4th Pacific Rim Int'l. Conf. Advanced materials and Processing (PRICM4)*, 2(2001) 1423.

[2] S. Matsumura, T. Soeda, M. Shimada, N.J. Zalusec, *Proc. 15th Int'l. Cong. Electron Microscopy (ICEM)*, 1(2002) 187.

7. 5 INFLUENCES OF HIGH ENERGY HEAVY IONS ON LONG- AND SHORT- RANGE STRUCTURES OF Li_2TiO_3

T. NAKAZAWA, V. GRISMANOVS[1], D. YAMAKI, Y. KATANO, T. ARUGA

Lithium metatitanate (Li_2TiO_3) has the rock-salt structure in which the cations occupy octahedral sites in a cubic close-packed oxide ion array [1]. The Li_2TiO_3 ceramics is regarded as one of the most suitable candidates for the solid tritium breeder material of D-T fusion reactors [2]. Radiation damages produced in Li_2TiO_3 under an operating fusion reactor result in the microstructure changes and hence have an influence on the tritium release behavior, and on thermal and mechanical properties of Li_2TiO_3. Thus, the study of microstructure changes and irradiation defects in Li_2TiO_3 is essential to evaluate its irradiation performance. Recently, the simultaneous exposure of Li_2TiO_3 to H^+, He^+ and O^{2+} ions has been reported to cause the appearance of TiO_2 (anatase) phase in its surface layer [3]. In order to obtain further information on structural changes, we irradiated Li_2TiO_3 with Xe and O ions, and performed X-ray diffraction (XRD) and Raman spectroscopy measurements.

Li_2TiO_3 has the cation-ordered structure. Long-range order in Li_2TiO_3 structure is identified from X-ray reflections of lattice planes which the cations lie on. Short-range order is done from the Raman spectrum of the location of

Table 1. Irradiation conditions of Li_2TiO_3

Ion	Xe	O
E (MeV)	160	80
Fluence (ions/m²)	$3.3 \times 10^{16}, 3.4 \times 10^{18}$	$4.6 \times 10^{19}, 1.4 \times 10^{20}$
D (GGy)	0.03, 3.4	2.6, 8.0
R_p (μm)	10	50
S_n (keV/nm)	0.03	2.0×10^{-4}
S_e (keV/nm)	20.0	1.2

E: energy of ions, D: accumulated radiation dose, R_p: mean projected range, S_n: nuclear stopping power at near surface, S_e: electronic stopping power at near surface. R_p, S_n, and S_e are calculated with the SRIM2000 code [4].

cations in the octahedral and tetrahedral coordination sites in Li_2TiO_3 structure. Influences of irradiation on long- and short-range orders are examined by XRD technique and Raman spectroscopy. Irradiation conditions are listed in Table 1. During XRD measurements, samples are masked with a gold foil of 10 μm in thickness leaving a hole 8 by 5 millimeters in order to remove diffractions from the unirradiated portion. The XRD peak intensities are normalized to a specified XRD peak from the gold foil. Raman spectra are measured for samples before and after irradiations at ambient temperature with JASCO NR 1100 Raman spectrometer operated at 100 mW using the 488 nm line Ar laser for the excitation source.

The changes in XRD patterns of samples irradiated have been observed in the range of 19° to 25° for 2Θ. In the case of the O ion irradiations, the XRD peaks decrease gradually with fluences. On the other hand, the peak entirely disappeares with the Xe ion irradiation at small fluences of about 10^{16} /m², that is, at the accumulated radiation dose of 0.03 GGy. Such decrease in XRD intensities means that long-range disorder is caused with the irradiation [5].

Raman spectra of samples before and after irradiation are shown in figure 1. The Raman intensities were normalized to the peak around 660 cm⁻¹. Raman spectrum gives information on short-range order in contrast with the XRD pattern. The vibrational spectra of lithium titanate oxides have been studied using the results of group-theoretical analyses [6, 7]. In lithium titanate, the frequencies in the 700-550cm⁻¹ region are known to be assigned to Ti-O stretches in TiO_6 octahedra. In oxides where lithium is octahedrally coordinated by oxygen the frequencies of the Li-O stretches are known to lie

within the 250-400 cm⁻¹ region. When the lithium coordination is tetrahedral, the Li-O stretches lie in the 400-550 cm⁻¹ region. In the Li_2TiO_3 structure the lithium occupies both octahedral and tetrahedral positions.

In the case of the O ion irradiations, no change in Raman spectrum occurs up to the maximum fluence of 1.4×10^{20} /m². On the other hand, in the case of the Xe ion irradiations, the peak intensities have been reduced even at the smaller fluence of 3.3×10^{16} /m² and still more at 3.3×10^{18} /m² with the Xe ion irradiation. The reductions suggest that most of the Li_2TiO_3 structures have been destroyed with the Xe ion irradiation: the destruction of Li_2TiO_3 structures means the short-range disorder. However, relative intensities of Raman peaks in the 250-400 cm⁻¹ region are observed to be increased by comparison with those before irradiation. In fact, note that the relative increments of the peaks signify that some parts of the coordinations remain undamaged or recover quickly. The increase in relative peak intensities in the 250-400 cm⁻¹ region with respect to those in the 400-700 cm⁻¹ region implies that in the irradiation region the surviving LiO_6 octahedra structures are more than the surviving TiO_6 octahedra and LiO_4 tetrahedra ones.

These changes of XRD patterns and Raman spectra due to the irradiation suggest that the

Figure 1. Raman spectra of Li_2TiO_3 irradiated with the 80 MeV O and 160 MeV Xe ions, and of Li_2TiO_3 before irradiation. Raman intensities are normalized to that around 660 cm⁻¹.

influence of the Xe ion irradiation on the disorder transformation is greater than that of the O ion irradiation with respect to the destruction of Li_2TiO_3 structure. This fact indicates that the disorder transformation, including short-range disordering, in Li_2TiO_3 takes place on irradiation with ions with the electronic stopping power ≥ 20.0 keV/nm. Note that the nuclear stopping power merely produces the number of displacements per atom (dpa) $\ll 0.1$ dpa, which is too small to destruct the lattice structure of Li_2TiO_3, in the near surface region for the present irradiations.

References

[1] M. Castellanos and A.R. West, J. Mater. Sci. 14 (1979) 450.

[2] P. Gierszewski, Review of properties of lithium metatitanate, Report no. CFFTP G-9561, 1995.

[3] T. Nakazawa, V. Grismanovs, D. Yamaki, Y. Katano, T. Aruga and A. Iwamoto, 2000 Int. Conf. on Ion Implantation Technology Proc. (2000) 753.

[4] J.F. Ziegler, J.P. Biersack and U. Littmark, The Stopping and Range of Ions in Solids, Pergamon, Oxford, 1985.

[5] T. Nakazawa, V. Grismanovs, D. Yamaki, Y. Katano, T. Aruga, JAERI-Review 2003-028 (2003) 102.

[6] E.V. Proskuryakova, O.I. Kondratov, N.V. Porotnikov and K.I. Petrov, Russ. J. Inorg. Chem. 28 (1983) 791.

[7] N.V. Porotnikov, N.G. Chaban and K.I. Petrov, Russ. J. Inorg. Chem. 28 (1983) 1402.

7. 6 ELECTRONIC EXCITATION EFFECTS ON THE MICROSTRUCTURAL EVOLUTION IN CeO₂ UNDER HIGH ENERGY ION IRRADIATION

T. SONODA[1], M. KINOSHITA[1], N. ISHIKAWA, Y. CHIMI and A. IWASE[2]

For progressing high burnup extension of LWR fuels, formation and growth mechanism of a crystallographic re-structuring in the periphery region of high burnup fuel pellets, as named "rim structure" [1] should be clarified. This structure is characterized by the existence of highly dense small sub-grains whose size is approximately 200 nm, and the accumulation of small pores with average size around 1 μm. The structure shall be formed by the accumulation and mutual interactions of radiation damages, fission products (FPs) and electronic excitations deposited partially by nuclear fissions [2].

In order to separate each of the processes as radiation damages, FPs and the effects of electric excitation, clarify the mutual interactions among them, and understand the formation mechanism of this restructuring, 70 – 210 MeV FP ions (Xe, I, Zr) irradiation examinations on CeO₂, as a simulation of fluorite ceramics of UO₂, have been done at JAERI-Tandem facility. Microstructural evolutions in the specimen are observed in a 300kV FE-TEM (HF-3000) at CRIEPI. This paper mainly reports electronic excitation effects on the microstructural evolution in CeO₂.

Fig. 1 shows typical micrographs of CeO₂ under irradiations with 100 MeV Xe at room temperature. This figure indicates that the irradiations of high energy FPs at room temperature cause the typical radiation damage, "ion tracks". Table 1 summarizes the mean diameter of ion tracks under several FP ions and temperature. This table suggests that the affected area of electronic excitation by fissions in CeO₂ seems to be around 5 ~ 7 nm φ, because the fission energies of Median light FPs and Median heavy FPs are around 95 MeV and 67 MeV, respectively. Fig. 2 shows the square of the mean diameter of ion tracks as a function of electronic stopping power (S_e). The dotted line in this figure indicates the estimated value derived from Szenes model [3], which is based on Thermal spike model [4]. In this figure, the square of track diameter tends to be proportional to S_e. This result suggests that the diameter of ion tracks, i.e. affected area by high-energy fission products, will be estimated by S_e.

In order to clarify the overlapping effect of ion tracks on the microstructural evolution, high fluence irradiation up to 1×10^{15} ions/cm² have been done, and observed microstructural exchanges by SEM/TEM. In the case of the irradiation on the wedge-shaped TEM specimen, the elliptical deformation of diffraction spots and faint "halo-pattern" become clear as the fluence becomes higher, $> 1 \times 10^{12}$ ions/cm², that means the inner structure of ion tracks under room temperature shall be disordered, like as amorphous or grain-subdivided [5]. Moreover, as shown in fig. 3, some part of grain surfaces under 210 MeV Xe irradiation to a fluence of 1×10^{15} ions/cm² are changed to concavo-convex, whose size of convex is around 1μm. Similar surface transient has also been observed in LWR fuels. This result suggests that this surface transient in CeO₂ is occurred by the mutual interaction between the overlapping effects of high-energy electronic excitation and the accumulation of radiation damage, estimated damage by SRIM code is around 9.0×10^{-2} dpa.

[1] Sector, Nuclear Power Generation Technology, Nuclear Technology Research Laboratory, Central Research Institute of Electric Power Industry (CRIEPI)
[2] Research Institute for Advanced Science & Technology, Osaka Prefecture University

Ion	Electric Charge	Irradiation energy (MeV)	Temp. (°C)	Mean diameter of ion tracks (nm ϕ)
Xe	+14	210	Room	9.30 ± 0.12
	+10	100	Room	7.91 ± 0.09
	+14	80	Room	5.68 ± 0.07
	+14	100	300	7.44 ± 0.11
I	+7	80	Room	5.14 ± 0.07
	+7	70	Room	~ 4.6
Zr	+9	100	Room	7.56 ± 0.16

Table 1. Mean diameter of ion tracks under several FP ions and temperature in CeO_2.

Fig. 1. Typical micrographs of CeO_2 under irradiation with 100 MeV Xe (left), and higher magnification image (right).

Fig. 2. Square of the mean diameter of ion tracks as a function of electronic stopping power (S_e). Dotted line indicates the estimated value by Szenes model [3].
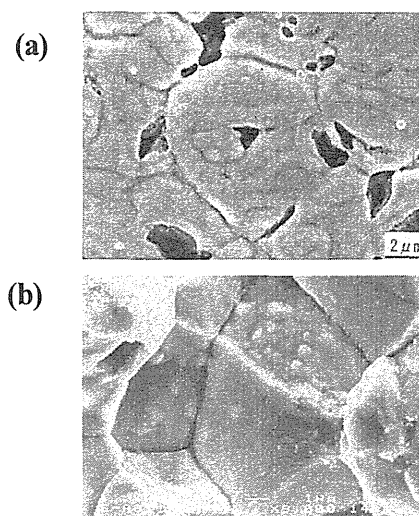
Fig. 3. SEM image of grain surfaces in CeO_2 under irradiation with 210 MeV Xe to a fluence of 1 x 10^{15} ions/cm^2 (a), and grain surface transient in LWR fuel (34 MWd/kgU,400°C) (b).

References

[1] J. O. Barner, M. E. Cunningham, M. D. Freshley, and D. D. Lanning, HBEP-61, 1990, Battelle Pacific Northwest Laboratories.

[2] T. Sonoda, M. Kinoshita, I.L.F. Ray, T. Wiss, H. Thiele, D. Pellottiero, V.V. Rondinella and Hj. Matzke, Nucl. Instr. and Meth. B, 191 (2002) 622-628.

[3] G. Szenes, Phys. Rev. B51 (1995) 8026.

[4] M. Toulemonde, J. M. Costantini, C. Dufour, A. Meftah, E. Paumier, F. Studer, Nucl. Instr. Meth. Phys. Res. B 116 (1996) 37.

[5] T. Sonoda, M. Kinoshita, N. Ishikawa, Y. Chimi, A. Iwase, JAERI-Rev. 2003-028 (2003) 104-105

7. 7 ELECTRONIC STOPPING POWER DEPENDENCE
OF ATOMIC MIXING INDUCED BY SWIFT HEAVY IONS IN Bi-Al$_2$O$_3$ INTERFACES

R. NAKATANI[1], R. TANIGUCHI[1], Y. CHIMI, N. ISHIKAWA, M. FUKUZUMI[1], Y. KATO[1], H. TSUCHIDA[2] and A. IWASE[1]

We have recently reported that the high-density electronic excitation due to 200 MeV Xe ion irradiation results in an effective atomic mixing at Bi-Al$_2$O$_3$ interface. In this report, we show that the amount of atomic mixing induced by swift heavy ion irradiations increases with increasing the electronic stopping power of irradiating ions.

Bismuth thin films (about 100 nm thick) were deposited on an α-Al$_2$O$_3$ single crystal substrates by vacuum evaporation at room temperature in a vacuum below 5×10^{-6} Torr. The specimens were irradiated at room temperature with 150 MeV ^{86}Kr, 200-MeV ^{136}Xe or 200 MeV ^{197}Au ions up to the fluence of 1×10^{14}/cm^2. After the irradiation, the mixing states of the Bi-Al$_2$O$_3$ interfaces were characterized by using Rutherford backscattering (RBS) spectroscopy. For comparison, irradiations with 3 MeV Si ions were also performed using 2MV tandem accelerator at Nara Women's University.

Figures 1, 2 and 3 show the RBS spectra of Bi-Al$_2$O$_3$ system for the Bi layer before and after the irradiation with Kr, Xe or Au ions, respectively. The figures indicate that the amount of atomic mixing at the interface increases with increasing the electronic stopping power, Se, of irradiating ions. For the irradiation with Kr ions, the electronic stopping power of which is much smaller than those for Xe and Au ions, the atomic mixing can rarely be observed. Figure 4 shows the result for 3 MeV Si ion irradiation up to 1×10^{15}/cm^2. Although the energy deposited elastically into the specimen is about 10-30 times larger for 3MeV Si irradiation than for Xe and Au irradiations, we cannot find any atomic mixing by 3MeV Si irradiation. The present results confirm that the atomic mixing can be induced by the high density electronic excitation at Bi-Al$_2$O$_3$ interface.

We thank Profs. N. Sakamoto and H. Ogawa for the irradiation experiments at Nara Women's University.
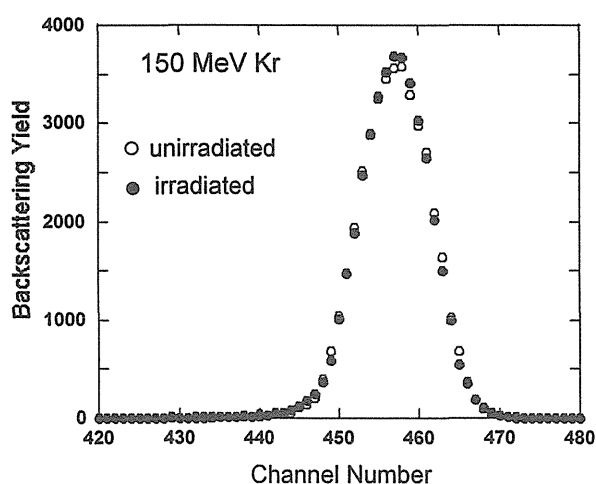
Fig.1 RBS spectra of Bi-Al$_2$O$_3$ system for Bi layer before irradiation (open circles) and after irradiation with 150 MeV Kr ions (solid circles). Se of 150 MeV Kr ions for Bi is 16keV/nm.

1 Osaka Prefecture University
2 Kyoto University
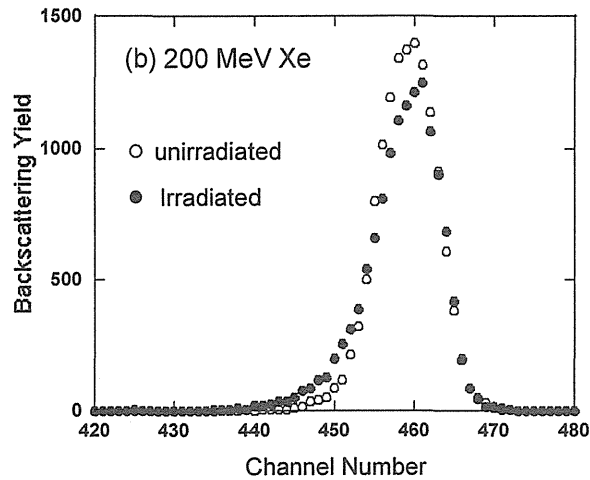
Fig. 2 RBS spectra of Bi-Al₂O₃ system for Bi layer before irradiation (open circles) and after irradiation with 200 MeV Xe ions (solid circles). Se of 200 MeV Xe ion for Bi is 24keV/nm.
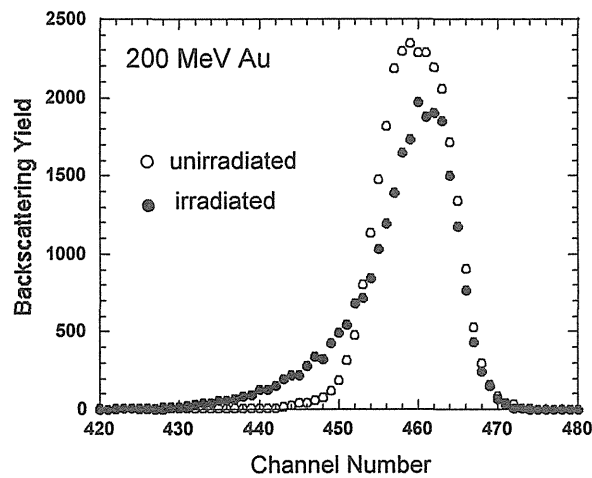
Fig. 3 RBS spectra of Bi-Al₂O₃ system for Bi layer before irradiation (open circles) and after irradiation with 200 MeV Au ions (solid circles). Se of 200 MeV Au ion for Bi is 27keV/nm.
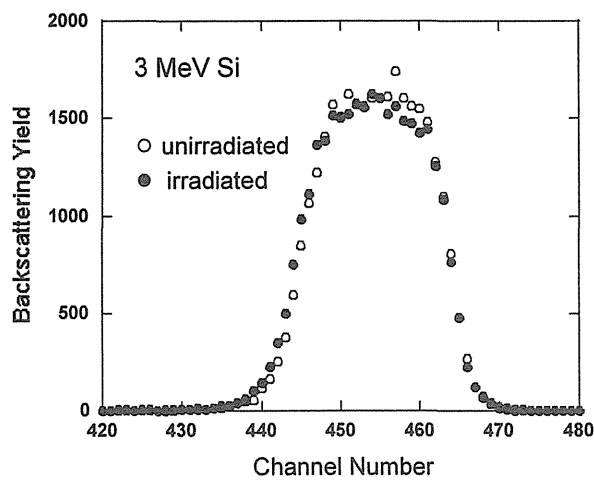
Fig. 4 RBS spectra of Bi-Al₂O₃ system for Bi layer before irradiation (open circles) and after irradiation with 3 MeV Si ions (solid circles).

7. 8 PRESSURE DEPENDENCE OF SUPERCONDUCTING PROPERTIES OF MgB$_2$ SINTERED SAMPLES

S. OKAYASU, H. IKEDA[1] and R. YOSHIZAKI[1]

A newly developed superconductor magnesium diboride MgB$_2$[1] has the highest transition temperature ($\sim$40K) in intermetallic compounds. This superconducting material is made up of two light elements, advantageous to practical applications of this material. However, the pinning properties of MgB$_2$ at this time; such as the critical current densities, the irreversibility fields, and so on; are inadequate level to industrial usages. Therefore, the improvements of these properties are needed. Though irradiation is known to be one of useful methods for improvement of superconductors, it can not be very effective in the improvement of MgB$_2$. Thus, we tried to improve these pinning properties by combined effects between irradiation and something. Here, we chose pressure effect, because the pressurization is commonly used for synthesis of new superconducting material. Firstly, we investigate the pressure effects on MgB$_2$ independently.

For magnetization measurements under pressure, we developed a new pressurized measurement cell for use in a commercial SQUID magnetometer (MPMS-5 Quantum Design). The schematic view is shown in figure 1. The filling liquid in the cell is the 1:1 mixture of flourinert FC-70 and FC-77. The filler is hermetically sealed with o-rings and metal gasket packings. From outside through a pressurize bar(⑦), the upper piston position (⑤) is shoved in the cell and the hydrostatic pressure is applied into the cell at room temperature. Then the clamp screw(②) is tightened to hold the upper piston position (⑤), and the pressure is maintained . The applied pressure is calibrated by the transition temperature of lead sealed with the sample in the cell[2].

The field dependence of the critical current densities (Jc) are shown in figure 2, comparing under the pressure (0.8GPa) to ambient pressure. The Jc decreases in all temperature range by applying the pressure. This disappointing result is explicable by the decrease of the transition temperature Tc. Considering the decrease of Tc due to the pressure, all Jc data lie on the universal line $Jc_0(H)[1-(T/Tc)^2]^{5/2}$. This suggests that the origin of decreasing Jc is decreasing Tc due to the applied pressure. With increase of pressure, Tc decreases monotonically. Using a linear extrapolation, dTc/dP is -1.5 [K/GPa], and the superconductivity will disappear at P=25GPa. For the purpose of improvement of the pinning properties of MgB$_2$, we must rethink strategy.

---

[1] Univ. of Tsukuba, Tsukuba, Ibaraki 305-8577, Japan

Authors extend our gratitude to Prof. J. Arai and Dr. T. Goko in Science University of Tokyo for development of the pressure cell.
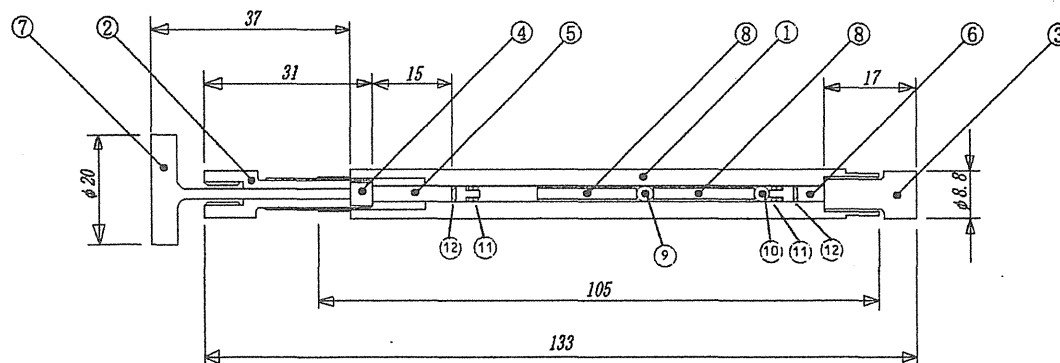
Fig. 1 Schematic view of the pressure cell.

①cell cylinder ②upper clamp screw ③lower clamp screw ④upper piston backup ⑤upper piston ⑥lower piston ⑦pressurize bar (removable) ⑧sapphire spacer ⑨MgB_2 sample ⑩Pb sample(for pressure calibration) ⑪o-ring ⑫metal gasket
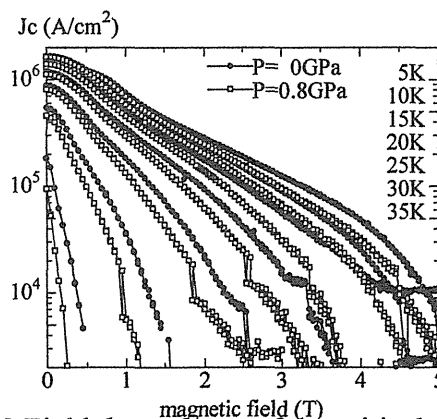
Fig.2 Field dependence of the critical current densities
solid circle(●) – 0 GPa, open circle(○) – 0.8GPa
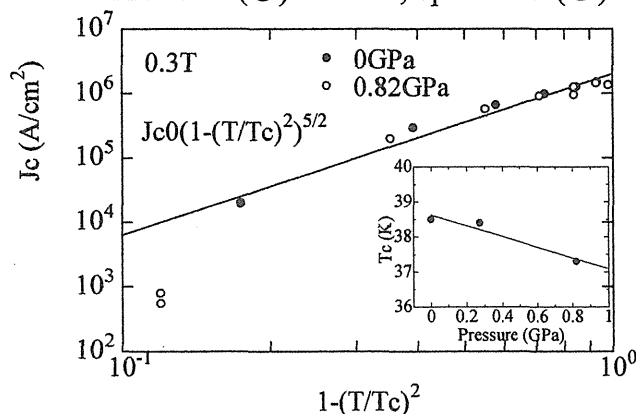
Fig.3 Scaling of Jc by an universal curve $Jc_0[1-(T/Tc)^2]^{5/2}$

Inset : decrease of Tc with increase of pressure

References

[1] J. Nagamatsu, et.al., Natue 410, 63 (2001)

[2] A.Eiling and J.S. Schilling,,J.Phys.F:Metal Phys.11(1981)623-39

7.9 ELECTRONIC EXCITATION EFFECTS ON SECONDARY IONS EMISSION FROM CONDUCTIVE MATERIALS BOMBARDED BY HEAVY IONS

T. SEKIOKA[1], M. TERASAWA[1] and M. SATAKA

It is recognized that high electronic excitations play an important role in the damage process of solid targets by high-energy heavy ions. However, the conversion mechanism of the energy of the excited electrons into kinetic energy for the target atom displacement is not well understood. In order to investigate the electronic excitation effects of high energy heavy ions in solids, we have studied the secondary ions mass spectra from thin conductive solid targets irradiated by swift heavy ion beams from the JAERI tandem accelerator in the energy region where the electronic stopping power $S_e = - (dE/dx)_e$ is dominant. In our earlier study, we measured the dependence of secondary Cu^+ ion yield from Cu on the electronic stopping power by bombarding a thin Cu foil target by swift Au ions. The secondary ion yields showed a significant increase with increasing electronic stopping power, which has approximately S_e^2 dependence [1]. We extend this study to the secondary ion yield measurement for Au target, in order to obtain the target mass dependence of the electronic excitation effect, and the more information about the conversion mechanism of the energy of the excited electrons into kinetic energy for the target atom displacement.

An Au foil target of 200 nm thickness evaporated on C-foils of 8.5 $\mu g/cm^2$ was irradiated with high-energy Au ions from the tandem accelerator. The secondary ions ejected from the front surface of the target were collected by a time of flight (TOF) mass spectrometer by applying an acceleration voltage of –500V and detected by an electron multiplier. Secondary electrons from the backside of the target were detected by another electron multiplier and this signal was used as the start signal of the TOF. Immediately before the measurement of the secondary Au^+ ion yield from the Au target, we cleaned the target by infrared radiation heating. We maintained the temperature of the target about 500°C for two hours in the vacuum of 1.6×10^{-6} Pa. Without cleaning, we could find no Au^+ secondary ion peak in the TOF spectrum because the weak Au^+ peak was buried in the background mainly due to hydrocarbon contaminants.

Figure 1 shows the yields of the secondary ions of Au^+ from Au target. The projectiles were 240 MeV Au^{15+} and 320 MeV Au^{25+} ions. Our earlier data of the yield of the secondary Cu^+ ions from Cu target as a function of the electronic stopping power is also shown in the fig.1. The values of the electronic stopping power are obtained from Ziegler's table by TRIM. The solid line in the figure represents the slope of S_c^2 and the dashed one represents the slope of

---

[1] University of Hyogo

S_e^4 for the eye guide. The yield of the Au^+ secondary ions from Au target is very small as compared with the yield of the Cu^+ secondary ion from Cu target, though Cu and Au have the same electronic structure ($^2S_{1/2}$). The tendency of the target mass dependence of the secondary ion yield agrees with the experimental results on the damage creation in metals by high electronic excitation effect by swift heavy ion irradiation [2]. The S_e dependence of the yield of the Au^+ secondary ions from Au target seems to be more sensitive than that of the Cu^+ secondary ions from Cu target. In order to confirm this result, we have tried to measure the secondary Au^+ from Au target at bombarding energy 280 MeV. However, we failed in finding the Au^+ peak in the spectrum, because of its low yield and the high background. We are now preparing for the improvement of the TOF mass spectroscopy system and installing a target cleaning system with an ion gun, in order to perform a low background experiment and obtain statistically much better data of the yield of the Au^+ secondary ions from Au target. Also we are planning to extend our study to the materials that are difficult to make a thin film target.
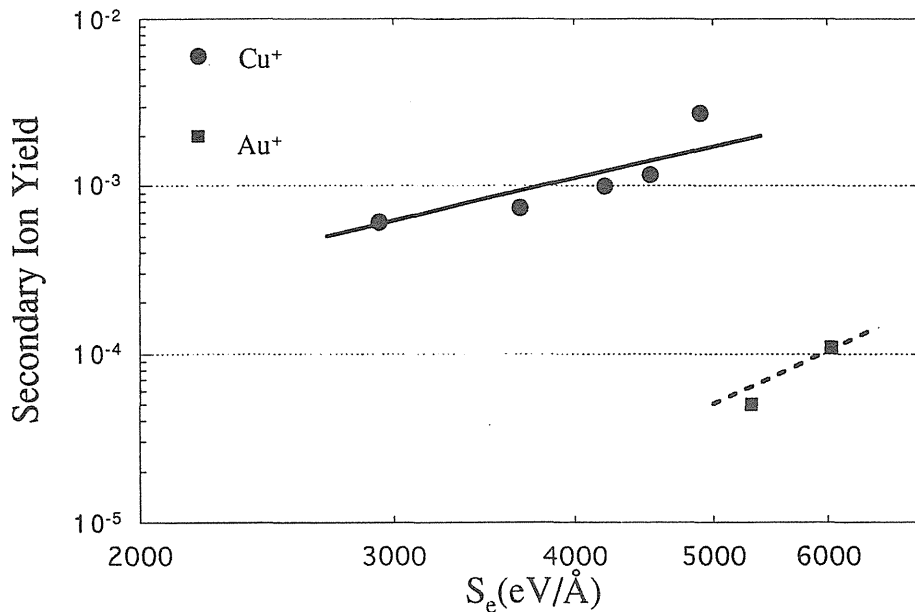
Fig. 1. The yields of the secondary ions of Cu^+ and Au^+ from Cu and Au target, respectively, normalized by the counts of secondary electrons, as a function of the electronic stopping power S_e. The values of the electronic stopping power are obtained by Ziegler's table (TRIM). The solid line in the figure represents the slope of S_e^2 and the dashed one represents the slope of S_e^4 for the eye guide.

Reference

[1] T. Sekioka, M. Terasawa, M. Sataka, S. Kitazawa, M. Niibe, Nucl. Instr. And Meth. B193 (2002) 751-754

[2] A. Dunlop and D. Lesueur, Radiat. Eff. Def. Solids 126 (1993) 123.

7. 10 SWIFT HEAVY-ION IRRADIATION EFFECTS IN BISMUTH THIN FILMS

Y. CHIMI, N. ISHIKAWA and A. IWASE[1]

Effects of swift heavy-ion irradiation in bismuth thin films have been studied by measuring the electrical resistivity at low temperature. We have already observed an abrupt resistivity increase around 20 K during annealing of ion-irradiated bismuth thin films, which implies re-crystallization of irradiation-induced amorphous regions [1]. Bismuth thin films in amorphous state are known to show not only a crystallization at 10–20 K, but also a superconducting transition below ~6.2 K [2]. In the present work, we have tried to detect a superconducting transition which may take place as a result of irradiation-induced amorphization [3].

A polycrystalline bismuth thin film of 340 Å thick was deposited on an α-Al_2O_3 single crystal substrate by vacuum evaporation at room temperature. The specimen was cooled to ~4.9 K by using a liquid-helium cryostat, and was irradiated below ~5.3 K with 200-MeV [197]Au ions up to a fluence of 3.1×10^{12} cm^{-2}. During irradiation, the electrical resistivity of the specimen, ρ, was measured *in situ* at ~4.9 K at appropriate fluence intervals. After irradiation, the temperature dependence of ρ was observed from ~4.9 K to ~13 K.

Figure 1 shows that the electrical resistivity of the specimen, ρ, increases monotonically as a function of ion fluence, Φ, for 200-MeV [197]Au ion irradiation. The resistivity increase exhibits a tendency toward saturation. The data can be fitted to ordinary exponential saturation behavior as expressed by equation (1).

$$\rho = \rho_0 + a\{1-\exp(-b\Phi)\} \tag{1}$$

Where ρ_0 is the resistivity before irradiation, and a and b are the parameters related to the defect production and annihilation cross-sections. In semi-metallic bismuth, however, it has to be considered that not only the change in carrier mobility but also that in carrier density contributes to the resistivity change due to accumulation of the irradiation-produced defects.

The temperature dependence of ρ below ~13 K after 200-MeV [197]Au ion irradiation is shown in Fig. 2. For the present specimen thickness of 340 Å, we can estimate the superconducting transition temperature as ~6.0 K from the thickness dependence [4]. However, up to the fluence of at least 3.1×10^{12} cm^{-2}, any resistivity decrease due to a superconducting transition has not been observed around 6.0 K, even in the temperature range down to ~4.9 K.

For 200-MeV [197]Au ion irradiation, a superconducting transition could not be detected, whereas the abrupt increase in resistivity reflecting the re-crystallization of irradiation-induced amorphous regions was observed. There are some possible reasons for the absence of superconducting transition after the irradiation: (a) the superconducting transition temperature may be below the measuring temperature of ~4.9 K, because not only the specimen thickness,

---

[1]Research Institute for Advanced Science and Technology, Osaka Prefecture University

but also the diameter of an amorphous track may determine the superconducting transition temperature, (b) the diameter of an amorphous track may be smaller than the coherence length of superconducting paired electrons, or (c) the superconducting region may be too narrow to be detected by measuring the electrical resistivity. Therefore, in order to detect a superconducting transition, the bigger volume of the amorphous region is necessary. In this sense, irradiation with 200-MeV ^{197}Au ions up to high fluence of more than 3.1×10^{12} cm^{-2} may induce detectable superconductivity in bismuth.
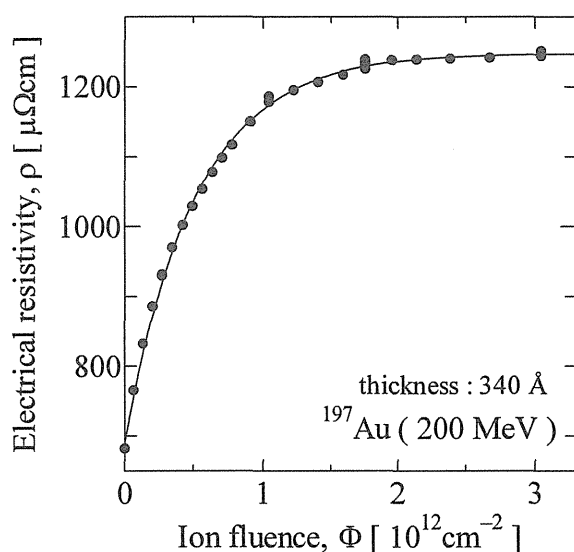
Fig. 1. Electrical resistivity, ρ, measured at ~4.9 K during irradiation below ~5.3 K with 200-MeV ^{197}Au ions as a function of ion fluence, Φ. A data fitting curve to ordinary exponential saturation behavior is also shown.
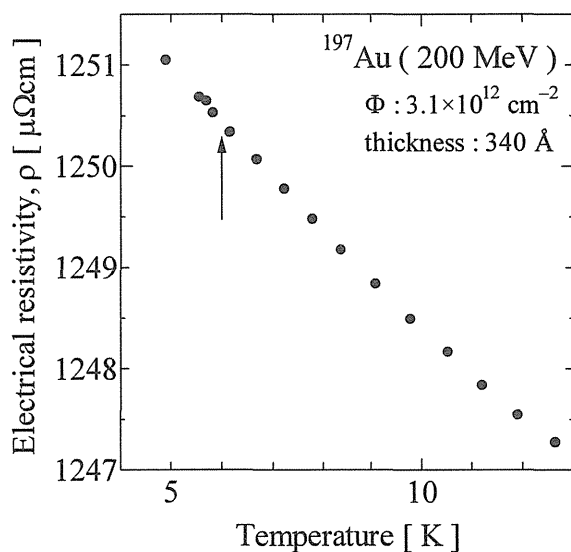
Fig. 2. Temperature dependence of resistivity, ρ, below ~13 K after 200-MeV ^{197}Au ion irradiation up to a fluence of 3.1×10^{12} cm^{-2}. An arrow indicates the expected superconducting transition temperature of ~6.0 K for the present specimen thickness of 340 Å [4].

References

[1] Y. Chimi, A. Iwase, N. Ishikawa, JAERI-Review 2003-028 (2003) 110.

[2] W. Buckel, R. Hilsch, Z. Phys. 138 (1954) 109.

[3] Y. Chimi, N. Ishikawa, A. Iwase, Mat. Res. Soc. Symp. Proc. 792 (2004) 379.

[4] D.G. Naugle, R.E. Glover, Phys. Lett. 28A (1969) 611; D.G. Naugle, R.E. Glover III, W. Moorman, Physica 55 (1971) 250.

7. 11 MODIFICATION OF THE MAGNETIC PROPERTIES
IN Fe-Ni INVAR ALLOYS BY HIGH-ENERGY HEAVY ION IRRADIATION

Y. MATSUSHIMA[1], F. ONO[1], H. KANAMITSU[1], S. KOMATSU[1], A. IWASE[2],
Y. CHIMI, N. ISHIKAWA and T. KAMBARA[3]

Fe-Ni alloys with the Ni-concentration around 35 at.% Ni show anomalous small thermal expansion and hence, called Invar alloys. These alloys also show various anomalies in magnetic properties. Those anomalies have been understood as a result of the instability of the 3d-band ferromagnetism in fcc metals and alloys. The Ni concentrations of those alloys are close to the boundary of the martensitic phase transition. Therefore, it is expected that the physical and magnetic properties in these alloys would be modified by high-energy particle irradiation. Actually, we observed large increase of the Curie temperature, T_C in Fe-Ni Invar alloys irradiated with high-energy heavy ions [1-4]. However, the mechanism of the large shift of T_C has not been clarified as yet, and further investigations are being carried on.

Thin disc specimens of Fe-Ni Invar alloys in a form of thin discs of 5×5 mm^2 and the thickness of 100-200 μm were irradiated with 50-200 MeV Xe-ions to the dose up to 10^{14} ions/cm^2. AC-susceptibility measurements were carried out using a specially designed apparatus suitable for rapid temperature variation. In those experiments the range of the Xe-ions was up to 7 μm, which was smaller than the thickness of the sample. Therefore, the modification of the magnetic properties has been expected within the range of the ion beams, which is around 4-8% of the thickness of the specimen. However, the AC-susceptibility signal from the irradiated portion was much larger than expected. A possible reason for this effect was given in [1] by considering the difference in the demagnetization factor between the modified part and the rest body of the specimen. However, the estimated intensity of the AC-susceptibility was still smaller than observed. To investigate the area distribution of the irradiation effect, the irradiated specimen was cut into thin needle-like pieces of the width around 400 μm, and the AC-susceptibility measurement was carried out for each piece.

Fig. 1 shows the observed AC-susceptibility versus temperature curves for Fe-30.6at.%Ni after 80 MeV-Xe ion irradiation. The first stage corresponds to the original Curie temperature that comes from the part where ion beams did not penetrate. The second stage is caused by the irradiation-induced ferromagnetism. In this figure it is clearly seen that the Curie temperature of the irradiated part increased as largely as 50 K.

---

[1] Department of Physics, Okayama University
[2] Research Institute for Advanced Science and Technology, Osaka Prefecture University
[3] Atomic Physics Laboratory, The Institute of Physical and Chemical Research
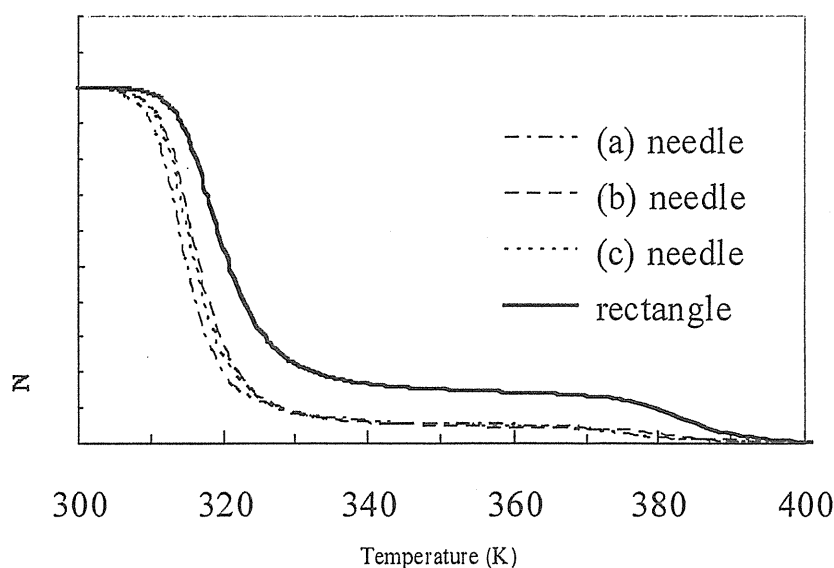
Fig.1 AC-susceptibility vs. Temperature curves for Fe-30.6at.%Ni alloy after Xe-ion irradiation. The curve (a) is from the needle-like sample cut from an edge, (b) from next to (a), (c) next to (b), and the last from the entire rectangular specimen.

In this figure observed AC-susceptibility vs. temperature curves for three thin sliced needle-like samples were also plotted. The sample (a) is cut from an end of the rectangular specimen, the sample (b) is cut from the area next to the sample (a), and (c) is cut from next to (b). In this figure it is seen that the intensities of the AC-susceptibility from the irradiated part in samples (a), (b) and (c) are smaller than that from the entire rectangular shape specimen. From these experimental results, it is concluded that the area distribution of the irradiation effect is uniform and that the intensity of the AC-susceptibility from the irradiated part depends upon the demagnetizing factor.

The present type of modification of introducing thin ferromagnetic needles in paramagnetic media has a possibility of applications for perpendicular high-density memory and giant magneto-resistance materials.

References

[1] A. Iwase, Y. Hamatani, Y. Mukumoto, N. Ishikawa, Y. Chimi, T. Kambara, C. Muller, R. Neumann and F. Ono, Nucl. Instrum. Methods Phys. Res. B 209 (2003) 323.

[2] A. Iwase, Y. Hamatani, Y. Mukumoto, N. Ishikawa, Y. Chimi, T. Kambara, C. Mueller, R. Neumann and F. Ono, RIKEN Accel. Prog. Rep. 36 (2003) 99.

[3] F. Ono, Y. Hamatani, Y. Mukumoto, S. Komatsu, N. Ishikawa, Y. Chimi, A. Iwase, T. Kambara, C. Muller, R. Neumann, Nucl. Instrum. Methods Phys. Res. B 206 (2003) 295.

[4] F. Ono, S. Komatsu, Y. Chimi, N. Ishikawa, T. Kambara and A. Iwase, MRS Fall Meetings (Boston, 2003).

7. 12 HARDENINGS AND DEPTH-DEPENDENT DAMAGE STRUCTURES IN Fe-P ALLOYS IRRADIATED WITH ENERGETIC Xe IONS

A. NAITO, T. ARUGA, T. NAKAZAWA AND K. ABIKO[1]

It has been argued that point defects might be produced in metals under irradiation with swift heavy ions through high density electronic energy excitation. However, the mechanism of the defect production through electronic energy excitation in metals is not yet fully established [1]. In this work damages produced in Fe-P alloys by swift heavy ion irradiations were studied and preliminary results are described, to contribute towards helping understand what may take place in metals irradiated with swift heavy ions.

Samples used in this study are high purity iron-phosphorus Fe-P alloys, with phosphorus of 0.02 to 0.3 wt%, which had been fabricated after the appropriate thermo-mechanical treatments to study behaviors of phosphorus in pure iron. The samples of 0.2 mm thickness in a disk of 3mm diameter, were irradiated with 160 MeV Xe^{+13} ions at ambient temperature to $4 \times 10^{14}/cm^2$. The irradiation to this dose produces the displacement damage of 0.05 dpa at the surface and 0.8 dpa at the peak around 8 μm of the depth. The elctronic energy deposition density is 35 keV/nm/ion at the surface and decreases to 5 keV/nm/ion at 8 μm. Cross sectional transmission electron microscopy (TEM) observation was performed with a JEOL 2000FX TEM, for specimens prepared from the irradiated samples using a focused ion beam (FIB) thinning apparatus. Nanoindentation test was performed using Shimadzu SPM-9500J3 instrument. The machine was equipped with the three-sided Berkovich indenter. The tests were done under a control of maximum load of 1 mN, to probe mechanical properties changes in the near-surface region of depths for the irradiated samples and also solution hardening for the samples before irradiation with the P contents varied.

In Fig. 1 (left), solid solution hardening of unirradiated Fe-P alloys due to phosphorus alloying from 0.02 to 0.3 wt % is shown for comparison with the hardening due to ion irradiations (right) for the sample alloyed with 0.02 wt% P or Fe-0.02P. Berkovich hardness H_B is defined as the maximum load divided by the projected area of the indentation, which is related to the indenter contact depth. Load-depth curves for phosphorus alloying to 0.02 and 0.05 wt% are very similar and these yield H_B of 2.1 GPa. The fact suggests that effects of phosphorus alloying up to 0.05 wt% on solution hardening can not be distinguished from that for 0.02 wt%. Upon alloying to 0.1 wt% P, the maximum indentation depth decreases 15 % of that for 0.02 and 0.05 wt% P, and H_B increases to 2.8 GPa. The irradiation of Fe-0.02P with 160 MeV Xe ions to $4 \times 10^{14}/cm^2$ exhibits a remarkable decrease in the maximum indentation depth (Fig.1 (right) curves a, c), which results in H_B increase from 2.1 GPa to 3.9 GPa, that is, increase of 85 %. Note that the load-depth curve for the Fe-0.02P sample irradiated to $4 \times 10^{14}/cm^2$ almost coincides with that for the unirradiated Fe-0.3P sample (Fig. 1). An hardness increase means the increase in the resistance to the plastic deformation, through the increase in the number density of obstacles and in the height of the barrier for dislocations to move. Therefore, the similarity observed in the load-depth curves for the unirradiated Fe-0.3P and irradiated Fe-0.02P samples implies that the Xe ion irradiation might form defect clusters having the same effects on hardening as solution hardening exhibited in Fe-0.3P sample. Cross sectional damage structures for the irradiated Fe-0.05P sample, which shows hardening of 5.1 Gpa, remarkably larger as compared with 2.1 GPa before irradiation, were examined using TEM and the typical photographs are given in Fig. 2, along with dislocation densities measured. Damage structures are characterized with defect clusters sized smaller than 5 nm in a high density of $9 \times 10^{16}/cm^3$ and dislocation lines with densities of $3 - 7 \times 10^{11}/cm^2$. Note that these densities are comparable to that observed in the similar sample irradiated in a high voltage (0.9MV) electron microscope JEM-1000D, with an electron flux of $1.7 \times 10^{19}/cm^2 s$ to a dose of 2 dpa, as compared with 0.05 dpa in the present ion irradiation, although in the HVEM irradiation, the temperature was higher a little. In addition, the dislocation densities are observed to decrease with

increasing depth (Fig.2 bottom), and to correlate with the depth profile of electronic stopping power, not with nuclear stopping power, although further investigations are needed to exclude other possibilities.
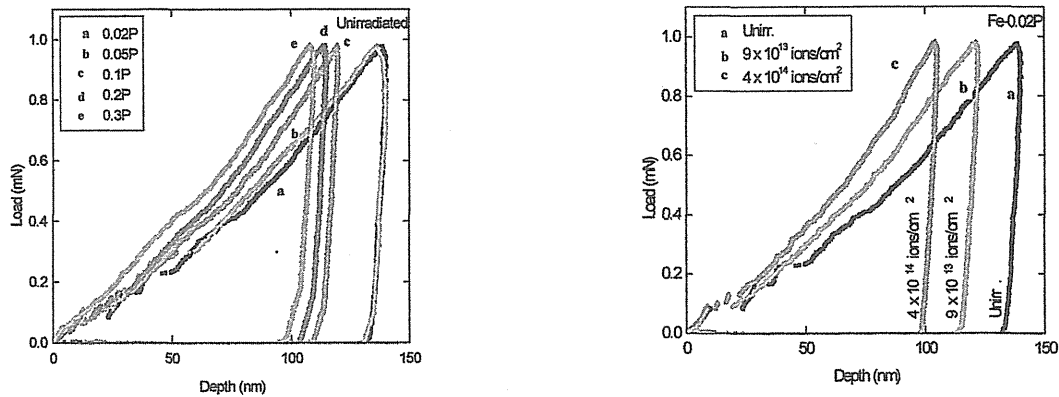
Fig. 1. Loads as a function of indentation depths for loading and unloading in nanoindentation tests:
(Left) for samples before irradiation with alloying phosphorus contents varied from 0.02 to 0.3 wt% , desiganted as curves a to e, corresponding to each P content as 0.02P for Fe-0.02wt% P. (Right) load-depth curves a to c for the Fe-0.02P sample irradiated to 4x 10^{14}/cm^2; curves a to c correspond to doses varied.
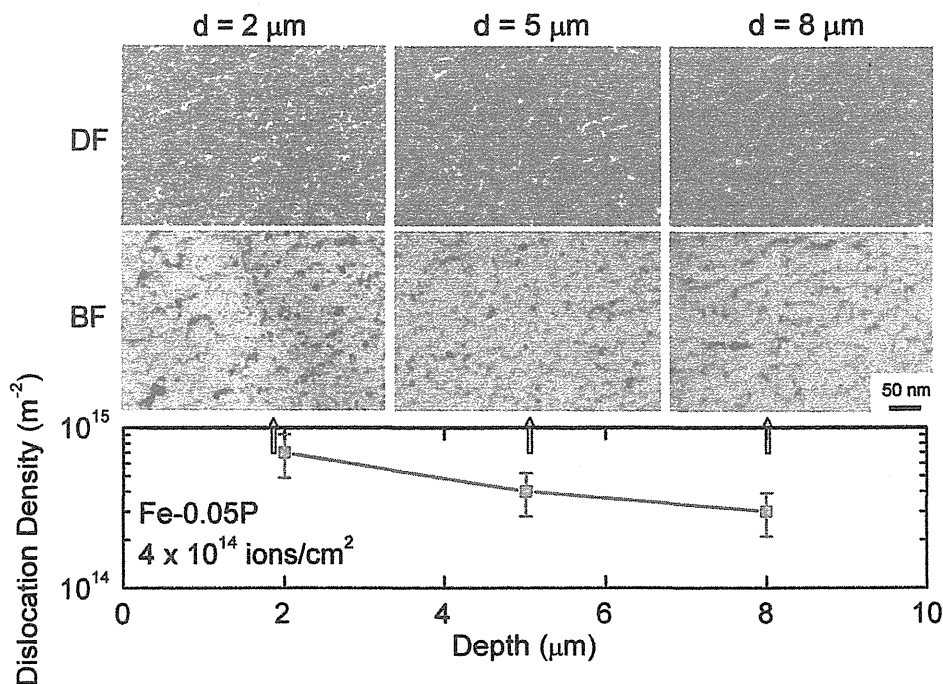
Fig. 2. Cross sectional damage structures as observed by TEM in dark (DF) and bright (BF) fields at the designated depths from the ion-incident surface for Fe-0.05P sample irradiated with 160 MeV Xe^{13+} ions to 4x10^{14}/cm^2, along with the dislocation densities measured on the images indicated by upwards arrows at the corresponding depths.

References
[1] A. Iwase, S. Ishino, J. Nucl. Mater. 276 (2000) 178.

7. 13 EFFECT OF HEAVY ION IRRADIATION ON β-FeSi₂ FILM

K. YAMAGUCHI, K. HOJOU, S. OKAYASU, K. SHIMURA and H. YAMAMOTO

β-FeSi$_2$ is a semiconducting silicide, which can be grown epitaxially on Si substrates, so that it is anticipated to play a key role in Si-based optoelectronics [1]. Since other phases of Fe-Si compounds are metallic [2], metal-semiconductor junction can be fabricated from the same compound if the phase transformation can be accomplished locally. For this purpose, ion beam irradiation is expected to serve as an ideal tool to modify the material properties of the confined region of the sample. Furthermore, due to the large electronic stopping power of heavy ions irradiated with high energy, electronic heating may be expected to induce phase transformation to high-temperature phase, for instance, to α-FeSi$_2$, which is metallic. However, little is known how iron silicides are affected by ion irradiation.

A thin film of β-FeSi$_2$ on Si (100) was fabricated by means of ion beam sputter deposition (IBSD) method, where a target of pure Fe (> 4 N) was sputtered by 35 keV Ar$^+$ ion beam onto a Si (100) substrate (0.5 mm thick) heated at 973 K [3]. The deposited thickness of Fe was 33 nm, so that in terms of β-FeSi$_2$ the thickness of the film is estimated to be about 100 nm, assuming that all the Fe atoms (density; 7.87 g cm^{-3}) are reacted to form β-FeSi$_2$ (4.93 g cm^{-3}). The 136 MeV Xe^{14+} ion beam from the tandem accelerator in JAERI was irradiated to β-FeSi$_2$ / Si samples and Si (100) substrates with the incident ion flux of 4x10^{13} Xe m^{-2} s^{-1}. Each sample, 5 mm x 5 mm in size, differs in the irradiated fluence, ranging from 3x10^{16} to 1x10^{18} Xe m^{-2}. The θ-2θ X-ray diffraction (XRD) analysis and Hall effect measurement were performed to determine respectively the change of crystal structure and electrical properties due to ion irradiation.

Figure 1 compares the XRD spectra of β-FeSi$_2$ film prepared on Si substrate before and after irradiation by Xe ions. Although the initial β-FeSi$_2$ film was highly oriented to (100) planes, the intensities of the peaks corresponding to β-FeSi$_2$ were found to decrease upon increasing the irradiation fluence, and were almost indistinguishable as the fluence exceeded 6x10^{17} Xe m^{-2}. This result indicates that disintegration of the crystal structure was more predominant than inducing phase transformation. According to TRIM calculation [4], the sputtering yield of β-FeSi$_2$ by 136 MeV Xe ion is estimated to be about 0.2, so that the lattice displacement may have taken a certain role.

Figure 2 shows the change in electrical resistivity of β-FeSi$_2$ / Si as evaluated by Hall effect measurement. One can see from the figure that Xe ion irradiation appears to increase the resistivity at around room temperature, while the resistivity tends to decrease in the temperature range of 400-600 K. Since the damage region reaches far beyond the film (estimated range; 17 µm), a part of Si substrate was also subject to irradiation. Therefore, it is not clear at present which (films or substrate) is responsible for the change in electrical properties. In the case of Si substrates irradiated with Xe ions, on the other hand, the samples did not show ohmic contact at low temperatures, so that the Hall effect measurements were not considered to be reliable.
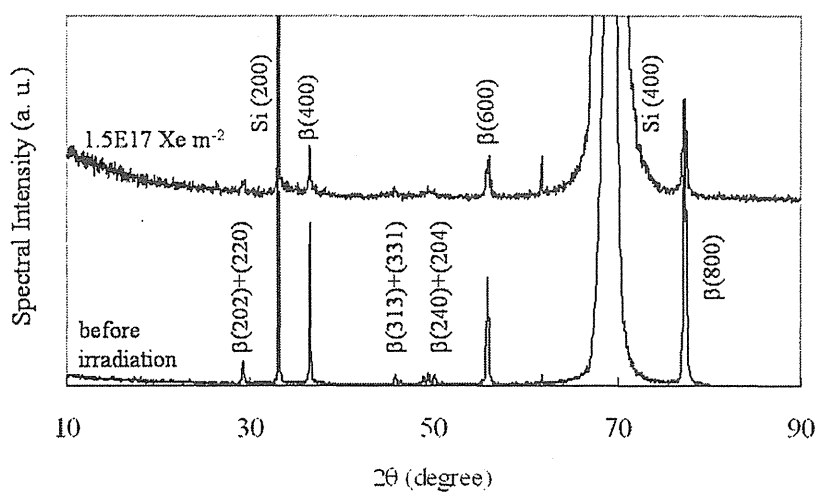
Fig.1: Comparison of XRD spectra of β-FeSi$_2$ / Si samples before and after irradiation (1.5×10^{17} Xe m^{-2}).
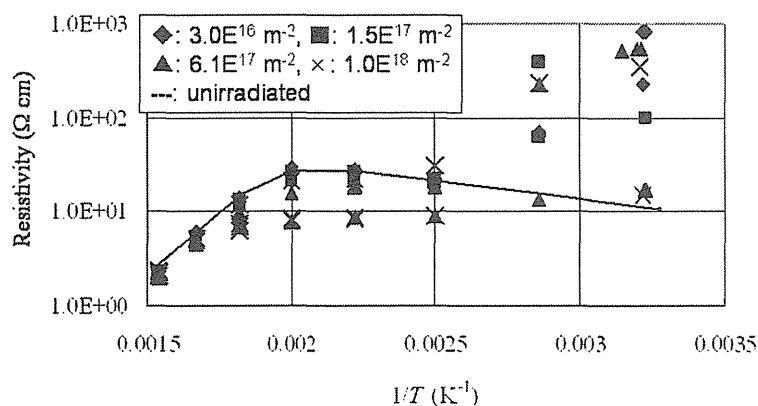
Fig.2: Effect of heavy ion irradiation on the electrical resistivity of β-FeSi$_2$ / Si. A curve indicates data obtained before ion irradiation.

References

[1] H. Lange, phys. stat. sol. (b) 201 (1997) 3.

[2] T. B. Massalski, in: H. Okamoto, P. R. Subramanian, L. Kacprzap (Eds.), Binary Alloy Phase Diagrams, ASM International, Metals Park, OH, 1990, p. 1772.

[3] M. Haraguchi, H. Yamamoto, K. Yamaguchi, T. Nakanoya, T. Saito, M. Sasase, K. Hojou, Nucl. Instrum. Method B 206 (2003) 313.

[4] J. F. Ziegler, J. P. Biersack, U. Littmark, The Stopping and Range of Ions in Solids, Pergamon Press, New York, 1985.

7. 14 ION IRRADIATION EFFECTS ON ELECTRIC RESISTIVITIES AND MICROSTRUCTURES OF CARBON FIBERS

A. KURUMADA[1], Y. IMAMURA[1], T. OKU[2], M. ISHIHARA, S. BABA and J. AIHARA

Carbon/Carbon composite materials have good nuclear characteristics, high thermal conductivity and excellent mechanical properties at high temperatures. They have been taken as one of the candidate materials for plasma facing components of the next fusion experimental reactors and for the cladding tube of the control rod of the High Temperature Engineering Test Reactor (HTTR). In order to apply them for their reactors, it needs to study on the changes in material properties and microstructures due to irradiation damage and to develop the excellent C/C composite materials with irradiation damage resistance. On the other hand, material properties of C/C composite materials are well known to depend on those of carbon fibers since carbon fibers in C/C composite materials are generally less crystalline than the carbon matrix part. In this study, high energy ions of carbon, nickel and argon are irradiated to carbon fibers with different microstructures and different properties, and the effects of ion irradiation damage on electric resistivities and microstructures are evaluated.

Materials tested in this study were eleven kinds of carbon fibers with different microstructures and different properties, which were three coal tar pitch based carbon fibers (K13C2U, K1352U, K1392U), a vapor growth carbon fiber (K1100X), three polyacrylonitrile based carbon fibers (T700SC, M55JB, M40JB) and four mesophase pitch based carbon fibers (YS-15-60S, YS-70-60S, XN-15-60S, XN-70-60S). Carbon ions ($^{12}C^{6+}$) of 100 MeV with 0.5 μ A were irradiated to 1×10^{-6}, 1×10^{-5}, 1.4×10^{-4} or 3×10^{-5} dpa, nickel ions ($^{59}Ni^{13+}$) of 200 MeV with 0.4 μ A were irradiated to 1×10^{-5} or 5×10^{-4} dpa by the TANDEM accelerator in Tokai, JAERI, and argon ions ($^{40}Ar^{8+}$) of 175 MeV with 1 μ A were irradiated to 1×10^{-3} dpa by the AVF cyclotron in Takasaki, JAERI. The ranges of carbon, nickel and argon ions calculated by TRIM-98 code were 161, 25.5 and 38.4 μ m for the carbon material of 2.2 g/cm^3 respectively. Therefore irradiation damages in carbon fibers were uniform across the cross section because the diameters of carbon fibers below about 20 μ m were enough smaller than the ranges.

A single carbon fiber was straightly put on the center of a frame paper with a square hole (10mm x 25mm) using conductive silver paste like the tensile specimen[1-3]. The electric resistivity was calculated after measuring of the electric resistance using a DC electric resistance tester (HIOKI Hi-Tester 3220) by four-terminal method. The cross section was observed by SEM and the mean value of the cross-sectional areas was evaluated from the photographs, and was used for calculation of the electric resistivity. The number of carbon fibers on a frame paper was confirmed by optical microscope.

---

[1] Faculty of Engineering, Ibaraki University   [2] Ibaraki Study Center, The University of the Air

Fig.1 and Fig.2 show electric resistivities (ρ μ Ωm) of carbon fibers before and after ion irradiation of 1×10^{-5} dpa respectively.   The ratio of electric resistivity after ion irradiation (ρ / ρ_0) was also indicated in Fig.2.   Electric resistivities of the YS-15-60S and XN-15-60S carbon fibers were large comparatively and those of the K13C2U and K1100X carbon fibers were small comparatively.   And electric resistivity of carbon fibers increased with increasing ion irradiation damage because of increase of lattice defects.   Electric resistivities of the K13C2U and K1100X carbon fibers, however, were also comparatively small after ion irradiation, so a coal tar pitch based carbon fiber and a vapor growth carbon fiber were considered to have irradiation damage resistance[4-5].   And the increase of the electric resistivity guessed the decrease of thermal conductivity of carbon fibers.   The K13C2U and K1100X carbon fibers were observed to have random structure by SEM.   The cross-sectional areas of carbon fibers increased with increasing ion irradiation damage due to lattice defects in graphite inter-layers, however, that of the K1100X carbon fiber was stable against ion irradiation damage.

As the results, a coal tar pitch based carbon fiber and a vapor growth carbon fiber with random structure were effective to develop the excellent C/C composite materials with irradiation damage resistance.

Fig.1   Electric resistivity of unirradiated carbon fibers ρ [μ Ωm]

Fig.2   Electric resistivity of carbon fibers
irradiated with 1×10^{-5}dpa ρ [μ Ωm]
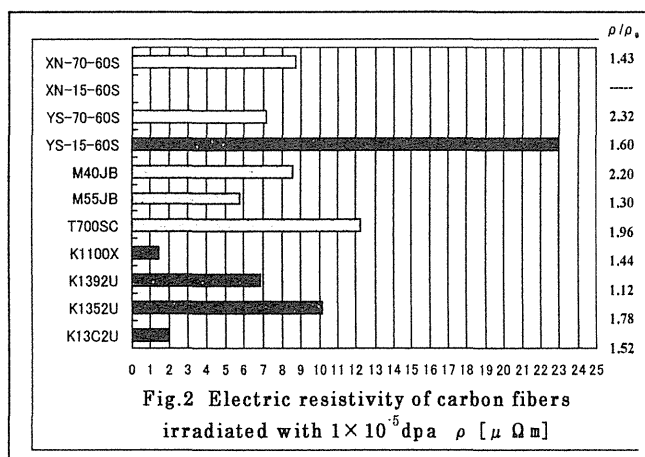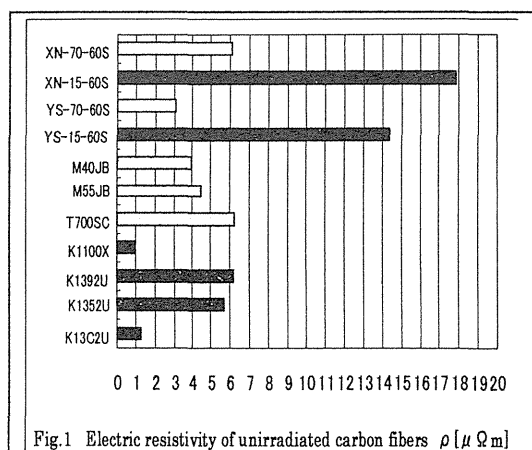
References

[1] T. Oku, Y. Imamura, A. Kurumada, M. Inagaki and K. Kawamata, TANSO, No.190 (1999) 262-266.

[2] T. Oku, A. Kurumada, B. McEnaney, T. D. Burchell, M. Ishihara, K. Hayashi, S. Baba and J. Aihara, Eurocarbon 2000, 1st World Conf. on Carbon, Berlin, Germany (2000.7.9-13) Vol.II, 947-948.

[3] T. Oku, A. Kurumada, K. Kawamata and M. Inagaki, J. of Nuclear Materials, 303 (2002) 242-245.

[4] A. Kurumada, Y. Imamura, T. Oku, M. Ishihara, S. Baba and J. Aihara, JAERI-Conf 2003-017 (2003.10) 139-141.

[5] A. Kurumada, Y. Imamura, T. Oku, M. Ishihara, S. Baba and J. Aihara, OECD 2004, NEA No.5309 (2004) 121-128.

7. 15 EVALUATIONS FOR THE STRUCTURE OF POWER-MOSFETS WITH HIGH RADIATION TOLERANCE

H. SATO[1], T. HIRAO, H. SHINDO[1], S. KUBOYAMA[1], T. KAMIYA, H. OHIRA[2] and S. MATSUDA[1]

The single-event effects (SEE) due to cosmic rays become the most serious problem in applying a high voltage to the semiconductor devices used in space environments. The Single Event Burnout (SEB) is known as a possible catastrophic failure mode for power-MOSFETs. The SEB is triggered when a high-energy heavy ion passes through a power-MOSFET under the off-state bias condition. The transient current generated by the heavy ion incidence turns on a parasitic-bipolar junction transistor (BJT) in MOSFET, which causes a shorted-circuit between the source and the drain due to carrier multiplication, and then destroys the device itself [1].

The epitaxial layers determine the electrical resistance affects the SEB tolerances of the MOSFETs. Generally, electrical characteristics of MOSFETs are worse when their on-resistance (R_{on}) increases with a thickness of an epitaxial layer. As a new way of improving SEB tolerance with low R_{on}, we adopted the device structure that has two epitaxial layers with different resistivity.

Figure 1 shows the scheme of the prepared sample in this experiment with the double-epitaxial layer, which was for appending an SEB tolerance by widening of the carrier transmission distance onto power-MOSFETs. In this structure, it is supposed that the thickness variations of the 1st-epitaxial layer are almost uninfluential, since its electrical resistivity is very low compared with the 2nd-epitaxial layer. Therefore, we performed experiment about the power-MOSFET in order to

Fig. 1. Cross section diagram of the epitaxial layer in the MOSFET.

elucidate the correlation between the SEB tolerance and the thickness of the 1st-epitaxial layer.

Three different samples were prepared, which varied the thickness of the 1st-epitaxial layer. The SEB tests were carried out by using an Energetic Particle Induced Charge Spectroscopy (EPICS) system [2]. EPICS is a specially designed for a pulse-height analyzer (PHA) to characterize the

---

[1] Space Component Engineering Center, Institute of Space Technology and Aeronautics, Japan Aerospace Exploration Agency (JAXA)

[2] Components Engineering Section, Engineering Dept., RYOEI TECHNICA Corporation, Japan

generated charges in a device. During the test, we used Ni ions of LET=28.0[MeV/(mg/cm^2)] from the TANDEM accelerator at JAERI. The beam current was about 1.0nA. The primary ion beam from the accelerator was scattered by Au thin foil for irradiating to entire Si-die surface of the MOSFET.
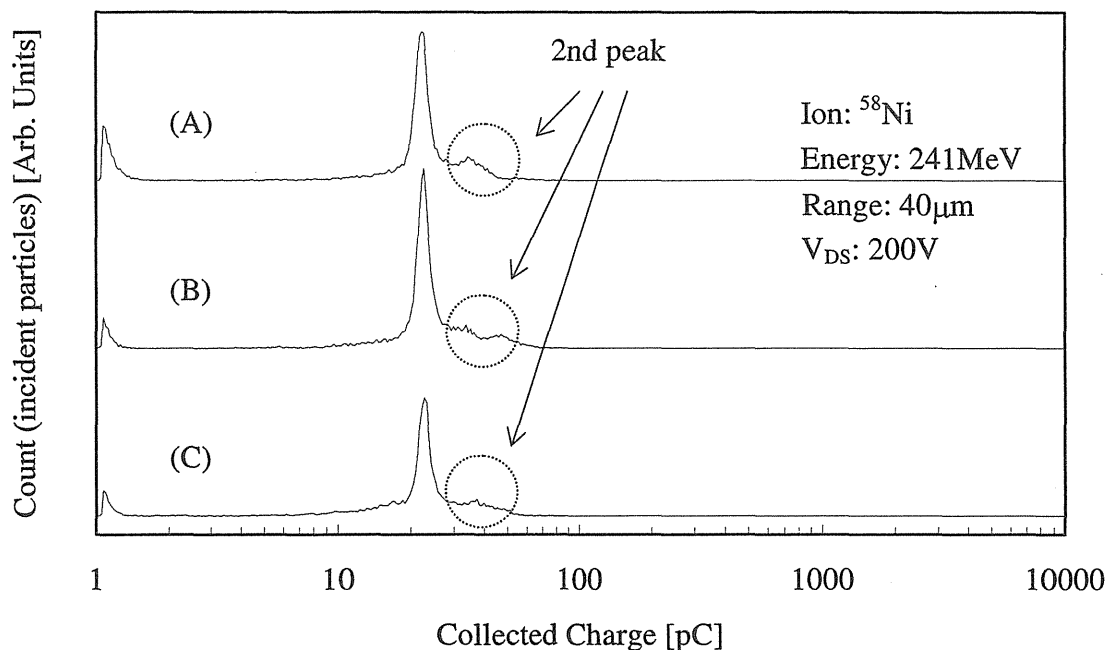
Fig. 2. EPICS spectra from the MOSFETs; the thickness of the 1st-epitaxial layer is a) thicker, b) middle and C) thinner.

Figure 2 shows the EPICS spectrum of each sample. In these spectra, the 2nd-peak involves the carrier that was amplified by the parasitic-BJT in the MOSFETs, and thus when its collected charge is higher, the SEB tolerance is worse. Comparing each spectrum shows that the 2nd-peak does not change significantly. This indicates that the thickness of the 1st-epitaxial layer does not influence the SEB tolerance within these ranges. In the device-simulation afterwards, it is in the range that the effective thickness of the 1st-epitaxial layer is up to ~10μm otherwise the influences do not appear at the 2nd-peaks. It is considered to be ineffective for the SEB tolerance in this experiment.

Some investigations mentioned above were conducted, and we obtained the optimal thickness of the 1st-epitaxial layer with a sufficient SEB tolerance. The SEB-free power-MOSFET with a low R_{on} is necessary for developing the DC/DC Converter with high efficiency. The power-MOSFET under development will be used for the DC/DC Converter of the next generation for space applications.

References

[1] M.Allenspach et al, IEEE Trans. Nucl. Sci., Vol. NS-43, No. 6 (1996) 2927.
[2] S.Kuboyama et al, IEEE Trans. Nucl. Sci., Vol. NS-39, No. 6 (1992) 1698.

This is a blank page.

−97−

8. Publication in Journal and Proceedings, and Contribution to Scientific Meetings

This is a blank page.

ACCELERATOR OPERATION AND DEVELOPMENT

Journal / Proceedings

S. Takeuchi, T. Nakanoya, H. Kabumoto, T. Yoshida
Improvement of High-voltage Performance of Acceleration Tubes by Cleaning the Walls with a High-pressure Water Jet
Nucl. Instrum. Method, A 513 (2003) 429

S. Takeuchi
The JAERI-KEK Joint RIB Project
Application of Accelerators in Research and Industry:17th Int'l Conf.
AIP 0-7354-0149-7/03, (2003) 229-236

T. Yoshida, S. Kanda, S. Takeuchi, K. Horie, I. Ohuchi, Y. Tsukihashi, S. Hanashima,
S. Abe, N. Ishizaki, H. Tayama, M. Matsuda. T. Nakanoya, H. Kabumoto, T. Kaneko
The Status of the JAERI Tandem Accelerator
Proc. of the 16th Workshop of the Tandem Accelerator and their Associated Technology
Kobe Univ. (Jun. 30-Jul. 1, 2003) 25-26

S. Takeuchi, T. Yoshida, T. Nakanoya, H. Kabumoto, N. Ishizaki, M. Matsuda. Y. Tsukihashi, S. Kanda,
H. Tayama, S. Abe, H. Nisugi, M. Satoh, H. Sakurayama, A. Iijima, T. Yoshida
Improvement of High-voltage Performance of new Acceleration Tubes by High-pressure Water Jet Cleaning and Status of the Tube Replacement
Proc. of the 16th Workshop of the Tandem Accelerator and their Associated Technology
Kobe Univ. (Jun. 30-July. 1, 2003) 71-72

S. Takeuchi, T. Nakanoya, H. Kabumoto, N. Ishizaki, M. Matsuda. Y. Tsukihashi, S. Kanda, H. Tayama,
S. Abe, T. Yoshida
Replacement of Accelerator Tubes of the JAERI Tandem Accelerator with the Tubes Cleaned by a High-pressure Water Jet
Proc. Of the 14th Symposium on Accelerator Science and Technology
KEK, Tsukuba (Nov. 11-13, 2003) 308-310

S. Takeuchi, M. Matsuda. N. Ishizaki, H. Tayama, A. Iijima, T. Yoshida
Operational Status of Superconducting Resonators of the JAERI Tandem –booster
Proc. Of the 10th Workshop on RF Superconductivity-2001
Tsukuba (Sep. 2001); KEK Proceedings 2003-2 JUNE 2003 A (2003) 591-593

S. Hanashima, M. Matsuda
Development of a Control Methodology for Peripheral Power Supplies using Optical Fibers
Proc. of the 16th Workshop of the Tandem Accelerator and their Associated Technology
Kobe Univ. (Jun. 30-Jul. 1, 2003) 84-87

Meetings

T. Yoshida, S. Kanda, S. Takeuchi, K. Horie,I. Ohuchi, Y. Tsukihashi, S. Hanashima, S. Abe, N. Ishizaki,
H. Tayama, M. Matsuda. T. Nakanoya, H. Kabumoto, T. Kaneko
The Status of the JAERI Tandem Accelerator
16th Workshop of the Tandem Accelerator and their Associated Technology
Kobe Univ. (Jun. 30-Jul. 1, 2003).

S. Takeuchi, T. Yoshida, T. Nakanoya, H. Kabumoto, N. Ishizaki, M. Matsuda. Y. Tsukihashi, S. Kanda,
H. Tayama, S. Abe, H. Nisugi, M. Satoh, H. Sakurayama, A. Iijima, T. Yoshida
Improvement of High-voltage Performance of new Acceleration Tubes by High-pressure Water Jet Cleaning and Status of the Tube Replacement
16th Workshop of the Tandem Accelerator and their Associated Technology
Kobe Univ. (Jun. 30-Jul. 1, 2003).

S. Takeuchi, T. Nakanoya, H. Kabumoto, N. Ishizaki, M. Matsuda. Y. Tsukihashi, S. Kanda, H. Tayama,
S. Abe, T. Yoshida
Replacement of Accelerator Tubes of the JAERI Tandem Accelerator with the Tubes Cleaned by a High-pressure Water Jet
14th Symposium on Accelerator Science and Technology, KEK, Tsukuba (Nov. 11-13, 2003)

S. Takeuchi, T. Yoshida, T. Nakanoya, H. Kabumoto, N. Ishizaki, M. Matsuda. Y. Tsukihashi, S. Kanda,
H. Tayama, S. Abe
Improvement of High-voltage Performance of Acceleration Tubes by High-pressure Purified Water Rinsing and the Status of Tube Replacement of the JAERI Tandem Accelerator
Fall Meeting of the Physical Society of Japan, Miyazaki (Sep. 11, 2003)

T. Kaneko (SATO), M. Matsuda, A. Osa, S. Ichikawa, T. Yoshida
JAERI-KEK Joint RNB Project
Symposium on Radiochemistry, Osaka (Oct. 1-3, 2003)

S. Hanashima, M. Matsuda
Development of a Control Methodology for Peripheral Power Supplies using Optical Fibers
Proc. of the 16th Workshop of the Tandem Accelerator and their Associated Technology
Kobe Univ. (Jun. 30-Jul. 1, 2003)

NUCLEAR STRUCTURE

Journal / Proceedings

Y.H. Zhang, M. Oshima, Y. Toh, M. Koizumi, A. Osa, T. Shizuma, T. Hayakawa, M. Sugawara,
H. Kusakari, T. Morikawa, S.X. Wen, L.H. Zhu
Rotational Bands of Odd-odd ^{172}Re
Phys. Rev. C68 (2003) 054313

T. Hayakawa, Y. Toh, M. Oshima, A. Osa, M. Koizumi, Y. Hatsukawa, J. Katakura, M. Matsuda,
Y. Utsuno, T. Morikawa, H. Kusakari, M. Sugawara, T. Czosnyka
Projectile Coulomb Excitation of ^{78}Se
Phys. Rev. C 67 (2003) 064310

T. Hayakawa, Y.Toh, M.Oshima, M.Matsuda, Y.Hatsukawa, N.Shinohara, H.Iimura, T.Shizuma,
Y.H.Zhang, M.Sugawara, H.Kusakari
Electric-dipole Transition Probabilities between Yrast Bands in ^{157}Gd
Phys. Lett. B551 (2003) 79

T. Shizuma, Y. Toh, M. Oshima, M. Sugawara, M. Matsuda,T. Hayakawa, M. Koizumi, A. Osa,
Y.H. Zhang, Z. Liu
Inelastic Excitation of ^{187}Re
Eur.Phys.J. A17 (2003) 159

M. Koizumi, A. Osa, M. Oshima, T. Sekine, T. Wakui, W.G. Jin, H. Katsuragawa, H. Miyatake, Y. Ishida
A Laser Ion Source with a Thin Ohmic-heating Ionizer for the TIARA-ISOL
Nucl. Instrum. Method. in Phys. Res. B 204 (2003) 359

M. Koizumi, A. Seki, Y. Toh, M. Oshima, A. Osa, A. Kimura, Y. Hatsukawa, T. Shizuma, T. Hayakawa,
M. Matsuda, J. Katakura, T. Czosnyka, M. Sugawara, T. Morikawa, H. Kusakari
Multiple Coulomb Excitation Experiment of ^{68}Zn
Nucl. Phys. A736 (2003) 46

M. Koizumi, A. Seki, Y. Toh, M. Oshima, A. Osa, A. Kimura, Y. Hatsukawa, T. Shizuma, T. Hayakawa,
M. Matsuda, J. Katakura, T. Czosnyka, M. Sugawara, T. Morikawa, H. Kusakari
Multiple Coulomb Excitation Experiment of ^{66}Zn
Euro. Phys. J. A18 (2003) 87

X. H. Zhou, M. Oshima, F. R. Xu, Y. Toh, Y. H. Zhang, Y. Zheng, Y. B. Xu, M. Koizumi, A. Osa,
T. Hayakawa, Y. Hatsukawa, T. Shizuma, M. Sugawara
Configuration-dependent Bands in ^{169}Re

Euro. Phys. J. A 19 (2004) 11

C. Y. Xie, BX. H. ZhouB, Y. Zheng, Y. H. Zhang, Z. Liu, Z. G. Gan, T. Hayakawa, M. Oshima, Y. Toh,
T. Shizuma, J. Katakura, Y. Hatsukawa, M. Matsuda, H. Kusakari, M. Sugawara, K. Furuno,
T. Komatsubara
Level Structure of ^{146}Tb
Euro. Phys. J. A 19 (2004) 7

Y. Zheng, BX. H. ZhouB, Y. H. Zhang, T. Hayakawa, M. Oshima, Y. Toh, T. Shizuma, J. Katakura,
Y. Hatsukawa, M. Matsuda, H. Kusakari, M. Sugawara, K. Furuno, T. Komatsubara
Multi-quasiparticle Excitations in ^{145}Tb
J. Phys. G: Nucl. Part. Phys. 30 (2004)1

L. T. Song, BX. H. Zhou, Y. H. Zhang, Y. X. Guo, X. G. Lei, Z. Y. Sun, M. Oshima, Y. Toh, A. Osa,
M. Koizumi, J. Katakura, Y. Hatsukawa, M. Matsuda, M. Sugawara
Rotational Band Built on the 1/2[660]($i_{13/2}$) Configuration in ^{179}Au
Phys. Rev. C69 (2004) 011403

T. Shizuma, Z.G. Gan, K. Ogawa, H. Nakada, M. Oshima, Y. Toh, T. Hayakawa, Y. Hatsukawa,
M. Sugawara, Y. Utsuno, Z. Liu
A new Isomer in ^{136}Ba Populated by Deep-inelastic Collisions
Euro. Phys. J. A20 (2004)207

M. Koizumi, A. Seki, Y. Toh, M. Oshima, A. Osa, Y. Utsuno, A. Kimura, Y. Hatsukawa, T. Hayakawa,
T. Shizuma, J. Katakura, M. Matsuda, M. Sugawara, T. Morikawa, H. Kusakari, T. Czosnyka
Coulomb Excitation of Stable even-even Zn Isotopes
The proceedings of "A New Era of Nuclear Structure Physics (NENS03)"

M. Sakama, M. Asai, K. Tsukada, S. Ichikawa, I. Nishinaka, Y. Nagame, H. Haba, S. Goto, M. Shibata,
K. Kawade, Y. Kojima, Y. Oura, M. Ebihara, H. Nakahara
α-decays of Neutron-deficient Americium Isotopes
Phys. Rev. C 69 (2004) 014308

M. Asai, S. Ichikawa, K. Tsukada, A. Osa, I. Nishinaka, Y. Nagame, Y. Kojima, M. Shibata
Gamma-ray Spectroscopy for Neutron-rich A=160–170 Nuclei: the β⁻Decay of ^{159}Pm, $^{160-162}$Sm, ^{162}Eu, $^{164-166}$Gd, and $^{166-168}$Tb
Proc. of the 3rd Int. Conf. on Fission and Properties of Neutron-rich Nuclei
Sanibel Island (Nov. 3–9, 2002 (World Scientific, Singapore, 2003)) 227–232

M. Asai, T. Ishii, A. Makishima, M. Ogawa, M. Matsuda
Nanosecond Isomers in Neutron-rich N=19 Nuclei

Proc. of the 3rd Int. Conf. on Fission and Properties of Neutron-rich Nuclei
Sanibel Island, USA, November 3–9, 2002 (World Scientific, Singapore, 2003) 295–297

L. Hou, T. Ishii, M. Asai, J. Hori, K. Ogawa, H. Nakada
Measurement of B(M1) for the $\pi p_{3/2} \nu p_{1/2}^{-1}$ Doublet in ^{68}Cu
Phys. Rev. C 68 (2003) 054306

T. Ishii, M. Asai, M. Matsuda, P. Kleinheinz, Hou Long, J. Hori, A. Makishima, T. Kohno, M. Ogawa,
K. Ogawa, H. Nakada,
Nano-second Isomers in Neutron-Rich Nuclei around ^{68}Ni
Proc. of 3rd Int. Conf. on Fission and Properties of Neutron-rich Nuclei,
(World Scientific, Singapore, 2003), 125

Y. Zheng, X. H. Zhou, Y. H. Zhang, T. Hayakawa, M. Oshima, Y. Toh, T. Shizuma, J. Katakura,
Y. Hatsukawa, M. Matsuda, H. Kusakari, M. Sugawara, K. Furuno, T. Komatsubara
Multi-quasiparticle Excitations in ^{145}Tb
J. Phys. G30(2004)465

T. Shizuma, S. Mitarai, G. Sletten, R.A.Bark, N.L.Gjorup, H.J.Jensen, M. Piiparinen, J. Wrzesinski,
Y.R. Shimizu
High-spin Structure in ^{185}Os
Phys. Rev. C 69 (2004) 024305

H. Iimura, M. Koizumi, M. Miyabe, M. Oba, T. Shibata, N. Shinohara, Y. Ishida, T. Horiguchi,
H.A. Schuessler
Nuclear-moments and Isotope Shifts of ^{135}La, ^{137}La, and ^{138}La by Collinear Laser Spectroscopy
Phys. Rev. C68 (2003) 054328

H. Hayashi, O. Suematsu, M. Shibata, Y. Kojima, A. Taniguchi, K. Kawase.
Q_b Measurement using a well-type HPGe Detector
JAERI-Conf 2004-005, 207

Meetings

M. Koizumi, A. Seki, Y. Toh, M. Oshima, A. Osa, Y. Utuno, A. Kimura, Y. Hatsukawa, T. Hayakawa,
T. Shizuma, J. Katakura, M. Matsuda, M. Sugawara, T. Morikawa, H. Kusakari, T. Czosnyka,
Coulomb Excitation of Stable even-even Zn Isotopes
A New Era of Nuclear Structure Physics (NENS03), Kurokawa Village, Niigata (Nov. 19-22, 2003)

T. Morikawa, M. Nakamura, T. Sugimitsu, H. Kusakari, M. Sugawara, M. Oshima, Y. Toh, M. Koizumi,
Y. Hatsukawa, A. Kimura, J. Goto

High-Spin States in ^{43}Sc
Annual Meeting of the Physical Society of Japan, Fukuoka (Mar. 30, 2004)

M. Asai, K. Tsukada, S. Ichikawa, Y. Nagame, T. Ishii, I. Nishinaka, K. Akiyama, A. Osa, M. Sakama,
Y. Oura, K. Sueki , M. Shibata
Nuclear Structure of ^{257}No Studied by Measuring Internal Conversion Electrons
2003 Annual Meeting of the Japan Society of Nuclear and Radiochemical Sciences, Izumisano (Oct. 1–3, 2003)

M. Asai, M. Sakama, K. Tsukada, T. Ishii, Y. Nagame, I. Nishinaka, K. Akiyama, S. Ichikawa, K. Sueki,
Y. Oura, M. Shibata
α–γCoincidence Measurement for ^{257}No
The 59th Annual Meeting of the Physical Society of Japan, Fukuoka (Mar. 27–30, 2004)

T. Ishii
γ-ray Spectroscopy of Neutron-rich Nuclei Produced in Deep-inelastic Collisions
Fall Meeting of the Physical Society of Japan, Miyazaki (Sep. 11, 2003)

T. Ishii
Nano-second Isomer Spectroscopy of Neutron-rich Nuclei Produced by Deep-inelastic Collisions
Sweden-Japan Joint Symposium on Accelerator Science and Accelerator based Sciences (Jan. 7, 2004).

T. Ishii, M. Asai, M. Matsuda, S. Ichikawa, T. Kohno, M. Ogawa
Nano-second Isomer Spectroscopy of the ^{48}Ca Region through Deep-inelastic Collisions
CNS-Riken Joint Symposium on Frontier of Gamma-ray Spectroscopy and its Application (Mar. 18, 2004)

T. Shizuma
Cross Section Measurements on Population and Depopulation of the Isomers in ^{176}Lu and ^{180}Ta by High Energy Synchrotron Radiation
Meeting on Application of High Energy Synchrotron Radiation from Superconducting Wigler, Spring-8 (Dec. 2003)

H. Wang, H. Ohba, M. Saeki, M. Miyabe, H. Miyatake, H. Iimura
Laser Induced Fluorescence Spectroscopy of Nd Atoms/Ions Produced by Laser Ablation
Fall Meeting of the Physical Society of Japan, Okayama, (Sep. 23, 2003)

H. Wang, H. Ohba, M. Saeki, M. Miyabe, H. Miyatake, H. Iimura
Laser Induced Fluorescence Spectroscopy of Neodymium Atoms Produced by Laser Ablation
5th Symposium on Advanced Photon Research, Kyoto, (Nov. 21, 2003)

NUCLEAR REACTIONS

Journal / Proceedings

K. Nishio, H. Ikezoe, S. Mitsuoka, K. Satou, C.J. Lin
Half-life of ^{228}Pu and α Decay of ^{228}Np
Phys. Rev. C68 (2003) 064305

K. Nishio, H. Ikezoe, Y. Nagame, S. Mitsuoka, I. Nishinaka, L. Duan, K. Satou, M. Asai, H. Haba,
K. Tsukada,S. Shinohara, S. Ichikawa
Fragment Mass Distribution of the $^{239}Pu(d,pf)$ Reaction via the Superdeformed β-vibrational Resonance
Proceedings of the International Workshop on New Applications of Nuclear Fission.
Bucharest, Romania (Sep. 7-12, 2003)

K. Nishio, H. Ikezoe, S. Mitsuoka, K. Satou, C.J. Lin
Half-life of ^{228}Pu and α Decay of ^{228}Np
JAERI-Conf 2004-005
Proceedings of the 2003 Symposium on Nuclear Data (Nov. 27-28, JAERI, Tokai, 167 (2004))

F.Camera, A.Bracco, V.Nanal, M.P.Carpenter, F.Della Vedova, S.Leoni, B.Million, S.Mantovani,
M.Pignanelli, O.Wieland, B.B.Back, A.M.Heinz, R.V.F.Janssens, D.Jenkins, T.L.Khoo, F.G.Kondev,
T.Lauritsen, C.J.Lister, B.McClintock, S.Mitsuoka, E.F.Moore, D.Seweryniak, R.H.Siemssen, R.J.Van
Swol, D.Hofman, M.Thoennessen, K.Eisenman, P.Heckman, J.Seitz, R.Varner, M.Halbert, I.Dioszegi,
A.Lopez-Martens
Radiative Fusion from very Symmetric Reactions: the Giant Dipole Resonance in the ^{179}Au Nucleus
Phys. Lett. B 560 (2003) 155

K.Nishio, H.Ikezoe, Y.Nagame, S.Mitsuoka, I.Nishinaka, L.Duan, K.Satou, S.Goto, M.Asai, H.Haba,
K.Tsukada, N.Shinohara, S.Ichikawa, T.Ohsawa
Fragment Mass Distribution of the $^{239}Pu(d, pf)$ Reaction via the Superdeformed Beta-vibrational Resonance
Phys. Rev. C 67 (2003) 014604

V.Nanal, T.L.Khoo, D.J.Hofman, B.B.Back, M.P.Carpenter, I.Dioszegi, K.Eisenman, M.L.Halbert,
P.Heckman, A.M.Heinz, D.Henderson, D.Jenkins, M.P.Kelly, F.G.Kondev, T.Lauritsen, C.J.Lister,
B.McClintock, S.Mitsuoka, T.Pennington, J.Seitz, R.H.Siemssen, M.Thoennessen, R.J.van Swol,
R.L.Varner, P.Wilt, Y.Alhassid
Highly Selective Studies of GDR in ^{164}Er
Nucl. Phys. A731 (2004) 153

H. Ishiyama, H. Miyatake, M-H. Tanaka, Y. X. Watanabe, N. Yoshikawa, S. C. Jeong, Y. Matsuyama,
Y. Fuchi, I. Katayama, T. Nomura, T. Hashimoto, T. Ishikawa, K. Nakai, S. S. Das, P. K. Saha, T. Fukuda,
K. Nishio, S. Mitsuoka, H. Ikezoe, M. Matsuda, S. Ichikawa, T. Furukawa, H. Izumi, T. Shimoda, Y. Mizoi,
M. Terasawa.
Study of Astrophysical (α, n) and (p, n) Reactions on Light Neutron-rich Nuclei by means of Low-energy RNB
American Institute of Physics Conference Proceedings 704 (2003) 453

H. Miyatake, H. Ishiyama, M-H. Tanaka, Y. X. Watanabe, N. Yoshikawa, S. C. Jeong, Y. Matsuyama,
Y. Fuchi, T. Nomura, T. Hashimoto, T. Ishikawa, K. Nakai, S. K. Das, P. K. Saha, T. Fukuda, K. Nishio,
S. Mitsuoka, H. Ikezoe, S. Ichikawa, M. Matsuda, Y. Mizoi, T. Furukawa, H. Izumu, T. Shimoda,
M. Terasawa
Exclusive Measurement of the Astrophysical $^8Li(α, n)$ Reaction Cross Section
Nucl. Phys. A738(2004)401

Meeting

K. Nishio, H. Ikezoe, Y. Nagame M. Asai, K. Tsukada, S. Mitsuoka, K. Tsuruta, K. Satou, C.J. Lin,
T. Ohsawa
Measurement of Evaporation Rresidue Cross Sections in the Sub-barrier $^{16}O+^{238}U$ Reaction
Spring Meeting of the Physical Society of Japan, Fukouka (Mar. 30, 2004)

K. Nishio, H. Ikezoe, S. Mitsuoka, K. Satou, and C.J. Lin
Half-life of the α Decaying Nucleus ^{228}Pu
Fall Meeting of the Atomic Energy Socierty of Japan, Shizuoka (Sep. 25, 2003)

S.Mitsuoka, H.Ikezoe, K.Nishio, K.Satou, K. Tsuruta, C.J. Lin
Total Fusion Cross Section in $^{64}Ni+^{154}Sm$ Reaction
Fall Meeting of the Physical Society of Japan, Miyazaki (Sep. 9, 2003)

S.Mitsuoka, H.Ikezoe, K.Nishio, K.Satou, K. Tsuruta, C.J. Lin
Dependence of Heavy-ion Fusion Reaction on Nuclear Deformation
International Conference FUSION03: From a Tunneling Nuclear Microscope to Nucelar Processes in Matter, Miyagi (Nov. 12-15, 2003)

S.Mitsuoka, H.Ikezoe, K.Nishio, K.Satou, K. Tsuruta, C.J. Lin
Hugging Fusion of Deformed Nuclei for Heavy Element Synthesis
5th Japan-China Joint Nuclear Physics Symposium, Fukuoka (Mar. 7-10, 2004)

H. Ishiyama, H. Miyatake, M-H. Tanaka, Y. X. Watanabe, N. Yoshikawa, S. C. Jeong, Y. Matsuyama,
Y. Fuchi, I. Katayama, T. Nomura, T. Hashimoto, T. Ishikawa, K. Nakai, S. S. Das, P. K. Saha, T. Fukuda,
K. Nishio, S. Mitsuoka, H. Ikezoe, M. Matsuda, S. Ichikawa, T. Furukawa, H. Izumi, T. Shimoda, Y. Mizoi,
M. Terasawa
Study of Astrophysical (α, n) and (p, n) Reactions on Light Neutron-rich Nuclei by means of Low-energy RNB
Tours Symposium on Nuclear Physics 5, Tours, France (Aug. 26-29, 2003)

T. Hashimoto, T. Ishikawa, T. Kawamura, K. Nakai, H. Ishiyama, Y. X. Watanabe, H. Miyatake,
M.H. Tanaka, N. Yoshikawa, S. C. Jeong, Y. Fuchi, I. Katayama, T. Nomura, S. K. Das, P. K. Saha, T.
Fukuda, K. Nishio, S. Mitsuoka, H. Ikezoe, M. Matsuda, S. Ichikawa, T. Furukawa, H. Izumi, T. Shimoda,
Y. Mizoi, M. Terasawa,
Measurement of the $^8Li(α, n)^{11}B$ reaction Cross Sections of Astrophysical Interest
The Sxth International Conference on Radioactive Nuclear Beams (RNB6), Argonne (Sep. 22-26, 2003)

H. Ishiyama, H. Miyatake, M-H. Tanaka, Y. X. Watanabe, N. Yoshikawa, S. C. Jeong, Y. Matsuyama,
Y. Fuchi, T. Nomura, T. Hashimoto, T. Ishikawa, K. Nakai, S. K. Das, P. K. Saha, T. Fukuda, K. Nishio,
S. Mitsuoka, H. Ikezoe, S. Ichikawa, M. Matsuda, Y. Mizoi, T. Furukawa, H. Izumu, T. Shimoda,
M. Terasawa
Direct Measurements of the Astrophysical (α, n) and (p, n) Reactions by using Low-energy Light Neutron-rich RNB.
The Third International Conference on Origin of Matter and Evolution of the Galaxies, RIKEN (Nov. 17-19, 2003)

H. Miyatake, H. Ishiyama, M-H. Tanaka, Y. X. Watanabe, N. Yoshikawa, S. C. Jeong, Y. Matsuyama,
Y. Fuchi, T. Nomura, T. Hashimoto, T. Ishikawa, K. Nakai, S. K. Das, P. K. Saha, T. Fukuda, K. Nishio,
S. Mitsuoka, H. Ikezoe, S. Ichikawa, M. Matsuda, Y. Mizoi, T. Furukawa, H. Izumu, T. Shimoda,
M. Terasawa
Exclusive Measurement of the Astrophysical $^8Li(α, n)$ Reaction Cross Section
The Eighth International Conference on Clustering Aspects of Nuclear Structure and Dynamics, Nara (Nov. 24-29, 2003)

NUCLER CHEMISTRY

Journal / Proceedings

Y. Nagame, M. Asai, H. Haba, K. Tsukada, I. Nishinaka, S. Goto, A. Toyoshima, K. Akiyama, M. Sakama,
Y. L. Zhao, S. Ichikawa, and H. Nakahara
Heavy Element Nuclear Chemistry at JAERI
Phys. At. Nucl. 66 (2003) 1131

Y. Nagame, H. Haba, K. Tsukada, M. Asai, K. Akiyama, M. Hirata, I. Nishinaka, S. Ichikawa, H. Nakahara,
S. Goto, T. Kaneko, H. Kudo, A. Toyoshima, A. Shinohara, M. Schädel, J. V. Kratz, H. W. Gäggeler, and
A. Türler
Transactinide Nuclear Chemistry at JAERI
Czech. J. Phys. 53 (2003) A299

Y. Nagame, H. Haba, K. Tsukada, M. Asai, A. Toyoshima, S. Goto, K. Akiyama, T. Kaneko, M. Sakama,
M. Hirata, T. Yaita, I. Nishinaka, S. Ichikawa, and H. Nakahara
Chemical Studies of the Heaviest Elements
Nucl. Phys. A734c (2004) 124

H. Haba, K. Tsukada, M. Asai, A. Toyoshima, K. Akiyama, I. Nishinaka, M. Hirata, T. Yaita, S. Ichikawa,
Y. Nagame, K. Yasuda, Y. Miyamoto, T. Kaneko, S. Goto, S. Ono, T. Hirai, H. Kudo, M. Shigekawa,
A. Shinohara, Y. Oura, H. Nakahara, K. Sueki, H. Kikunaga, N. Tsuruga, A. Yokoyama, M. Sakama,
S. Enomoto, M. Schädel, W. Brüchle, and J. V. Kratz
Fluoride Complexation of Element 104, Rutherfordium
J. Am. Chem. Sci. 126 (2004) 5219

I. Nishinaka, Y. Nagame, H. Ikezoe, Y. L. Zhao, K. Sueki, and H. Nakahara
Partition of Total Excitation Energy between Fragment Pairs in Asymmetric and Symmetric Fission Modes
Phys. Rev. C 70 (2004) 014609-1

Y. Hatsukawa, Y. Toh, M. Oshima, T. Hayakawa, N. Shinohara, K. Kushita, T. Ueno, K. Toyota
New Technique for the Determination of Trace Elements using Multiparameter Coincidence Spectrometry
J. Radioanal. Nucl. Chem. 255 (2003) 111

Y. Toh, M. Oshima, R. Matsumoto, M.H. Mahmudy Gharaie, Y. Hatsukawa, N. Shinohara, A. Kimura,
J. Goto
Trace Element Analysis by Multiple Gamma Ray Detection Method
Geochim. Cosmochim. Acta, 67, No18S (2003) A483

M. H. Mahmudy Gharaie, R. Matsumoto, Y. Kakuwa, P.G. Milroy, Y. Toh, M. Oshima
Geochemical Evidence for Environmental Changes at Frasnian-famennian Boundary leading to the Mass Extinction
Geochim. Cosmochim. Acta, 67, No18S (2003) A268

Y. Hatsukawa, M. H. Mahmudy Gharaie, R.Matsumoto, Y. Toh, M. Oshima, A. Kimura, T. Noguchi,
T. Goto, Y. Kakuwa
Ir Anomalies in Marine Sediments: Case Study for the Late Devonian Mass Extinction Event
Geochim. Cosmochim. Acta, 67 (2003) A138

A.Kimura, Y. Toh, M. Oshima, Y. Hatsukawa, J. Goto
Determination of Trace Elements in Iron and Steel by Neutron Activation Analysis with Multiple Gamma-ray Detection
J. Nucl. Radiochem. Sci. 4 (2003) 183

H. Miyahara, K Katoh, N. Marnada, K.Ikeda, K. Fujiki, I. Nishinaka, K. Tsukada, Y. Nagame, M. Asai,
S. Ichikawa, H. Haba
Emission Probability Measurement of Principal γ-rays of ^{147}Eu
Nucl. Instrum. Method. A 523 (2004) 96

Meeting

K. Tsukada, H. Haba, M. Asai, K. Akiyama, A. Toyoshima, I. Nishinaka, M. Hirata, K. Hashimoto,
S. Ichikawa, Y. Nagame, K. Yasuda, Y. Miyamoto, Y. Tani, H. Hasegawa, W. Sato, A. Shinohara, S. Goto,
M. Ito, J. Saito, H. Ishizu, H. Kudo, Y. Oura, K. Sueki, H. Nakahara, N. Kinoshita, H. Kikunaga,
A. Yokoyama, M. Sakama, M. Schadel, J.V. Kratz
Anion-exchange Behavior of Rutherfordium and Dubnium in P ure HF Solution
The Second International Conference on The Chemistry and Physics of the Transactinide Elements (TAN03), Napa, California (Nov. 16-20, 2003)

K. Tsukada, H. Haba, M. Asai, A. Toyoshima, K. Akiyama, I. Nishinaka, M. Hirata, K. Hashimoto, S.I.
Ichikawa, Y. Nagame, H. Nakahara, K. Yasuda, Y. Miyamoto, J. Saito, M. Ito, H. Ishizu, S. Goto,
H. Kudo, Y. Tani, H. Hasegawa, W. Sato, A. Shinohara,K. Sueki,Y. Oura, N. Kinoshita, H. Kikunaga,
A. Yokoyama
Anion-exchange Behavior of Db in HF
2003 Annual Meeting of the Japan Society of Nuclear and Radiochemical Sciences, Osaka (Oct. 1-3, 2003)

Y. Toh, M. Oshima, R. Matsumoto, M.H. Mahmudy Gharaie, Y. Hatsukawa, N. Shinohara, A. Kimura,
J. Goto
Trace Element Analysis by Multiple Gamma Ray Detection Method
Thirteenth Annual V. M. Goldschmidt Conference, Kurashiki (Sep. 7, 2003)

M. H. Mahmudy Gharaie, R. Matsumoto, Y. Kakuwa, P.G. Milroy, Y. Toh, M. Oshima
*Geochemical Evidence for Environmental Changes at Frasnian-famennian Boundary leading to the Mass
Extinction*
Thirteenth Annual V. M. Goldschmidt Conference, Kurashiki (Sep. 7, 2003)

Y. Hatsukawa, M. H. Mahmudy Gharaie, R. Matsumoto, Y. Toh, M. Oshima, A. Kimura, T. Noguchi,
T. Goto, Y. Kakuwa
Ir Anomalies in Marine Sediments: Case Study for the Late Devonian Mass Extinction Event
Thirteenth Annual V. M. Goldschmidt Conference, Kurashiki (Sep. 7, 2003)

NUCLEAR THEORY

Journal / proceedings

T. Tanigawa, M. Matsuzaki, S. Chiba

Possibility of ΛΛ Pairing and Its Dependence on Background Density in a Relativistic Hartree-Bogoliubov Model

Phys. Rev. C 68 (2003) 015801

P. Möller, A. J. Sierk, A. Iwamoto, T. Ichikawa

Calculation of High-dimensional Fission-fusion Potential Energy Surfaces in the SHE Region

AIP Conference Proceedings 704 (2004) 49

Tom. Maruyama, S. Chiba

In-medium Effects in Eta-photo-production through the S_{11} Resonance in the Relativistic Approach

Prog. Theor. Phys. 11 (2004) 229

Meetings

T. Ichikawa, A. Iwamoto, P. Möller, A. J. Sierk

Study of Effective Fusion Barrier for Production of Super Heavy Elements

Spring Meeting of Physical Society of Japan, Fukuoka (Mar. 29, 2004)

P. Möller, A. J. Sierk, T. Ichikawa, A. Iwamoto

Calculation of High-dimensional Fission-fusion Potential Energy Surfaces in the SHE Region

Tours Symposium on Nuclear Physics V, Tours, France (Aug. 26, 2003)

P. Möller, A. J. Sierk, T. Ichikawa, A. Iwamoto

Fission and Fusion at the End of the Periodic System

FUSION03: From a Tunneling Nuclear Microscope to Nuclear Processes in Matter, Matsushima, Miyagi (Nov. 12, 2003)

A. Iwamoto, T. Ichikawa, P. Möller, A. J. Sierk

Cluster Expression in Fission and Fusion

Cluster03: Clustering Aspects of Nuclear Structure and Dynamics, Nara (Nov. 27, 2003)

T. Tanigawa, M. Matsuzaki, S. Chiba

ΛΛ Pairing and Neutrino Emissivity in a Relativistic Model

2003 Autumn Meeting of the Physical Society of Japan

Miyazaki World Convention Center Summit, Miyazaki (Sep. 9-16, 2003)

T. Tanigawa, M. Matsuzaki, S. Chiba
$^1S_0$ Proton Pairing in Neutron Star Matter within a Relativistic Model
59th Annual Meeting of the Physical Society of Japan
Kyushu University, Hakozaki Campus, Fukuoka (Mar. 27-30, 2004)

Y. Utsuno
Monte Carlo Shell Model Study of Structure of Unstable Nuclei around N=20
ECT Workshop on "Recent Advances in Nuclear Shell Model", Trento (July 11, 2003)

Y. Utsuno
Varying Shell Gap and Deformation in N~20 Unstable Nuclei around N=20 Studied by the Monte Carlo Shell Model
Fall Meeting of the Physical Society of Japan, Miyazaki (Sep. 11, 2003)

Y. Utsuno, T. Otsuka, T. Mizusaki, M. Honma
Structure of Neutron-rich Na Isotopes and the Shell Evolution
RCNP Workshop on "Nuclear Force and Nuclear Structure", Osaka (Mar. 24, 2004)

Y. Utsuno
Mechanism of anomalous Magnetic Moment of ^9C by the Shell Model
The 59th annual Meeting of the Physical Society of Japan, Fukuoka (Mar. 28, 2004)

T. Maruyama, T. Tatsumi, D.Voskresensky, T. Tanigawa, S. Chiba
Kaon Condensation and the Non-uniform Nuclear Matter
Tours Symposium on Nuclear Physics V, Tours, France (Aug. 26-29, 2003).

Tos. Maruyama, T. Tatsumi, D.N. Voskresensky, T. Tanigawa, S. Chiba, Tom. Maruyama
Coulomb Screening Effect on the Nuclear-pasta Structure
Int. Symp. on Origin of Matter and Evolution of the Galaxy OMEG03, RIKEN (Nov. 17-19, 2003)

S. Chiba, T. Maruyama, T. Tanigawa, S. Gojuki, S. Nakamura, K. Samata, S. Oryu
Effective Inter-cluster Potentials Generated by RGM, OCM and EST Expansion
The 8th International Conference on Clustering Aspects of Nuclear Structure and Dynamics, Nara (Nov. 24-29, 2003)

Tos. Maruyama, T. Tatsumi, D.N. Voskresensky, T. Tanigawa, S. Chiba, Tom. Maruyama
Coulomb Screening Effect on the Nuclear-pasta Structure
The 8th International Conference on Clustering Aspects of Nuclear Structure and Dynamics, Nara (Nov. 24-29, 2003)

Tos. Maruyama, T. Tatsumi, D.N. Voskresensky, T. Tanigawa, S. Chiba. Tom. Maruyama
Kaon Condensation and the Structured Mixed Phase
The 8th International Conference on Clustering Aspects of Nuclear Structure and Dynamics, Nara (Nov. 24-29, 2003)

Tos. Maruyama, T. Tatsumi, D.N. Voskresensky, T. Tanigawa, S. Chiba, Tom. Maruyama
Kaon Condensation and the Non-uniform Nuclear Matter
YITP Workshop on Nuclear Matter under Extreme Conditions (Matter03), Kyoto (Dec. 2003)

ATOMIC PHYSICS AND SOLID STATE PHYSICS

Journal / Proceedings

K. Kawatsura, K. Takahiro, M. Imai, M. Sataka, K. Komaki, H. Shibata
Ejected Electron Spectra from Highly Excited States in High-energy Collisions of O^{q+} with He
Nucl. Instrum. Method B205 (2003) 528

M. Imai, M. Sataka, K. Kawatsura, K. Takahiro, K. Komaki, H. Shibata
Zero-degree Electron Spectroscopy of Highly Charged Argon and Titanium Ions
Atomic Collision Research in Japan 29 (2003) 23

S.C. Jeong, I. Katayama, H. Kawakami, H. Ishiyama, H. Miyatake, M. Sataka, A. Iwase, S. Okayasu,
H. Sugai, S. Ichikawa, K. Nishio, Y. Sugiyama, M. Yahagi, K. Takada, M. Watanabe
Simulation Study on the Measurement of Diffusion Coefficient in Solid Materials by Short-lived Radiotracer Beams
Jpn. J. Appl. Phys. (2003) 42 (2003) 4576

S.C. Jeong, I. Katayama, H. Kawakami, H. Ishiyama, H. Miyatake, M. Sataka, A. Iwase, S. Okayasu,
H. Sugai, S. Ichikawa, K. Nishio, Y. Sugiyama, M. Yahagi, K. Takada, M. Watanabe
Simulation of Radiotracer Method for Diffusion Studies using Short-lived Radioactive Nuclear Beams
Nucl. Instrum. Method. B212 (2003) 483

H. Kito, A. Iyo, A. I. Crisan, M. Hirai, M. Tokumoto, S. Okayasu, M. Sasase, H. Ihara Y. Tanaka
Heavy-ion Irradiation Dependence of the Superconducting Properties of $(Cu,C)Ba_2Ca_3Cu_4O_{10.5-\delta}$
Physica C388-389 (2003) 711

H. Kito, A. Iyo, M. Hirai, A. Crisan, M. Tokumoto, S. Okayasu, M.Sasase, M. Sataka, H. Ihara
Y. Tanaka
Heavy-ions Irradiation Dependence of Superconducting Properties of the Cu-based $(Cu,C)Ba_2Ca_3Cu_4O_{11-\delta}$
Physica C392-396 (2003) 181

Meetings

M. Imai, M. Sataka, S. Kitazawa, K. Nishio, K. Kawatsura, K. Takahiro, K. Komaki, H. Shibata H. Tawara
Coster-Kronig Electron Spectra of Silicon, Sulfur, Argon and Titanium Ion Excited through C-foil Target
XXIII International Conference on Photonic, Electronic and Atomic Collisions, Stockholm (Jul. 2003)

K. Kawatsura, K. Takahiro, M. Sataka, M. Imai, K. Komaki, H. Shibata
Coster-Kronig and Auger Electrons from Highly Excited States in High-energy Collisions of O^{q+} with He
XXIII International Conference on Photonic, Electronic and Atomic Collisions, Stockholm (Jul. 2003)

H. Kito, A. Iyo, M. Hirai, M. Tokumoto, S. Okayasu, M. Sasase, M. Sataka, H. Ihara, Y. Tanaka
Ion Irradiation Dependence of the Superconducting Properties of $(Cu,C)Ba_2Ca_3Cu_4O_{10.5-\delta}$
The 7th International Conference on Materials and Mechanisms of Superconductivity and High Temperature Superconductors (M2S-HTSC VII), Rio de Janeiro (May. 27, 2003)

RADIATION EFFECTS IN MATERIALS

Journal / proceedings

N. Matsunami, M. Sataka, A. Iwase, S. Okayasu
Electronic Excitation Induced Sputtering of Insulating and Semiconducting Oxides by High Energy Heavy Ions
Nucl. Instrum. Method. B203 (2003) 288

H. Maeta, T. Kato, H. Ohtsuka, M. Sataka. N. Matsumoto, H. Sugai
X-ray Diffuse Scattering of Radiation Induced Defects in Ions -irradiated Ni
JAERI-Conf-2003-017

T. Nakazaawa, V. Grismanovs, D. Yamaki, Y. Katano, T. Aruga
Disordering in Li_2TiO_3 Irradiated with High Energy Ions
Nucl. Instrum. Method. B206 (2003) 166

T. Sonoda, N. Ishikawa, Y. Chimi, A. Iwase
Radiation Effects in Fluorite Structure Ceramics CeO_2 under Fission Energy Ion Irradiation as Simulations of Fission Field in Nuclear Fuels
CRIEPI Rep. T03069 (2003) (in Japanese)

Y. Chimi, A. Iwase, T. Iwata
Defect Production and Radiation Annealing in Platinum Irradiated with High-energy Heavy Ions
Nucl. Instrum. Method. B209 (2003) 159

S. Ishino, Y. Chimi, Bagiyono, T. Tobita, N. Ishikawa, M. Suzuki, A. Iwase
Radiation Enhanced Copper Clustering Processes in Fe-Cu Alloys during Electron and Ion Irradiations as Measured by Electrical Resistivity
J. Nucl. Mater. 323 (2003) 354

Y. Chimi, N. Ishikawa, A. Iwase
Effects of High-energy Ion Irradiation in Bismuth Thin Films at Low Temperature
Mat. Res. Soc. Symp. Proc. 792 (2004) 379

F. Ono, Y. Hamatani, Y. Mukumoto, S. Komatsu, N. Ishikawa, Y. Chimi, A. Iwase, T. Kambara, C. Mueller R. Neumann
Modification of Fe-Ni Invar Alloys by High-energy Ion Beams
Nucl. Instrum. Method. B206 (2003) 295

A. Iwase, Y. Hamatani, Y. Mukumoto, N. Ishikawa, Y. Chimi, T. Kambara, C. Mueller, R. Neumann, F. Ono
Anomalous Shift of Curie Temperature in Iron-nickel Invar Alloys by High-energy Heavy Ion Irradiation
Nucl. Instrum. Method. B209 (2003) 323

A. Iwase, Y. Hamatani, Y. Mukumoto, N. Ishikawa, Y. Chimi, T. Kambara, C. Mueller, R. Neumann, F. Ono
Modification of Magnetic Properties of Fe-Ni Invar Alloys by GeV Heavy Ion Irradiation
RIKEN Accel. Prog. Rep. 36 (2003) 99

A. Kurumada, Y. Imamura, T. Oku, M. Ishihara, S. Baba, J. Aihara
Ion Irradiation Effects on Tensile Properties of Carbon Fibers
OECD 2004, NEA No.5309, (2004) 121

A. Kurumada, Y. Imamura, T. Oku, M. Ishihara, S. Baba, J. Aihara
Effects of Ion Irradiation on Mechanical Properties of Carbon Fibers
JAERI-Conf 2003-017, 139

Meetings

M. Shimada, K. Yasuda, S. Matsumura, C. Kinoshita
Radiation Defects in Oxide Ceramics Irradiated with 200 MeV Xe
Fall Meeting of the Japan Institute of Metal, Sapporo (Oct. 11, 2003)

M. Shimada, S. Matsumura, C. Kinoshita.
Precise Analysis of Atomic Configurations by Electron Channeling X-ray Spectroscopy
Fall Meeting of the Japan Institute of Metal, Sapporo (Oct. 13, 2003)

M. Shimada, S. Matsumura, K. Yasuda and C. Kinoshita, N. Ishikawa, Y. Chimi
Atomic Disordering around Ion Tracks in Magnesium Aluminate Spinel
Spring Meeting of the Japan Institute of Metal, Sapporo (Mar. 31, 2004)

M. Shimada, S. Matsumura, K. Yasuda and C. Kinoshita, Y. Chimi, N. Ishikawa, A. Iwase
Radiation-induced Disordering in Magnesium Aluminate Spinel Subjected to Ionizing Radiation
11th International Conference on Fusion Reactor Materials, Kyoto (Dec. 7-12, 2003)

T. Nakazawa, A. Naitou, D. Yamaki, T. Aruga
Disordering in Li_2TiO_3 Irradiated with High Energy Ions
2004 Annual Meeting of the Atomic Energy Society of Japan, Okayama (Mar. 29-31, 2004)

T. Sonoda, M. Kinoshita, Y. Chimi, N. Ishikawa, A. Iwase, K. Yasuda

Microstructural Evolution and Electronic Excitation Effects in CeO$_2$ under High Energy Ion and Electron Irradiation

Fall Meeting of Japan Institute of Metals, Sapporo (Oct. 11, 2003)

T. Sonoda, Y. Chimi, N. Ishikawa, A. Iwase

Microstructural Evolution and Electronic Excitation Effects in CeO$_2$ under High Energy Ions

Materials Science Symposium "High-Density Electronic Excitation Effects", JAERI Tokai (Nov. 26-27, 2003)

R. Nakatani, A. Iwase, R. Taniguchi, Y. Chimi, N. Matsunami

Atomic Mixing Induced by High-energy Heavy Ion Irradiations

Fall Meeting of the Physical Society of Japan, Okayama (Sep. 21, 2003)

R. Nakatani, A. Iwase, R. Taniguchi, Y. Chimi, N. Ishikawa, H. Tsuchida

Atomic Mixing Induced by Electronic Excitation

Spring Meeting of the Physical Society of Japan, Fukuoka (Mar. 28, 2004)

A. Iwase

Interactions between Swift Heavy Ions and Materials

Symposium of Quantum Science and Engineering Center, Kyoto (Oct. 3, 2003)

R. Nakatani

Swift Heavy Ion Induced Atomic Mixing

Forum 21 (Jan. 10, 2004)

A. Iwase

Materials Science under High Energy Irradiation Fields

Symposium on Development of Quantum Beam for Nano-Technology and Application, Ibaraki (Feb. 3, 2004)

M. Fukuzumi, R. Taniguchi, F. Hori, Y. Chimi, S. Komatsu, F. Ono, T. Kambara, A. Iwase

Lattice Structure and Magnetic Properties of FeRh Intermetallic Compounds Irradiated with High Energy Particles

Fall Meeting of the Physical Society of Japan, Okayama (Sep. 21, 2003)

M. Fukuzumi, R. Taniguchi, F. Hori, S. Komatsu, Y. Chimi, T. Kambara, F. Ono, A. Iwase

Modification of Lattice Structure and Magnetic Properties of Fe-Rh Alloys by using Energetic Particle Irradiation

Materials Research Society 2003 Fall Meeting, Boston (Dec. 1, 2003)

M. Fukuzumi, R. Taniguchi, N. Ishikawa, Y. Chimi, T. Kambara, S. Komatsu, F. Ono, F. Hori, A. Iwase
Swift Heavy Ion Induced Magnetic Phase Transition of Fe-Rh Alloy
Spring Meeting of the Physical Society of Japan, Fukuoka (Mar. 28, 2004)

Y. Chimi, N. Ishikawa, A. Iwase
Effects of High-energy Ion Irradiation in Bismuth Thin Films at Low Temperature
Fall Meeting of the Physical Society of Japan, Okayama (Sep. 21, 2003)

Y. Chimi, N. Ishikawa, A. Iwase
Effects of High-energy Ion Irradiation in Bismuth Thin Films at Low Temperature
Materials Research Society 2003 Fall Meeting, Boston (Dec. 1, 2003)

S. Ishino, Y. Chimi, A. Iwase, N. Soneda, A. Takahashi
On the Solute Migration during Irradiation
11th International Conference on Fusion Reactor Materials, Kyoto (Dec. 8, 2003)

S. Komatsu, Y. Hamatani, A. Iwase, N. Ishikawa, Y. Chimi, T. Kambara, F. Ono
Modification of Magnetic Properties in Fe-Ni Invar Alloys by Effect of Ion Irradiation
Fall Meeting of the Physical Society of Japan, Okayama (Sep. 21, 2003)

F. Ono, S. Komatsu, Y. Chimi, N. Ishikawa, T. Kambara, A. Iwase
Magnetic Properties in Fe-Ni Invar Alloys Irradiated by High-energy Ions
2003 Materials Research Society (MRS) Fall Meeting, Boston (Dec. 3, 2003)

A. Naito, T. Nakazawa, T. Aruga, A. Iwase, K. Abiko
Nanoindentation Hardening of High Purity Fe-P Alloys Irradiated MeV/u Xe Ions
2003 Spring Meeting of Japan Institute Metals, Chiba (Mar. 27-29, 2003)

A. Naito, T. Nakazawa, T. Aruga, A. Iwase, K. Abiko
Damage Structures of High Purity Fe-P Alloys Irradiated MeV/u Xe Ions
59-th Annual Meeting of the Japanese Society of Microscopy, Sapporo (Jun. 7-9, 2003)

K. Yamaguchi, T. Katsumata, K. Shimura, H. Yamamoto, K. Hojou
Effect of High-energy Heavy Ion Irradiation on Iron Silicide Thin Films
The 64th Autumn Meeting of the Japan Society of Applied Physics (Sep. 2, 2003)

A. Kurumada, Y. Imamura, T. Oku, M. Ishihara, S. Baba, J. Aihara, T. D. Burchell
Effects of Ion Irradiation on Tensile Properties of Carbon Fibers
International Nuclear Graphite Specialists Meeting-4, Marugame (Sep. 13-16, 2003)

A. Kurumada, Y. Imamura

Irradiation Damage Effects on Properties and Microstructures of Materials for HTTR

Oarai Research Reports, Institute for Materials Research, Tohoku University (Aug.21-22, 2003) 182

9. Personnel and Committees

This is a blank page.

(1) Personnel(FY 2003)

Department of Materials Science

Zenko	Yoshida	Director
Katsuyuki	Tomatsuri	Administrative Manager

Tandem Accelerator Group

Scientific Staff

Tadashi	Yoshida※
Suehiro	Takeuchi
Susumu	Hanashima
Makoto	Matsuda
Takamitsu	Nakanoya
Hiroshi	Kabumoto
Tetsuya	Sato

Technical Staff

Susumu	Kanda
Yoshihiro	Tsukihasi
Katsuzo	Horie
Isao	Ohuchi
Shinichi	Abe
Nobuhiro	Ishizaki
Hidekazu	Tayama

Entrusted Operators

Akihiko	Iijima
Takahiro	Yoshida
Hisashi	Sakurayama
Hikaru	Nisugi
Manabu	Satou
Teruo	Onodera

Entrusted Assistants

Yasuharu	Sugiyama
Yoshio	Fujii
Teruo	Kozawa

Research Group for Innovative Nuclear Science

Masumi	Oshima※
Hideki	Iimura
Tetsuya	Hirade
Yuichi	Hatsukawa
Akihiko	Osa
Yutaka	Utsuno
Yosuke	Toh
Mitsuo	Koizumi

Atsushi Kimura   (Post Doc.)
Jun   Goto   (Post Doc.)
Haiming Wang   (Visiting Researcher)
Akiyuki Seki   (Student)
Mahamudy Gharaie Mohamad Hosein   (Student)

Research Group for Nuclear Physics of Heavy Elements

Hiroshi Ikezoe※
Tetsuro Ishii
Shin-ichi Ichikawa
Katsuhisa Nishio
Shin-ichi Mitsuoka
Cheng-Jian Lin   (JSPS Research Fellow)
Kaoru   Tsuruta   (Post Doc.)
Trang Thi Kieu Hoang   (MEXT)
Ken-ichirou Satou   (Student)

Research Group for Radiation Effects and Analysis

Kiichi   Hojou※
Masao   Sataka
Hideo   Ohtsuka
Satoru   Okayasu
Teruo   Kato
Norito   Ishikawa
Yasuhiro Chimi
Takeo   Aruga
Tetsuya Nakazawa
Daijyu   Yamaki
Akira   Naito
Ken-ichiro Shimura   (Post Doc.)
Atsushi Hirose   (Student)
Seiji   Komatsu   (Student)

Advanced Science Research Center

Research Group for Many Body Theory of Hadron Systems

Satoshi Chiba※
Toshiki Maruyama
Tomonori Tanigawa   (JSPS Domestic Research Fellow)

Research Group for Atom-at-a-chemistry of the Heaviest Elements

Yuichiro Nagame※
Kazuaki Tsukada
Ichiro Nishinaka
Masato Asai
Kazuhiko Akiyama   (Post Doc.)

Takatoshi Ichikawa	(Post Doc.)
Atsushi Toyoshima	(Student)

Neutron Science Research Center

Research Group for Nanostructure

Yukio Morii※
Hiroyuki Yamamoto
Kenji Yaguchi

Department of Research Reactor

Division of Isotope Research and Development

Hiroyuki Sugai

Department of Health Physics

Radiation Control Division

Hitosi Ogose
Minako Yokoyama
Hutao Niino

Advanced Photon Research Center

Free Electron Laser Research Group

Takehito Hayakawa
Toshiyuki Shizuma

Takasaki Radiation Chemistry Research Establishment

Research Group for Severe Environment Materials

Toshio Hirao

Oarai Research Establishment

High Temperature Irradiation Laboratory

Masahiro Ishihara※
Shin-ichi Baba
Jun Aihara

※ Head

(2) Tandem Consultative Committee

(Chairman)	Toru	Nomura	(Professor, Prime Scientist, High Energy Accelerator Research Organization (KEK))
(Vice Chairman)	Hiroshi	Ikezoe	(Deputy Director, Department of Materials Science)
	Hiroyasu	Ejiri	(Professor Emeritus of Osaka University)
	Akihiko	Iwase	(Professor, Osaka Prefecture University)
	Kenji	Katori	(RI Beam Science Laboratory, RIKEN)
	Ken-ichiro	Komaki	(Professor, The University of Tokyo)
	Shigeru	Kubono	(Professor, The University of Tokyo)
	Hiroshi	Kudo	(Professor, Tsukuba University)
	Hisaaki	Kudo	(Professor, Niigata University)

Kenji	Morita	(Professor, Meijo University)
Tetsuo	Noro	(Professor, Kyushu University)
Tsutomu	Ohtsuki	(Associate Professor, Tohoku University)
Hiromi	Shibata	(Associate Professor, Kyoto University)
Kazuhiro	Yabana	(Associate Professor, Tsukuba University)

(Secretary)	Masao	Sataka	(Research Group of Radiation Effects and Analysis)
	Suehiro	Takeuchi	(Tandem Accelerator Group)
	Tadashi	Yoshida	(Head, Tandem Accelerator Group)
	Katsuyuki	Tomatsuri	(Administrative Manager, Department of Materials Science)

(3) Research Planning and Assessment Committee

(a) Sub-committee for Nuclear Physics and Nuclear Chemistry

(Chairman)	Shigeru	Kubono	(Professor, The University of Tokyo)
	Tetsuo	Noro	(Professor, Kyushu University)
	Tsutomu	Ohtsuki	(Associate Professor, Tohoku University)
	Kazuhiro	Yabana	(Associate Professor, Tsukuba University)
	Motoharu	Mizumoto	(Nuclear Transmutation Group)
	Nobuo	Shinohara	(R&D Group for Nonproliferation Technology)
	Suehiro	Takeuchi	(Tandem Accelerator Group)
(Secretary)	Susumu	Hanashima	(Tandem Accelerator Group)
(Secretary)	Tadashi	Yoshida	(Head, Tandem Accelerator Group)

(b) Sub-committee for Materials and Radiation Damage

(Chairman)	Kenji	Morita	(Professor, Meijo University)
	Ken-ichiro	Komaki	(Professor, The University of Tokyo)
	Hiroshi	Kudo	(Professor, Tsukuba University)
	Hiromi	Shibata	(Associate Professor, Kyoto University)
	Shiro	Jitsukawa	(Head, Research Group for Radiation Effects and Analysis)
	Hiroshi	Naramoto	(Head, Research Group for Design of New Materials with Energy Beams)
	Suehiro	Takeuchi	(Tandem Accelerator Group)
(Secretary)	Susumu	Hanashima	(Tandem Accelerator Group)
(Secretary)	Tadashi	Yoshida	(Head, Tandem Accelerator Group)

10. Cooperative Researches

This is a blank page.

Title	Contact person Organization
1. Decay study on neutron-rich nuclei produced with the fission of actinide elements	Michihiro SHIBATA Nagoya University
2. Study of heavy-ion fusion via reverse fission process	Hiroari MIYATAKE High Energy Accelerator Research Organization
3. Nuclear structure of the neutron-rich Ni region produced in deep-inelastic collisions	Masao OGAWA Tokyo Institute of Technology
4. Aqueous chemistry of elements 104(Rf) and 105(Db)	Atsushi SHINOHARA Osaka University
5. Studies on the shape coexistence in ^{70}Ge and the coexistence phenomenon of magnetic and anti-magnetic rotors	Masahiko SUGAWARA Chiba Institute of Technology
6. Ion source development for mass-separation of short-lived exotic nuclei	Sun Chan JEONG High Energy Accelerator Research Organization
7. Study of the explosive nucleo-synthesis by using RNB	Hiroari MIYATAKE High Energy Accelerator Research Organization
8. Study of superdeformed Nucleus by the fission experiment	Takaaki OHSAWA Kinki University
9. Synthesis of actinide metallofullerenes	Motomi KATADA Tokyo Metropolitan University
10. Studies on nuclear isomers at the A=180 mass region	Hiroaki UTSUNOMIYA Konan University
11. Nuclear chemical study on transactinide elements by use of gas phase chemistry	Hisaaki KUDO Niigata University

12. Nuclear structure study for heavy and transactinide nuclei

Yasuji OURA
Tokyo Metropolitan University

13. Study of collective motion in deformed high-spin isomers

Hideshige KUSAKARI
Chiba University

14. Systematic study of signature inversion and deformation at high spin in deformed nuclei

Masahiko SUGAWARA
Chiba Institute of Technology

15. Study of nuclear deformation using Coulomb excitation

Tsuneyasu MORIKAWA
University of Kyushu

16. Laser spectroscopy of radioactive isotopes around mass number 180

Takayoshi HORIGUCHI
Hiroshima International University

17. Ion irradiation effects on new superconducting material MgB_2

Hiroshi IKEDA
University of Tsukuba

18. Study of diffusion process in solid using short-lived nuclei

Ichiro KATAYAMA
High Energy Accelerator Research Organization

19. Interaction between columnar defects and vortices

Takanobu KISS
Kyushu University

20. Modification of magnetic properties using high density electronic excitation

Fumihisa ONO
Okayama University

21. Study of radiation defects in materials irradiated at low temperature with heavy ions by X-ray diffuse scattering

Hiroshi MAETA
Hiroshima Kokusai Gakuin University

22. Electronic excitation effects in ceramics by high-energy ion beams

Noriaki MATSUNAMI
Nagoya University

23. Electronic excitation effects on secondary ion emission from material surfaces bombarded by high energy

Tsuguhisa SEKIOKA
Himeji Institute of Technology

24. Electronic processes in highly charged ion collisions

Ken-ichiro KOMAKI
University of Tokyo

25. Study on recovery of properties of new carbon composite materials and carbon fibers with anti-irradiation damage due to high heat treatment after irradiation

Akira KURUMADA
Ibaraki University

26. Fine structures of oxide crystals under high density electronic excitation

Chiken KINOSHITA
Kyushu University

27. Research in the effect of heavy-ion irradiation for multi-layered (Cu,C)-12n(n-1) superconductors

Hijiri KITO
National Institute of Advanced Industrial Science and Technology (A.I.S.T)

28. Evaluation of single event effect in semiconductor device

Sumio MATSUDA
National Space Development Agency of Japan

29. Basic research on radiation effects of fission products in light water reactor fuels

Motoyasu KINOSHITA
Central Research Institute of Electric Power Industry (CRIEPI)

This is a blank page.

国際単位系 (SI) と換算表

表1 SI基本単位および補助単位

量	名 称	記 号
長 さ	メ ー ト ル	m
質 量	キログラム	kg
時 間	秒	s
電 流	アンペア	A
熱力学温度	ケ ル ビ ン	K
物 質 量	モ ル	mol
光 度	カンデラ	cd
平 面 角	ラ ジ ア ン	rad
立 体 角	ステラジアン	sr

表3 固有の名称をもつSI組立単位

量	名 称	記号	他のSI単位による表現
周 波 数	ヘ ル ツ	Hz	s^{-1}
力	ニュートン	N	$m \cdot kg/s^2$
圧 力, 応 力	パスカル	Pa	N/m^2
エネルギー, 仕事, 熱量	ジュール	J	$N \cdot m$
工 率, 放 射 束	ワ ッ ト	W	J/s
電 気 量, 電 荷	クーロン	C	$A \cdot s$
電位, 電圧, 起電力	ボ ル ト	V	W/A
静 電 容 量	ファラド	F	C/V
電 気 抵 抗	オ ー ム	Ω	V/A
コンダクタンス	ジーメンス	S	A/V
磁 束	ウェーバ	Wb	$V \cdot s$
磁 束 密 度	テ ス ラ	T	Wb/m^2
インダクタンス	ヘンリー	H	Wb/A
セルシウス温度	セルシウス度	℃	
光 束	ルーメン	lm	$cd \cdot sr$
照 度	ル ク ス	lx	lm/m^2
放 射 能	ベクレル	Bq	s^{-1}
吸 収 線 量	グ レ イ	Gy	J/kg
線 量 当 量	シーベルト	Sv	J/kg

表2 SIと併用される単位

名 称	記 号
分, 時, 日	min, h, d
度, 分, 秒	°, ′, ″
リ ッ ト ル	l, L
ト ン	t
電 子 ボ ル ト	eV
原子質量単位	u

$1\,eV = 1.60218 \times 10^{-19}\,J$

$1\,u = 1.66054 \times 10^{-27}\,kg$

表4 SIと共に暫定的に維持される単位

名 称	記 号
オングストローム	Å
バ ー ン	b
バ ー ル	bar
ガ ル	Gal
キ ュ リ ー	Ci
レ ン ト ゲ ン	R
ラ ド	rad
レ ム	rem

$1\,Å = 0.1\,nm = 10^{-10}\,m$

$1\,b = 100\,fm^2 = 10^{-28}\,m^2$

$1\,bar = 0.1\,MPa = 10^5\,Pa$

$1\,Gal = 1\,cm/s^2 = 10^{-2}\,m/s^2$

$1\,Ci = 3.7 \times 10^{10}\,Bq$

$1\,R = 2.58 \times 10^{-4}\,C/kg$

$1\,rad = 1\,cGy = 10^{-2}\,Gy$

$1\,rem = 1\,cSv = 10^{-2}\,Sv$

表5 SI接頭語

倍数	接頭語	記 号
10^{18}	エ ク サ	E
10^{15}	ペ タ	P
10^{12}	テ ラ	T
10^9	ギ ガ	G
10^6	メ ガ	M
10^3	キ ロ	k
10^2	ヘ ク ト	h
10^1	デ カ	da
10^{-1}	デ シ	d
10^{-2}	センチ	c
10^{-3}	ミ リ	m
10^{-6}	マイクロ	μ
10^{-9}	ナ ノ	n
10^{-12}	ピ コ	p
10^{-15}	フェムト	f
10^{-18}	ア ト	a

(注)

1. 表1−5は「国際単位系」第5版, 国際度量衡局 1985年刊行による。ただし, 1eV および1uの値はCODATAの1986年推奨値によった。
2. 表4には海里, ノット, アール, ヘクタールも含まれているが日常の単位なのでここでは省略した。
3. barは, JISでは流体の圧力を表わす場合に限り表2のカテゴリーに分類されている。
4. EC閣僚理事会指令ではbar, barnおよび「血圧の単位」mmHgを表2のカテゴリーに入れている。

換 算 表

力	N(=10^5dyn)	kgf	lbf
	1	0.101972	0.224809
	9.80665	1	2.20462
	4.44822	0.453592	1

粘 度 $1\,Pa \cdot s(N \cdot s/m^2) = 10\,P$(ポアズ)$(g/(cm \cdot s))$

動粘度 $1\,m^2/s = 10^4\,St$(ストークス)(cm^2/s)

圧	MPa(=10 bar)	kgf/cm²	atm	mmHg(Torr)	lbf/in²(psi)
力	1	10.1972	9.86923	7.50062×10^3	145.038
	0.0980665	1	0.967841	735.559	14.2233
	0.101325	1.03323	1	760	14.6959
	1.33322×10^{-4}	1.35951×10^{-3}	1.31579×10^{-3}	1	1.93368×10^{-2}
	6.89476×10^{-3}	7.03070×10^{-2}	6.80460×10^{-2}	51.7149	1

エネルギー・仕事・熱量	J(=10^7erg)	kgf·m	kW·h	cal（計量法）	Btu	ft・lbf	eV
	1	0.101972	2.77778×10^{-7}	0.238889	9.47813×10^{-4}	0.737562	6.24150×10^{18}
	9.80665	1	2.72407×10^{-6}	2.34270	9.29487×10^{-3}	7.23301	6.12082×10^{19}
	3.6×10^6	3.67098×10^5	1	8.59999×10^5	3412.13	2.65522×10^6	2.24694×10^{25}
	4.18605	0.426858	1.16279×10^{-6}	1	3.96759×10^{-3}	3.08747	2.61272×10^{19}
	1055.06	107.586	2.93072×10^{-4}	252.042	1	778.172	6.58515×10^{21}
	1.35582	0.138255	3.76616×10^{-7}	0.323890	1.28506×10^{-3}	1	8.46233×10^{18}
	1.60218×10^{-19}	1.63377×10^{-20}	4.45050×10^{-26}	3.82743×10^{-20}	1.51857×10^{-22}	1.18171×10^{-19}	1

$1\,cal = 4.18605\,J$（計量法）

$\qquad = 4.184\,J$ （熱化学）

$\qquad = 4.1855\,J$ （15 ℃）

$\qquad = 4.1868\,J$（国際蒸気表）

仕事率 $1\,PS$（仏馬力）

$\qquad = 75\,kgf \cdot m/s$

$\qquad = 735.499\,W$

放射能	Bq	Ci
	1	2.70270×10^{-11}
	3.7×10^{10}	1

吸収線量	Gy	rad
	1	100
	0.01	1

照射線量	C/kg	R
	1	3876
	2.58×10^{-4}	1

線量当量	Sv	rem
	1	100
	0.01	1

R100

古紙配合率100%
白色度70%再生紙を使用しています